Student thesis series INES nr 791

Evaluating uncertainty in Sweden's national methane inventory for landfills: A UAV-based case study at Filborna

Fleur van Kampen

2026
Department of
Earth and Environmental Sciences
Lund University
Sölvegatan 12
S-223 62 Lund
Sweden

Fleur van Kampen (2026).

Evaluating uncertainty in Sweden's national methane inventory for landfills: a UAV-based case study at Filborna

Master degree thesis, 30 credits in Physical Geography and Ecosystem Science

Department of Earth and Environmental Sciences, Lund University

Level: Master of Science (MSc)

Course duration: *September* 2025 until *June* 2026

Evaluating uncertainty in Sweden's national methane inventory for landfills: a UAV-based case study at Filborna

A case study using UAV-based methane measurements at Filborna landfill to assess how site-scale emissions compare with Sweden's national inventory estimates and associated uncertainties.

Fleur van Kampen

Master thesis, 30 credits, in *Physical Geography and Ecosystem Science*

Marko Scholze
Dep. of Earth and Environmental Sciences, Lund University

Tim Arnold
Dep. of Earth and Environmental Sciences, Lund University

Thesis evaluator:
Per-Ola Olsson

Course examiner:
Martin Berggren

Acknowledgements

I would like to express my sincere gratitude to my supervisor, Marko Scholze, for his valuable guidance, support, and constructive discussions throughout this project. Our meetings helped me shape the direction of the thesis and develop the work further. I am also very grateful to my co-supervisor, Tim Arnold, for his feedback, advice, and guidance whenever I needed it.

I would also like to thank everyone at ReSource Sverige for giving me the opportunity to work with their UAV processing workflow and data from Filborna. Their support and willingness to share knowledge and data made this project possible. A special thanks to Alessandro Sarno for the meetings and ideas that helped shape this thesis.

Finally, I would like to thank Ben for his endless support, patience, and encouragement throughout this process. I am also deeply grateful to my parents for supporting me throughout all these years of university.

Abstract

Methane (CH_4) emissions from landfills are a key uncertainty in Sweden's national greenhouse gas inventory. This thesis evaluates whether UAV-based CH_4 measurements can complement inventory-based estimates, using Filborna landfill in southern Sweden as a case study. UAV-derived emissions from 2022–2024 were compared with an IPCC Tier 2 First Order Decay model, reproduced from Sweden's national inventory methodology and applied to the Filborna Waste Facility. For the UAV-derived emissions, uncertainty was assessed for wind speed, wind direction, kriging interpolation, sensor precision, and background estimation. Wind direction was the dominant source of uncertainty in the UAV-based flux estimates. The reproduced First Order Decay model showed good agreement with Sweden's national inventory estimates at the national scale, while UAV measurements revealed short-term, site-specific variability that the model cannot capture directly. UAV methods cannot replace inventory modelling, but can provide independent observations to evaluate assumptions, identify variability, and improve confidence in landfill CH_4 emission estimates.

Table of Contents

Glossary

DOC - Dissolved organic content

FOD-Model - First Order Decay model. An IPCC method used to estimate methane (CH_4) generation from landfilled organic waste. The model assumes that degradable organic matter breaks down gradually over time, so methane production is highest after waste is deposited and then decreases exponentially as the remaining degradable material is depleted.

GHG - Greenhouse gas

GMP – Global Methane Pledge

MSW - Municipal solid waste

NIR - National inventory report

RSS - Root sum of squares

SW – Solid waste

SWDS - Solid waste disposal site

TDM - Tracer gas dispersion method

UAV - Unmanned aerial vehicle

1 Introduction

Methane (CH_4) is a potent greenhouse gas (GHG), with a 100-year global warming potential 27.2 times greater than that of carbon dioxide (CO_2) for non-fossil methane (IPCC, 2021). CH_4 is estimated to account for nearly a third of global warming observed since the industrial revolution and is the second most significant driver of climate change (Ministry of the Environment, 2022; Saunois et al., 2025). According to the Global Methane Pledge (GMP), reducing CH_4 emissions is essential for limiting global warming to 1.5 °C. Because CH_4 has a relatively short atmospheric lifetime of about 12 years, compared with the centuries-long persistence of CO_2, it is a particularly effective target for near-term climate mitigation (Saunois et al., 2025). To meet these goals, national action must take place (Ministry of the Environment, 2022), which includes improvements in the transparency, accuracy and consistency of national GHG inventory reporting (Climate and Clean Air Coalition, 2021).

Human activities are responsible for at least two-thirds of global CH_4 emissions (Jackson et al., 2024). These anthropogenic sources of CH_4 come from fossil fuels, agriculture, waste handling and burning of biomass and biofuel. Sweden aims to achieve net-zero GHG emissions by 2045 (Swedish Environmental Protection Agency, 2024) and is a supporter of the GMP, of which the aim is to reduce global CH_4 emissions by at least 30% by 2030 compared to 2020 (Climate and Clean Air Coalition, 2021). In Sweden, landfills are the second largest source for CH_4 emissions after livestock farming (Swedish Environmental Protection Agency, 2026 p. 99). In 2024, the Swedish waste sector emitted 0.98 Mt CO_2-equivalents, with CH_4 being the dominant GHG in the sector, accounting for 68% of total waste-sector emissions, equivalent to approx. 0.67 Mt CO_2-equivalents. CH_4 emissions from solid waste disposal amounted to 0.39 Mt CO_2-equivalents, indicating that landfills were responsible for approx. 58% of total CH_4 emissions from the waste sector.

National policies, including the 2002 ban on landfilling combustible materials, have contributed to a substantial decline in waste-sector CH_4 emissions. Between 1990 and 2024, these emissions decreased by 84%, and they are projected to fall further, reaching an 88% reduction by 2030 relative to 1990 levels (Swedish Environmental Protection Agency, 2026, p. 97; Ministry of Climate and Enterprise, 2022). Despite this decline, significant uncertainties remain in the measurement and modelling of emissions. In Europe, landfill operators are required to report annual CH_4 emissions (Mønster et al., 2019), yet existing methods vary in accuracy and reliability. Addressing these uncertainties is essential for improving emission inventories and supporting progress toward climate targets (Fosco et al., 2025).

Waste disposal sites are classified as an IPCC CH_4 emission source category (Referred to as CRT 5.A: Common Reporting Tables, Sector 5, A: solid waste disposal). This sub-category entails managed, unmanaged and uncategorised waste deposited in landfills (Swedish Environmental Protection Agency, 2026 p. 99). For Sweden in particular, only data for managed waste disposal sites are reported, as unmanaged and uncategorised landfill sites are considered not to occur. These managed waste disposal sites are among the ten largest contributors to GHG uncertainty in Sweden's National Inventory Report (NIR) (Swedish

Environmental Protection Agency, 2024), with a combined uncertainty of 55.9%. Overall, waste disposal sites contributed 3.96 % to the uncertainty in national total GHG emissions in 2022, excluding changes in land use (Table A1, Appendix). Improving landfill emission estimation methods could therefore reduce the uncertainty in the national inventory.

While Sweden's annual landfill measurements are used to enforce local environmental permits and to ensure Sweden complies with binding EU and United Nations climate treaties (Naturvårdsverket, n.d.; Mønster et al., 2019), there is no standardised approach for using these CH_4 measurements for the Swedish NIR. The NIR is not based on direct CH_4 measurements, but on the IPCC Tier 2 First Order Decay (FOD) model. Parameters in the model used for all landfills in Sweden, such as dissolved organic carbon content (DOC), the CH_4 generation rate constant, and oxidation factors, are assumed or derived from default values. Incorporating emission factors based on site-specific measurements into the FOD model could therefore reduce the current uncertainty associated with landfill CH_4 emissions in Sweden.

There is still a lack of methodologically consistent, site-scale measurements of CH_4 emissions from Swedish landfills; this motivates the exploration of UAV-based approaches in this thesis. Recent advances in lightweight CH_4 sensors and UAV platforms enable high-resolution spatial measurements of CH_4 concentrations, making UAV-based monitoring an increasingly promising and accessible tool for landfill emission assessment (Liu et al., 2021). UAVs can cover large, heterogeneous, and inaccessible areas, potentially leading to more accurate CH_4 emission measurements. This thesis investigates the potential of using UAV-based measurements over landfills to reduce uncertainty in the NIR. By reviewing existing estimation practices and their associated uncertainty sources, this study evaluates whether UAV-based measurements can provide accurate and spatially representative emission measurements.

This thesis uses the Filborna landfill in southern Sweden as a case study to evaluate the potential of UAV-based CH_4 measurements for improving landfill CH_4 emission assessment. The main objective is to assess how UAV-derived CH_4 emission estimates compare with inventory-based approaches, and to determine whether UAV measurements can provide a useful complementary method for reducing uncertainty in landfill CH_4 reporting. In addition, tasked satellite observations over Filborna are used as a supplementary assessment of the current possibilities and limitations of CH_4 detection for this type of landfill emission source.

To address this objective, the thesis is guided by the following research questions:

1. How do CH_4 emission estimates derived from UAV-based measurements at Filborna compare with emissions reported in the national inventory?
2. What are the main sources of uncertainty in UAV-based CH_4 flux estimates at landfill scale?
3. To what extent does the FOD model capture observed CH_4 emissions from a heterogeneous, actively managed landfill such as Filborna?

4. How do modifications to key processing steps and parameter choices in the UAV-based CH_4 flux calculation pipeline affect the resulting emission estimates and associated uncertainties?
5. What do tasked satellite observations over Filborna indicate about the current detectability of landfill CH_4 emissions from space?

The underlying hypothesis is that UAV-based measurements can capture site-specific spatial and operational variability that is not fully represented by inventory-based FOD modelling. As a result, UAV observations are expected to provide a more direct estimate of landfill-scale CH_4 emissions and may help identify key sources of uncertainty in national inventory reporting. By addressing these questions, this thesis evaluates whether UAV-based methodologies can complement existing CH_4 measurement approaches and contribute to a more accurate and reliable assessment of landfill CH_4 emissions in Sweden.

2 Background

2.1: Landfills and methane emissions in Sweden

In Sweden, approximately 1.9 million tonnes of waste were sent to landfill in 2024. This total includes several waste streams and is broader than municipal or household waste. Household waste now represents only a small fraction of landfilled material: in 2024, 28,150 tonnes of household waste were landfilled, corresponding to 1.5% of the total landfilled waste stream (Avfall Sverige, 2025). This reflects a shift away from landfilling, particularly for household waste, alongside increased biological treatment, material recycling, and energy recovery. Fig. 1 shows reported national data for landfilled waste.

In GHG inventory reporting, landfill methane emissions are estimated for solid waste disposed at solid waste disposal sites (SWDS). Municipal solid waste (MSW) generally includes household waste and similar waste from sources such as shops, offices, institutions, and small businesses, whereas household waste refers more narrowly to waste generated by households.

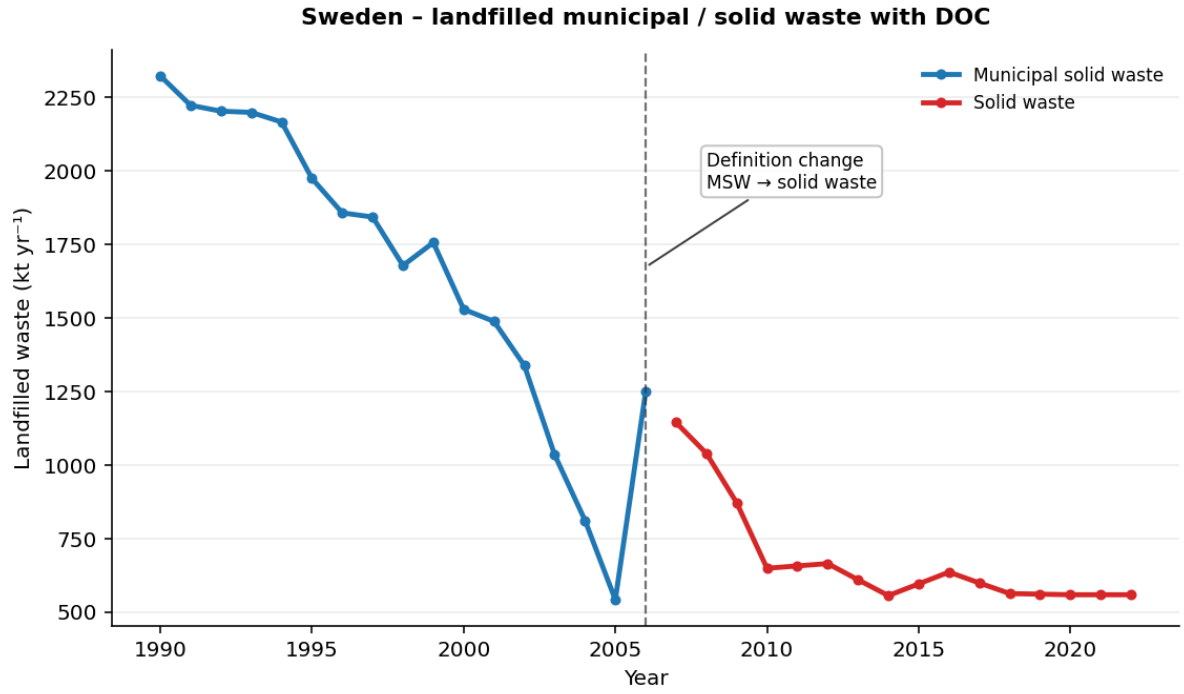

Source: UNFCCC. Reported statistics: 2006, 2008, 2010, 2012, 2014, 2016, 2018, 2020.
Inter/extrapolated statistics: 2007, 2009, 2011, 2013, 2015, 2017, 2019, 2021, 2022.

Fig. 1: Reported landfilled waste in Sweden, 1990–2023. The dashed line marks the 2006 definition change from municipal solid waste (MSW) to the broader solid waste category. Data are from the National Inventory Report submitted to the UNFCCC (2024).

The reduction in landfilling was driven by increasing awareness of the environmental, health, and social impacts associated with landfill disposal (Corvellec and Hultman, 2012). Municipalities have been responsible for the collection, transportation, and treatment of waste since 1972. In the 1970s and 1980s, many municipalities started incinerating waste to recover energy. In the 1990s, efforts were made to increase recycling through policies requiring waste producers to promote recycling (Björklund and Finnveden, 2007). In the early 2000s,

landfilling decreased further due to the European Landfill Directive, which required reductions in landfilled biodegradable waste and the collection of CH_4 from landfills (Swedish Government, Ministry of Climate and Enterprise, 2022). Around the same time, in 2001, a tax on landfilled waste was introduced. Expanding on the 2001 EU directive, landfilling of combustible material and organic material was also banned in 2002 and 2005 respectively (Corvellec and Hultman, 2012).

The decline in landfilling has led to a decrease in the number of landfills in Sweden. In 1974 there were 742 active landfills (Swedish Environmental Protection Agency, 2026 p. 399) in Sweden, 300 active landfills in 1994 (Corvellec and Hultman, 2012), while only 239 active landfills remained in 2025 (Naturvårdsverket, 2025). Of these active landfills, landfilling of household waste was only conducted at 47 sites in 2024 (Avfall Sverige, 2025). Landfills are still being shut down and capped through 2030 (Avfall Sverige, 2023), and the number of active sites is therefore expected to decline further. However, closed landfills may still emit landfill gases, of which primarily CH_4 (Avfall Sverige, 2025). It is estimated that there are between 4,000 and 8,000 closed landfills containing organic waste in Sweden (Montoya et al., 2020), some of which continue to emit CH_4. Fig. 2 shows that CH_4 emissions decreased gradually, despite a much sharper decline in landfilling. This delayed response can be explained by the slow degradation of DOC in previously deposited waste. Even after organic waste inputs are reduced or landfilling stops, older waste continues to decompose and produce CH_4 over several decades. Closed landfills may still emit landfill gases for up to three decades after closure (Petrovic, 2026). Therefore, landfill CH_4 monitoring should also be carried out at sites that are no longer active (Scheutz and Kjeldsen, 2019).

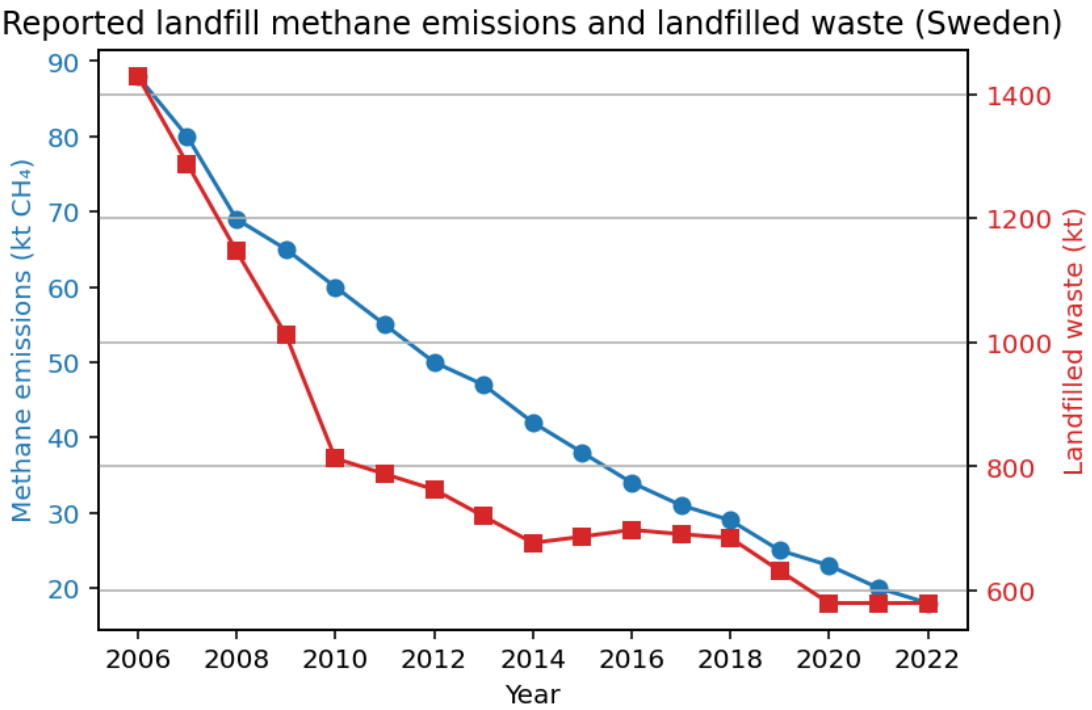

Fig. 2: Estimated landfill CH_4 emissions in kt CH_4 (left, in blue) and landfilled solid waste 2006-2022 in kt (right, in red). Data from National Inventory Report, UNFCCC (2024).

388.7 kt CO_2-equivalents of CH_4 emissions, with a combined uncertainty of 55.9%, were reported from managed waste disposal sites in 2024 in Sweden (Naturvårdsverket, 2025). Emissions from the waste sector (CRT 5) originate from solid waste disposal, biological treatment of waste, wastewater handling, and incineration and open burning of waste. Landfills fall under CRT 5.A (SW disposal) and represent the largest source of CH_4 within the waste sector; in 2024, CH_4 emissions from managed waste disposal sites corresponded to about 39.7% of total waste-sector GHG emissions (Swedish Environmental Protection Agency, 2026 p. 390). Worldwide, the waste sector contributes around 20% of total anthropogenic CH_4 emissions (Scarpelli et al., 2024). In Sweden in 2024, the waste sector contributed 15% of Sweden's total CH_4 emissions and total waste-sector CH_4 emissions amounted to approx. 0.67 Mt CO_2-equivalents. In 2020, total CH_4 emissions from the waste sector amounted to 0.68 Mt CO_2-equivalents, of which 0.58 Mt CO_2-equivalents originated from landfills. CH_4 emissions from landfills have decreased strongly since the 1990s (Fig. 2), and CH_4 emissions from landfilling are projected to decrease further, by 88% compared to 1990 by 2030.

To meet the GMP target, global CH_4 emissions need to be reduced by at least 30% by 2030 relative to 2020 levels (Climate and Clean Air Coalition, 2021). However, UNEP estimates that reductions of 40–45% by 2030 are needed to keep the Paris Agreement's 1.5 °C target within reach (UNFCCC, 2015, Article 4, para. 1; Avfall Sverige, 2024). Sweden has therefore developed a national action plan aimed at reducing CH_4 emissions. Avfall Sverige (2024) notes that, although CH_4 emissions from landfills have already decreased substantially, there is still a lack of knowledge regarding emissions from the waste sector. CH_4 emissions from landfills are difficult to quantify directly because they are diffuse and highly variable in space and time (Petrovic et al., 2026). Improving knowledge of accurate and effective emission measurement techniques is therefore necessary to meet both national and international targets. Uncertainty remains not only regarding emissions from current landfilling, but also regarding emissions from (temporary) waste storage.

2.2: Current methods for measuring methane emissions

2.2.1: Reporting practices in Sweden

Active landfill sites must report annual CH_4 emissions to the Swedish Pollutant Release and Transfer Register. Currently, there is no standardised method for measuring and monitoring CH_4 emissions from landfills in Sweden (Avfall Sverige, 2024). Each landfill may choose how to report its emission estimates: landfills can report CH_4 values as measured (M), estimated (E), or calculated (C) (Naturvårdsverket, 2016) (Fig. 3). M refers to CH_4 values based on continuous or periodic measurements. C refers to calculations using emission factors and mass balance; one example is the IPCC's FOD model, which uses standard emission factors. E is used when neither calculation nor measurement is possible, and no formal calculation or measurement method is applied.

There are different ways of measuring CH_4 emissions from landfills. Two common techniques are chamber flux measurements and the tracer gas dispersion method (TDM) (Avfall Sverige, 2016). Because the methodology for estimating emissions varies between landfills, the reported

data are inconsistent. Therefore, the IPCC FOD model is used in the national inventory to ensure consistency, while individually reported emissions are only used for comparison and verification.

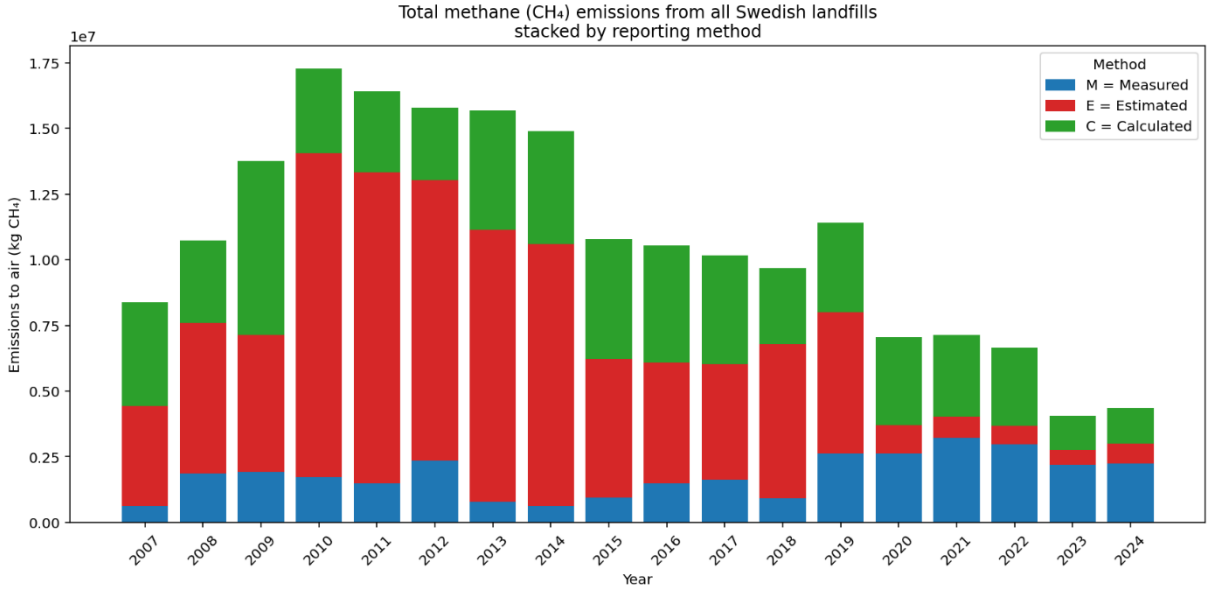

Fig. 3: Self-reported total CH_4 emissions in kg CH_4 from Swedish landfills, 2007–2024. Blue indicates measured emissions (M), red indicates estimated emissions (E), and green indicates calculated emissions (C). Data from Naturvårdsverket: Swedish Pollutant Release and Transfer Register (n.d.).

2.2.2: Chamber measurements

Chamber measurements using closed and open surface flux chambers are an accurate method for measuring emissions, but taking enough measurements is impractical, especially for large heterogeneous landfills, often leading to underestimation of emissions due to poor representation of emission hotspots (Gålfalk et al., 2021; Scheutz and Kjeldsen, 2019). This is because chambers only measure a small, localised part of a landfill site and are therefore unable to capture the spatial variability of emissions across a heterogeneous landfill. For this reason, methods that quantify emissions at the scale of the entire site are often preferred, such as the tracer gas dispersion method (TDM).

2.2.3: Tracer gas dispersion method

The TDM is the most well-documented technique for estimating landfill CH_4 emissions (Scheutz and Kjeldsen, 2019). The method follows several steps, beginning with on-site and off-site screening to identify the main emission areas. This is followed by the release of a tracer gas, based on the emission pattern established during the initial screening. The tracer gas must be released at a known and constant rate to quantify CH_4 emissions. Measurements are then taken downwind of the site. CH_4 emissions are estimated through a plume traverse, which is successful when CH_4 and the tracer gas disperse similarly in the atmosphere (Fredenslund et al., 2019). Because the background concentrations of both CH_4 and the tracer gas can be identified outside the plume, CH_4 emissions can be derived from the ratio between CH_4 and tracer gas enhancements, multiplied by the known tracer gas release rate (Scheutz and Kjeldsen, 2019). The setup, however, is complex: the tracer gas needs to be released correctly

and the TDM can be prone to measurement errors. The TDM also does not allow emission hotspots and CH_4 leaks to be detected easily.

2.2.4: Satellite observations

In addition to ground-based measurement techniques, recently developed remote sensing approaches have been used to quantify CH_4 emissions from landfills. In recent years, the use of satellites for CH_4 detection has increased (Ferrari et al., 2025). Shortwave infrared satellite sensors can quantify CH_4 plumes and concentrations at spatial resolutions of up to 30 m. Ferrari et al. (2025) suggest that multi-satellite observations may have strong potential for consistent and accurate CH_4 emission monitoring from landfills. Compared with in situ measurement strategies, satellites allow repeated and potentially near-continuous monitoring. However, observations may be limited by atmospheric effects such as wind and clouds, temporal variability, and sensor-specific factors.

The commercial sensors from GHGSat have been used to quantify landfill emissions successfully, particularly for urban landfills with high emission rates (GHGSat, n.d.; Gillespie et al., 2025). Krause et al. (2025) suggest that combining satellite observations with ground-based sensors, operational information, and meteorological data could improve understanding of site-specific landfill emissions throughout the year. One major source of uncertainty in the measurements from the GHGSat sensors is variation in wind speed (McLinden et al., 2024). In addition, each scene is observed under different conditions, and measurements perform best over flat and reflective surfaces. The sensors from GHGSat also have a CH_4 detection threshold of approx. 100 kg h^{-1} (Dogniaux et al., 2025), meaning that emissions below this threshold are usually not detected. Both wind speed and the reflected sunlight collected by the instrument significantly affect the sensor's detection limit. Jervis et al. (2025) report that GHGSat has a 50% probability of detection at 100 kg h^{-1} under a wind speed of 3 m s^{-1}, although the detection threshold varies depending on observation conditions. GHGSat is not the only satellite-based option; other systems, such as Carbon Mapper, are also being developed and applied for methane point-source detection (Carbon Mapper, n.d.).

Satellite-based CH_4 detection and quantification has considerable potential, but the method is still in an early stage of development. Despite its current limitations, it offers a valuable approach for CH_4 monitoring, particularly when used in combination with in situ measurements.

2.3: UAV-based methane measurements

The use of gas-detecting sensors mounted on UAVs may provide a cost-efficient way to measure and monitor CH_4 emissions (Montoya et al., 2020). UAVs allow different areas of a landfill site to be surveyed and can help identify CH_4 emission hotspots.

2.3.1: Principles of UAV methane measurements

UAV-based CH_4 measurements typically involve mounting fast-response gas concentration sensors, such as laser-based CH_4 analysers, together with a navigation system on a multirotor

or fixed-wing platform. This setup enables georeferenced, high-frequency sampling of CH_4 concentrations within the atmospheric boundary layer.

During operation, the UAV is flown along predefined transects, typically perpendicular to the mean wind direction and downwind of the emission source, to intercept the gas plume. The sensor records CH_4 mole fractions at high temporal resolution while meteorological parameters such as wind speed, wind direction, pressure, and temperature are measured either onboard or from nearby stations.

Fluxes are commonly derived using a mass-balance or inverse modelling approach. In this approach, excess CH_4 concentrations above background levels are integrated across a vertical control plane downwind of the source and multiplied by the perpendicular wind component to estimate the emission rate. Post-processing generally includes synchronisation of sensor and navigation data, calibration drift correction, background subtraction, and uncertainty analysis accounting for wind variability, sensor precision, and flight geometry (Fosco et al., 2025).

2.3.2: Current applications

The use of UAVs for CH_4 measurements has become increasingly common due to developments in sensor technology and the ability to mount lightweight measurement equipment on UAV platforms (Fosco et al., 2025). UAV-based measurements allow CH_4 concentrations to be mapped at high spatial resolution across landfill sites and can help identify emission hotspots that may be missed by ground-based measurements. This makes UAVs particularly useful for heterogeneous sites such as landfills, where emissions may vary significantly across different areas.

2.3.3: Limitations and uncertainty

Despite their advantages, UAV-based CH_4 measurements have several limitations.
CH_4 emissions from landfills can vary over time due to factors such as weather conditions and seasonal changes. For example, CH_4 oxidation is influenced by air and soil temperature; lower temperatures can reduce oxidation rates and may lead to higher CH_4 emissions during winter (Maurice and Lagerkvist, 2003). Continuous monitoring across different seasons would therefore improve estimates of landfill gas emissions. However, continuous measurements are difficult to achieve with UAV-based approaches because UAVs are, for example, limited by battery life, weather conditions (Mønster et al., 2019).

In addition, the accuracy of UAV-based emission estimates can be affected by topographic conditions and wind variability, if such factors are not properly accounted for (Scheutz and Kjeldsen, 2019). UAV measurements can provide high spatial resolution data, but translating concentration measurements into reliable emission fluxes requires careful consideration of plume transport and atmospheric conditions.

In many UAV-based workflows, CH_4 concentrations measured along flight paths are interpolated to a two-dimensional concentration field, for example using geostatistical kriging.

This interpolated concentration field is then combined with wind measurements to estimate surface fluxes by integrating CH_4 concentrations across a vertical plane downwind of the source. Although this framework enables estimation of landfill CH_4 emissions, several uncertainties remain. These uncertainties relate to the physical consistency of the plume representation, assumptions used in the processing workflow, and the quantification of overall uncertainty. Uncertainties in CH_4 measurements may arise from sensor precision, methodological assumptions, temporal variability, or the aggregation of emissions from multiple sources (IOGP, Ipieca, OGCI & Energy Institute, 2025). These limitations highlight the importance of understanding how UAV-based measurements compare with existing approaches for estimating CH_4 emissions, such as the modelling methods used in national GHG inventories.

2.4: Methane estimation in the Swedish national inventory

The NIR for GHG emissions prioritises time-series consistency. This means that even when facility-level measurements are available, national emissions are estimated using the same underlying model structure across all years, with recalculations applied retrospectively when parameters or data sources are updated. National CH_4 emissions from landfills are therefore estimated using a bottom-up modelling approach in which parameters and assumptions are standardised across the country.

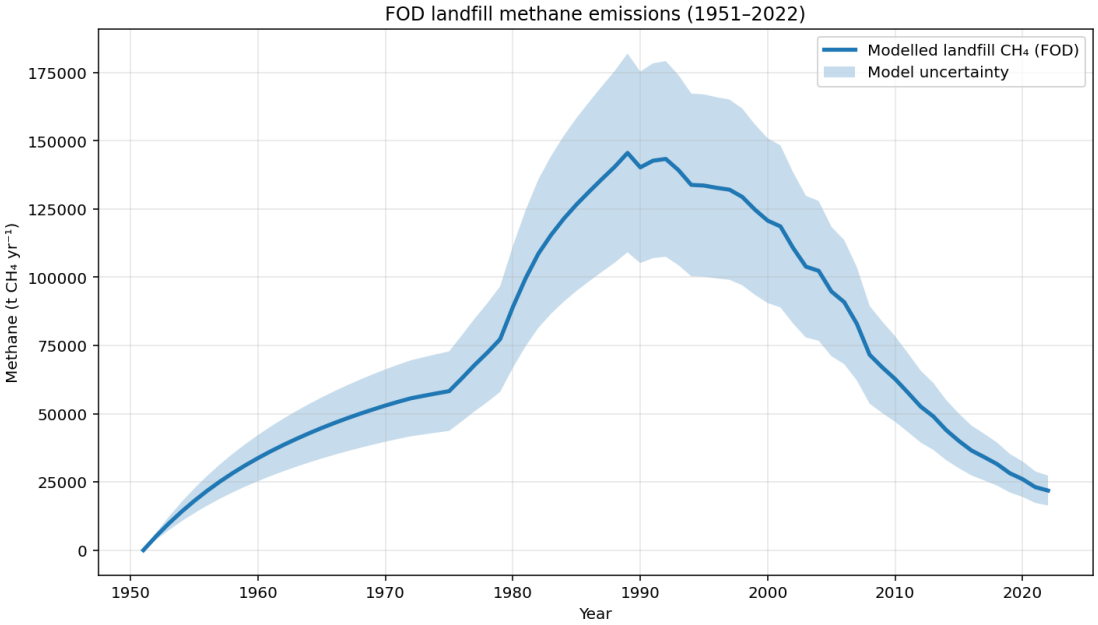

Fig. 4: CH_4 emissions from Swedish landfills estimated using the FOD parameters applied in the National Inventory Report (NIR, 2024) with the blue line showing the modelled CH_4 and the light blue envelope showing the model uncertainty.

2.4.1: The IPCC First Order Decay model

Several FOD models can be used to estimate CH_4 generation and emissions from landfilled waste, including LandGEM, Afvalzorg and the IPCC model. These models share the assumption that CH_4 generation declines exponentially over time as DOC is depleted, but they differ in complexity and application. LandGEM is a relatively simple landfill-scale model, Afvalzorg uses a more detailed multiphase approach, and the IPCC model is designed for consistent national GHG inventory reporting (Vu et al., 2017). In Sweden, CH_4 emissions from

landfilled waste are estimated using a national implementation of the IPCC Tier 2 FOD model (Fig. 4). The model estimates CH_4 generation from DOC deposited in landfills using nationally reported activity data consisting of solid waste. Parameters used for the model, such as decay rates, CH_4 correction, recovery and oxidation, are derived from measurements, national statistics, and IPCC guidance; this methodology is further described in Chapter 3.3 (Fosco et al., 2025). The uncertainty band for the FOD is estimated using IPCC values for emission factors and a combination of IPCC and expert judgement for activity data. The uncertainty analysis is performed following the IPCC 2006 guidelines for approach 1 (UNFCC, 2026 p.191). As seen in Fig. 4, uncertainty peaks in 1990, following a decrease. The decrease following 1990 is due to the use of new data sources, particularly, in DOC values after the change in IPCC guidelines in 2006 (UNFCCC, 2025 p. 423).

2.4.2: Limitations of the FOD-approach

One limitation of the FOD-approach is that its accuracy depends strongly on assumed parameters. The parameters applied in the Swedish inventory are based on national averages, climate conditions, and IPCC recommendations. However, site-specific landfill conditions are not fully represented. Citrasari et al. (2025) report that CH_4 emissions from landfills may be underestimated by up to 200% when using simplified modelling approaches. Similarly, Fosco et al. (2025) highlight that bottom-up approaches often underestimate CH_4 emissions observed in the atmosphere.

Several factors may contribute to these discrepancies. CH_4 emissions from landfills depend on waste composition, the degradation stage of the landfill, and CH_4 oxidation processes within the landfill cover (Maurice and Lagerkvist, 2003). These factors can vary substantially between landfill sites. When national average parameters are applied in a model such as the FOD framework, this variability may not be fully captured.

Direct, top-down measurements may therefore help improve our understanding of the differences between inventory-based estimates and observed CH_4 emissions. For example, satellite observations have been used to detect CH_4 plumes from large emission sources (Zhang et al., 2026). Such measurements can be used both to validate inventory estimates and to improve parameter values used in emission models. UAV-based measurements may also contribute to validating key parameters such as decay rates, and gas recovery. Improving measurement-based estimates of landfill CH_4 emissions may therefore help reduce uncertainty in national GHG inventories and provide valuable constraints for model-based approaches.

Overall, estimating CH_4 emissions from landfills remains challenging due to the spatial and temporal variability of emissions, as well as limitations in both measurement and modelling approaches. While modelling frameworks such as the IPCC's FOD model provide consistent national-scale estimates, they may not fully capture site-specific variability. Measurement-based approaches, including UAV observations, offer the potential to complement these models by providing spatially resolved emission data. Understanding how such measurements compare with inventory-based estimates is therefore important for improving the accuracy and reliability of GHG inventories.

3 Study Site and data

This study focuses on CH_4 emissions from the Filborna waste facility in Helsingborg, Sweden (Fig. 5). The site was selected due to the availability of UAV-based CH_4 measurements and long-term waste monitoring data. Filborna has a long history of CH_4 monitoring, with UAV measurement campaigns conducted in 2022, 2023, and 2024.

Fig. 5: Location of Filborna waste facility in Helsingborg, southern Sweden. Basemap sources: Esri, DigitalGlobe, GeoEye, i-cubed, USDA FSA, USGS, AEX, Getmapping, Aerogrid, IGN, IGP, swisstopo, and the GIS User Community. Inset basemap: OpenStreetMap contributors.

3.1: Study site: Filborna landfill, Helsingborg

The Filborna waste facility landfill covers approx. 32 hectares and has been in operation since 1951. Although landfilling of organic waste has been prohibited in Sweden since 2005, several landfill cells remain active sources of CH_4 emissions due to the ongoing anaerobic degradation of previously deposited waste.

The landfill contains a heterogeneous mix of waste types, including household, industrial, and commercial waste, as well as ash, sewage sludge, and garden waste. The site is subdivided into multiple functional areas, including composting facilities, waste storage areas, and an

incineration plant (Fig. 6). These sub-areas represent potential CH_4 emission hotspots and introduce spatial variability in surface fluxes. Filborna is equipped with a landfill gas recovery system; however, fugitive emissions remain a significant component of total CH_4 release.

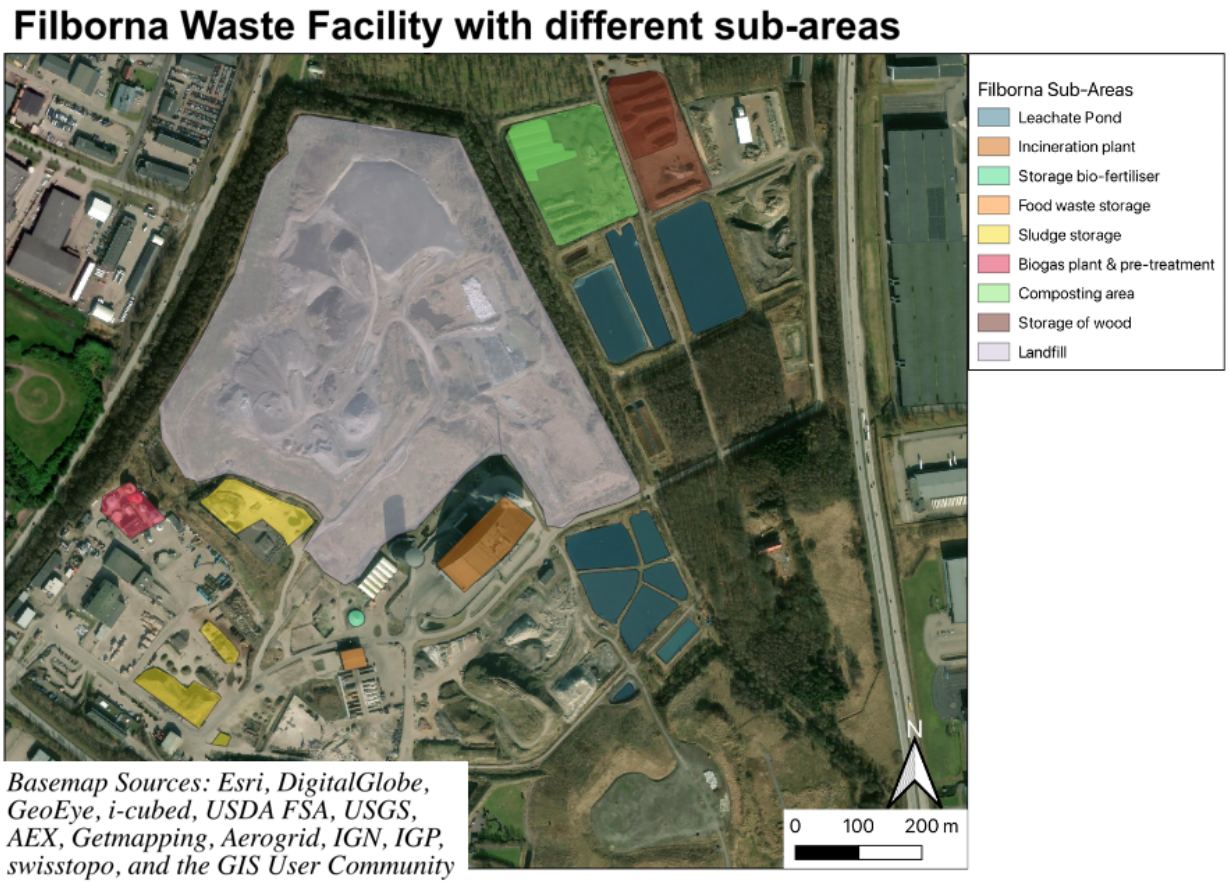

Fig. 6: Study site Filborna Waste Facility with sub-areas marked in colours defined in legend. Sub-areas based on data from ReSource International (2022), Basemap sources: Esri, DigitalGlobe, GeoEye, i-cubed, USDA FSA, USGS, AEX, Getmapping, Aerogrid, IGN, IGP, swisstopo, and the GIS User Community.

3.2: Data for Filborna

Fig. 7 summarises the different datasets used to estimate and compare CH_4 emissions from the Filborna waste facility. The analysis combined site-specific data, including UAV campaigns, GHGSat satellite observations, and reported site emissions from Naturvårdsverket, with national-level data used for model-based estimation. Reported waste quantities for Filborna were applied together with FOD model parameters to estimate methane generation and emissions. The resulting estimates from the different approaches were then compared to evaluate differences between measurement-based, reported, satellite derived, and modelled emissions.

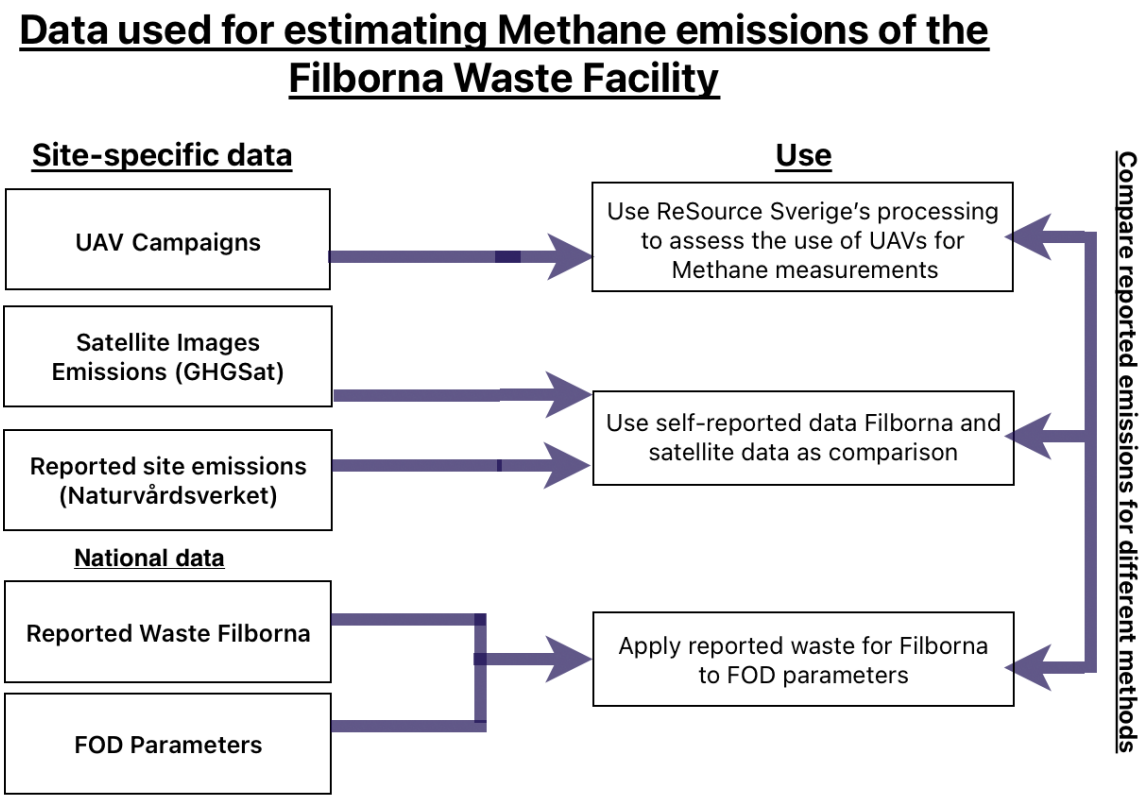

Fig. 7: Overview of the datasets used to estimate and compare CH_4 emissions from the Filborna waste facility. Site-specific data included UAV campaigns, satellite observations, and reported site emissions, while national-level data included reported waste quantities and FOD model parameters. These datasets were used to compare CH_4 emission estimates derived from different methodological approaches, for more detailed workflow, see Appendix Fig. A1.

3.2.1: UAV Campaigns

UAV data were provided by ReSource Sverige, a Swedish environmental consultancy specialising in landfill gas measurement, CH_4 emission quantification, and waste-sector environmental assessments. The data originate from field campaigns conducted at the Filborna landfill on the following dates:

1) 12 October 2022 **2)** 17 October 2023 **3)** 15 November 2024

The datasets include CH_4 concentration measurements along UAV flight trajectories, as well as meteorological observations including wind speed, wind direction, temperature, and atmospheric pressure. These data form the basis for site-scale CH_4 flux estimates.

Raw CH_4 concentration data were initially processed using the CH_4 flux calculation pipeline developed by ReSource Sverige. Subsequent sensitivity analyses and uncertainty quantification were implemented in Python as part of this study.

3.2.1.1: 2022 Campaign

The 2022 data used for the analysis consisted of three transects with a total of five flights conducted during the afternoon of 12 October 2022. The altitude range for all flights from 2022

was 23 – 141 m above ground. Mean wind speed ranged between 3.2 m/s and 4.1 m/s with a wind direction between 186 ° and 207°.

Transect B was located west of the biogas plant and sludge storage area. Transect W was located north of the landfill, crossing the composting area and leachate ponds. Transect WB was positioned west of the landfill and north of the biogas plant (Fig. 8).

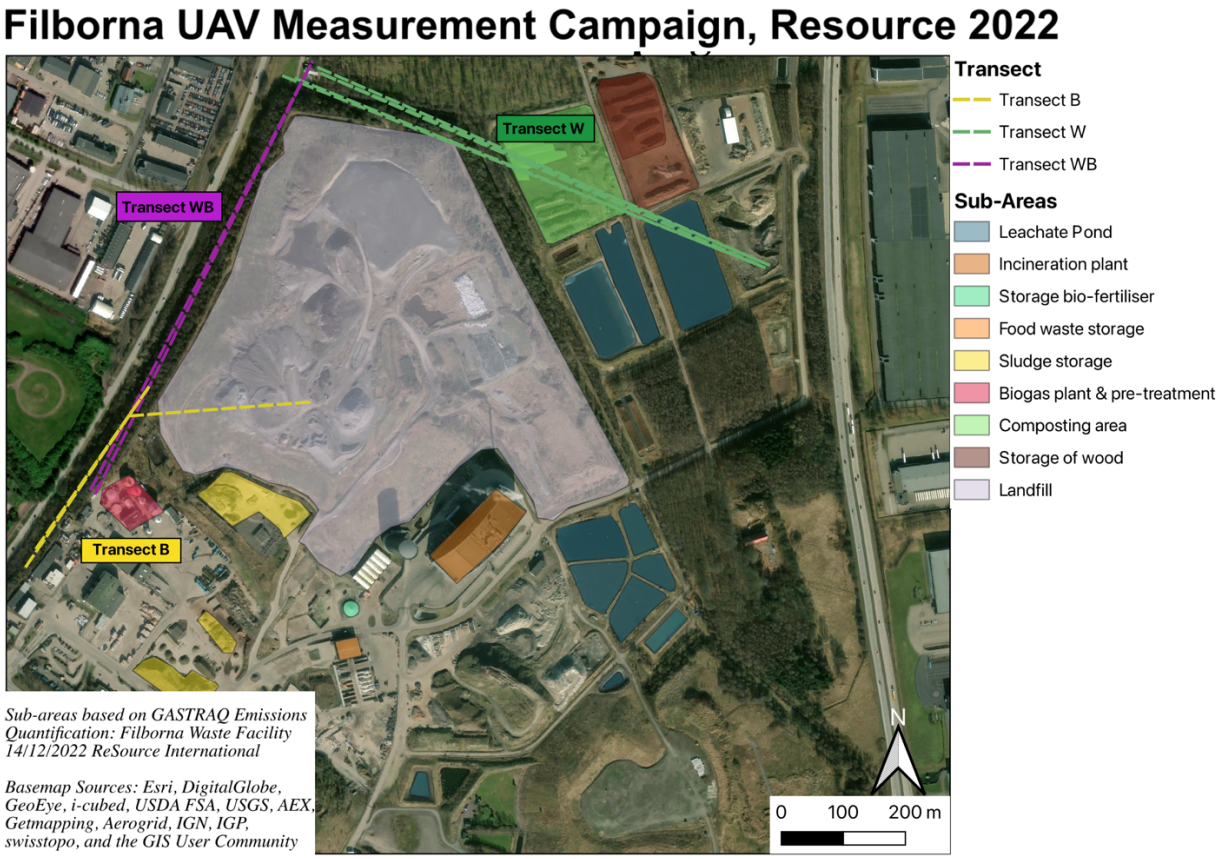

Fig. 8: Filborna campaign, ReSource (2022) with Transect B (yellow), W (green) and WB (purple). Sub-areas are marked in colours defined in the legend and are *based on data from ReSource International (2022)*, B*asemap sources: Esri, DigitalGlobe, GeoEye, i-cubed, USDA FSA, USGS, AEX, Getmapping, Aerogrid, IGN, IGP, swisstopo, and the GIS User Community*.

3.2.1.2: 2023 Campaign

The 2023 campaign consisted of a single transect with eight flights conducted during the afternoon of 17 October 2023. The altitude range for all flights from 2022 was 36 – 107 m above ground. For the measurements on 17/10/2023, wind speed ranged between 5.5 m/s and 7.9 m/s with a wind direction between 276 ° and 294°.

The transect (C) was located east of the landfill, between the leachate ponds, the composting area, and the wood storage sub-area in the northern part of the Filborna waste facility (Fig. 9).

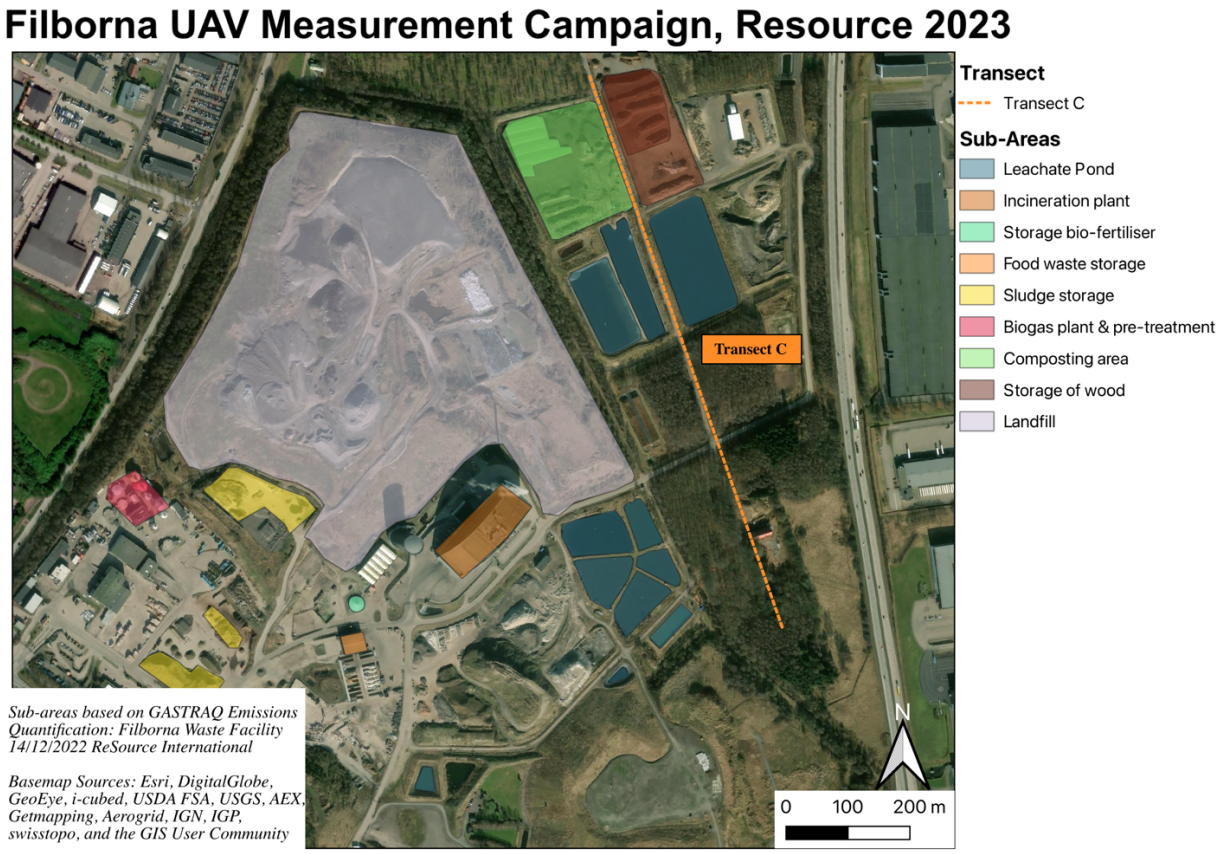

Fig. 9: Filborna campaign, ReSource (2023) with Transect C (orange). Sub-areas are marked in colours defined in the legend and are based on data from ReSource International (2022), Basemap sources: Esri, DigitalGlobe, GeoEye, i-cubed, USDA FSA, USGS, AEX, Getmapping, Aerogrid, IGN, IGP, swisstopo, and the GIS User Community.

3.2.1.3: 2024 Campaign

The 2024 campaign followed the same transect as in 2023 (Fig. 9) with a total of nine flights conducted during the afternoon of 15 November 2024. The altitude range for all flights from 2022 was 32 – 107 m above ground. For the measurements on 17/10/2024 wind speed ranged between 5.2 m/s and 7.2 m/s with a wind direction between 270 ° and 284°.

3.2.2: Additional measured data

In addition to the UAV campaign data, this study uses historical emission data and landfill-specific information from Bergström and Fråne (2011) and Naturvårdsverket for comparison with the UAV-derived measurements. A visual of the data and usage is available in Appendices Fig. A1.

3.2.2.1: Satellite observations (GHGSat)

Satellite images of Filborna retrieved from GHGSat were also used for comparison. These images have a spatial resolution of approx. 25 m (GHGSat, 2026). Historical catalogue data and newly tasked observations were requested through the European Space Agency. For this study, 12 observations were granted. The dates and acquisition times for 10 of these scenes are listed in Table 1. GHGSat detects and quantifies CH_4 emissions with a minimum detection threshold of approx. 100 kg h^{-1} under wind speeds of around 3 m s^{-1}. Scenes that do not meet this CH_4 detection threshold result in a “no methane detected” classification.

Table 1: GHGSAT Catalogue and tasked data including date, time ID of measurements and sensor used (GHGSat, n.d.).

GHGSAT Data	Date	Time (UTC)	Observation ID	Sensor
Catalogue data	01/02/2024	13:06:32	Ii98UjV	GHGSat-C4
	07/05/2024	13:09:16	Ejd-zjV	GHGSat-C3
	14/02/2025	13:41:41	Mo48zjV	GHGSat-C5
Weekly Tasking	03/02/2026	13:10:51	Ita9zjV	GHGSat-C12
	14/02/2026	13:09:35	ItlB3mi	GHGSat-C12
	19/02/2026	14:45:40	CtqAUjV	GHGSat-C3
	04/03/2026	14:34:14	Cu3EYmi	GHGSat-C3
	06/03/2026	11:01:49	hu54UjV	GHGSat-C11
	10/03/2026	11:18:04	hu94Ymi	GHGSat-C11
	16/04/2026	09:43:16	Wui83mi	GHGSat-C8
	23/04/2026	15:15:10	KupDYmi	GHGSat-C5
	27/04/2026	09:36:17	Our-Ymi	GHGSat-C6
	05/05/2026	14:56:03	Gv1CYmi	GHGSat-C4

3.2.2.2: Historical emission data

In Sweden, landfill operators are required to report CH_4 emissions annually using either measured, calculated, or estimated values. Data from Naturvårdsverket represent annual totals of CH_4 emissions (kg CH_4 yr^{-1}) derived using different methodological approaches over time. Emissions for the period 2007–2011 are based on estimated values, whereas emissions from 2012–2021 were derived using measurement-based approaches (TDM). From 2022 onwards, emissions have been quantified using UAV-based measurements (overview available in Appendices, Fig. A2).

3.2.2.3: Tracer dispersion method measurements

TDM measurements reported by Linn Möller (2022) were originally expressed as instantaneous emission rates (kg CH_4 h^{-1}). To enable comparison with annual emission totals, these measurements were annualised by multiplying the hourly emission rates by 8,760 h yr^{-1}. When multiple tracer measurements were available within the same year, the annualised values were averaged to obtain a single representative annual estimate. Measurement uncertainty was propagated by combining the reported ± uncertainties for each year using a root-mean-square (RMS) approach. These uncertainties are shown as vertical whiskers (± uncertainty) around the annualised mean values (Fig. 10).

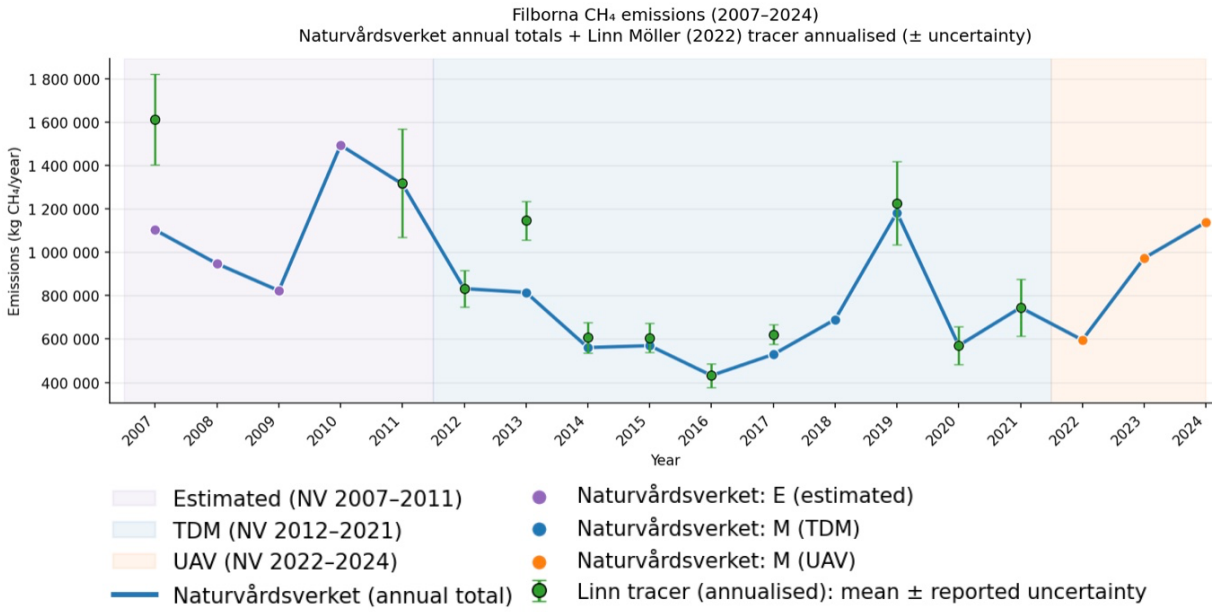

Fig. 10: Measured and estimated CH_4 Emissions at Filborna landfill for 2007-2024. Filborna's self-reported (to Naturvårdsverket) CH_4 Emissions for 2007-2024 indicated by the blue line. Measured TDM data 2007-2021 averaged with uncertainty whiskers in green (Möller, 2022). Data reported to Naturvårdsverket as E (estimated) in purple, M (TDM) in blue, M (UAV) in orange.

3.3: FOD parameters

Table 2 summarises the key parameters used in the FOD calculation for landfill CH_4 emissions in Sweden, including the CH_4 correction factor (MCF), CH_4 fraction in landfill gas (F), fraction of degradable organic carbon that decomposes (DOCf), oxidation factor (OX), and decay rate ($T_{1/2}$). The table also provides the parameter values applied in the NIR and the source for each assumption.

In Sweden's NIR, landfills are treated as managed anaerobic systems and are therefore assigned a CH_4 correction factor (MCF) of 1. CH_4 generation is further determined by assumptions regarding the DOC content of the deposited waste, the fraction of DOC that decomposes (DOCf), the CH_4 fraction in landfill gas, set to 50%, and a fixed oxidation factor (OX), set to 10%. The decay rate is a half-life of 7.5 years, which is the rate at which DOC is converted to CH_4 over time. These parameters are based on a combination of IPCC default values and national assessments, as summarised in Table 2.

Table 2: Parameters used for FOD calculation Sweden. Adapted Table 7.6 from the NIR Sweden, 2024.

Parameter	Value	Motivation
MCF - 1979	0.6	IPCC Uncategorised SWDS
MCF 1980 -	1	IPCC Managed anaerobic
F	50%	IPCC Default
DOCF	0.5	IPCC Default
OX	10%	National parameter (Swedish EPA, 1997b)
$T_{1/2}$	7.5 years	National parameter (Swedish EPA, 1993b)

Activity data describing the amount and composition of waste deposited in Swedish landfills are compiled over long historical periods. Since 2006, the quality of Swedish landfill activity data has improved due to harmonised waste statistics introduced under the EU Waste Statistics Regulation. For earlier years, activity data rely on reconstructed estimates based on population, per-capita waste generation, and estimated landfilling fractions.

The same parameter values for MCF, F, OX and $T_{1/2}$ from the NIR are assumed for the Filborna FOD (Table 3). A DOCF value of 0.54 was used instead of the default of 0.50 based on Filborna-specific evaluation by Börjesson et al. (2007) and from the IPCC (2000)'s GHG inventory's guidance. For the Filborna landfill, historical landfill data used as activity data were obtained from Bergström and Fråne (2011). These activity data and parameter assumptions are applied within the standard IPCC FOD-formulation to estimate annual CH_4 generation from landfilled waste.

Table 3: Parameters used for FOD calculation Filborna. Table 7.6 from the NIR Sweden, 2024 adapted to fit Filborna

Parameter	Value	Motivation
MCF - 1979	0.6	IPCC Uncategorised SWDS
MCF 1980 -	1	IPCC Managed anaerobic
F	50%	IPCC Default
DOCF	0.54	IPCC Default
OX	10%	National parameter (Swedish EPA, 1997b)
$T_{1/2}$	7.5 years	National parameter (Swedish EPA, 1993b)

4 Methods

4.1: Study design

The study integrates national-scale modelling, site-level measurements, and methodological evaluation, split into 3 different parts:

1. National and site-scale inventory reproduction using Sweden's implementation of the IPCC Tier 2 First Order Decay (FOD) model (Fig. 11A).
2. Site-specific comparison of CH_4 emission estimation methods at Filborna landfill (Fig. 11A).
3. Evaluation and modification of UAV CH_4 flux processing workflows (Fig. 11B).

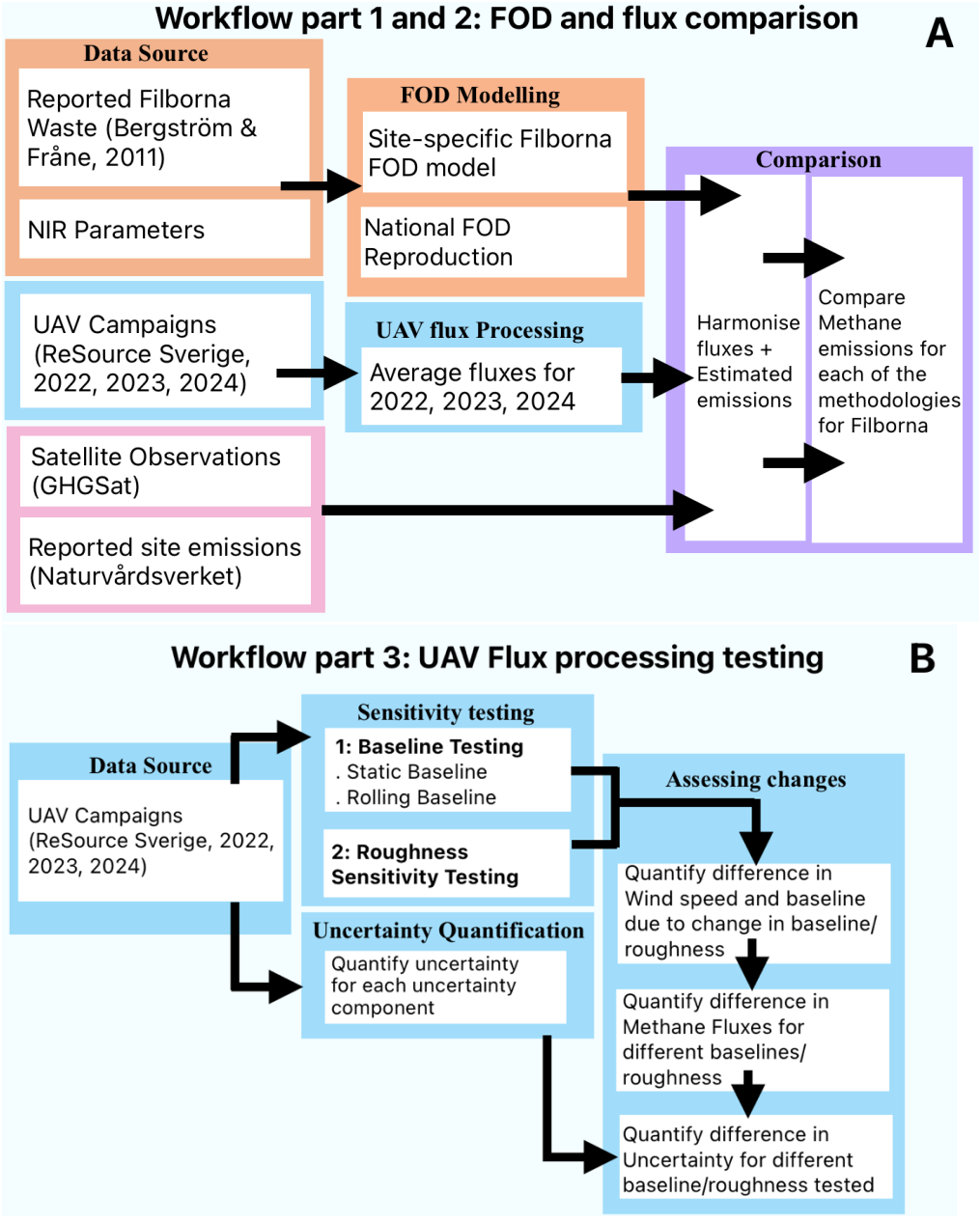

Fig. 11: Workflow part 1,2 (A) and part 3 (B). Colours used to differentiate between data sources with orange indicating the FOD-data, blue the UAV-derived data, and pink the other measured data. The purple block displays the comparison of all CH_4 values.

4.2: FOD modelling approach

4.2.1: National model reproduction

Swedish landfill CH_4 emissions are quantified using the IPCC Tier 2 FOD model, as implemented in the NIR 2024 submitted to the UNFCCC by Naturvårdsverket. The FOD model estimates annual CH_4 generation from deposited waste using IPCC FOD structure with national activity data and Swedish inventory parameters. CH_4 emissions are calculated using the following equation:

$$CH_4 Emissions = \left[\sum_x CH_4 generated_{x,T} - R_T\right] * (1 - OX_T) \quad (1)$$

where $CH_4 Emissions$ is the amount of CH_4 emitted in year T (Gg), T is inventory year, x is waste category, R_T is recovered CH_4 in year T (Gg) and OX_T is the oxidation factor in year T.

To calculate the CH_4 generated, national waste disposal data is used to calculate the decomposable DOC using the following equation:

$$DDOCm = W * DOC * DOC_f * MCF \quad (2)$$

where $DDOCm$ is the mass of decomposable DOC deposited (Gg), W is the mass of waste deposited (Gg), DOC is a fraction or Gg C per Gg waste, DOC_f is the fraction of DOC that can decompose and MCF is the CH_4 correction factor for aerobic decomposition in the year of deposition.

The total accumulated $DDOCm$ ($DDOCma_T$) and the total decomposed $DDOCm$ ($DDDOCm\ decomp_T$) are calculated for the end of year T as following:

$$DDOCma_T = DDOCmd_T + (DDOCma_{T-1} * e^{-k}) \quad (3)$$

$$DDOCm\ decomp_T = DDOCma_{T-1} * (1 - e^{-k}) \quad (4)$$

where $DDOCma_T$ is the $DDOCm$ accumulated in the SWDS at the end of year T (Gg), $DDOCma_{T-1}$ is the $DDOCm$ accumulated in the SWDS at the end of year *(T-1)* (Gg), $DDOCmd_T$ is the $DDOCm$ deposited in the SWDS in year T (Gg), $DDOCm\ decomp_T$ is the $DDOCm$ deposited in the SWDS in year (Gg) and k is the reaction constant.

Lastly, the CH_4 formed from decomposable material is calculated by multiplying the CH_4 fraction in generated landfill gas and the CH_4 /C molecular weight ratio.

$$CH_4 generated_T = DDOCm\ decomp_T * F * 16/12 \quad (5)$$

where $CH_4 generated_T$ is the amount of CH_4 generated from decomposable material, F is the fraction of the CH_4 by volume in generated landfill gas and 16/12 is the molecular weight ratio CH_4/C.

Model parameters (k, OX, and MCF) were taken directly from the NIR 2024 alongside the (rounded) waste statistics. In this study, uncertainty in the national FOD model was estimated using a Monte Carlo approach with 10,000 simulations. Key model parameters were sampled from uncertainty ranges based on IPCC guidance, including DOCf, CH_4 fraction, decay rate, CH_4 correction factor, oxidation, recovery, and activity data (Appendix Table A2). For each year, the 2.5th and 97.5th percentiles of the simulated emission estimates were used to define the 95% uncertainty interval. The FOD model is independently implemented in Python to reproduce reported national emission estimates.

4.2.2: Site-Specific FOD Model for Filborna

A site-specific FOD model is constructed for Filborna landfill by applying national parameters to site-specific waste deposition data (1951–2024) This approach assumes identical FOD parameters to those used in the national inventory (Table 4), except for DOCf, which has a site-specific value of 0.54, as described in chapter 3.3. For flux calculations, emissions are averaged temporally and spatially across the reported landfilling area of approx. 32 ha.

Similar to the reconstructed national model, uncertainty in the Filborna model was estimated using a Monte Carlo simulation with 10,000 simulations. For each iteration, annual CH_4 emissions were recalculated using the sampled parameter set. This produced a distribution of modelled emissions for each year. The 2.5th and 97.5th percentiles were used as the 95% uncertainty interval, while the median represented the Monte Carlo central estimate. Key model parameters were sampled from uncertainty ranges based on IPCC guidance.

Table 4: Data and Parameters used for reproduction Filborna FOD model (Full table with sources for each value/assumption in Appendix Table A3).

Parameter	Value / Assumption
CH_4 observations (2001-2006)	Surface flux study scaled to $CH_4 yr^{-1}$
CH_4 observations (2007-2024)	Annual site-scale CH_4 measurements
DOCf values	0.50 for national reconstruction. 0.54 for Filborna
F (CH_4 fraction)	0.5 (default NIR)
Oxidation factor (OX)	0.1 (default NIR)
Half-life ($t_{1/2}$)	7.5 y (default NIR)
Mehane correction factor (MCF)	0.6 before 1980; 1.0 after (default NIR)
Site-specific waste input	Annual deposited waste by category (1951-2009)
DOC conversion	Category-specific DOC fractions
Post-2009 DOC input	Mean 2000-2008 DOC input scaled to match waste inputs for 2022-2024 from Avfall Sverige

4.3: Comparison of methane emission estimates

4.3.1: UAV Processing workflow

The UAV CH_4 processing workflow provided by ReSource Sverige was evaluated to assess how methodological choices influence the derived emission estimates. The workflow converts UAV-based CH_4 and meteorological measurements into site-level CH_4 flux estimates through a series of processing steps, including data filtering, wind processing, background correction, spatial interpolation, and flux calculation. The processed CH_4 enhancement data were used to reconstruct the plume measurement plane and estimate total CH_4 flux using a mass balance approach. The resulting estimates represent landfill-scale emissions for individual flights under the meteorological and operational conditions at the time of measurement.

4.3.2: Comparing estimated emissions

To ensure comparability, UAV surface fluxes are annualised and all estimates are expressed in kg CH_4 yr^{-1}. FOD estimates total generated CH_4 (minus recovery and oxidation assumptions). UAV measurements quantify surface (primarily fugitive) emissions. Satellite data detect plume-based enhancements. Comparisons therefore evaluate magnitude and consistency rather than assuming direct methodological equivalence.

4.4: UAV processing workflow analysis

4.4.1: Uncertainty quantification

The uncertainty of the CH_4 flux estimates was quantified by propagating five main sources of uncertainty: wind speed, wind direction, kriging interpolation, sensor precision, and baseline estimation (Eq. 6). The aim of the uncertainty analysis was to express each component on a common scale before combining them into a total uncertainty estimate. Therefore, all uncertainty terms were first converted to absolute flux-equivalent uncertainty in kg CH_4 h^{-1}. The absolute components were then combined using a root-sum-of-squares (RSS) approach, assuming that the individual uncertainty sources were independent.

$$U_{\text{total}} = \sqrt{U^2_{\text{wind speed}} + U^2_{\text{wind direction}} + U^2_{\text{kriging}} + U^2_{\text{measurement}} + U^2_{\text{background}}} \tag{6}$$

where U_{total} is the total absolute uncertainty in kg CH_4 h^{-1}.

The total relative uncertainty was then calculated by normalising the total absolute uncertainty by the final CH_4 flux estimate:

$$u_{\text{rel,total}} = \frac{U_{\text{total}}}{|F_{CH_4}|} \tag{7}$$

where F_{CH_4} is the final estimated CH_4 flux in kg CH_4 h^{-1}.

This approach avoided combining relative and absolute uncertainty terms directly and ensured that each uncertainty component contributed consistently to the final uncertainty budget. It also allowed the relative importance of each source of uncertainty to be compared across flights.

4.4.1.2: Wind speed uncertainty

Wind speed uncertainty was estimated based on the variability of the wind speed time series during each flight. The relative uncertainty of the mean wind speed was calculated from the standard error of the mean. Because consecutive wind measurements are not fully independent, the standard error was adjusted using an effective sample size based on the lag-1 autocorrelation of the wind-speed series as following:

$$n_{\text{eff}} = n\frac{1 - r_1}{1 + r_1} \tag{8}$$

where n_{eff} is the effective sample size, n is the number of observations, and r_1 is the lag-1 autocorrelation-coefficient.

The effective sample size was constrained to avoid unrealistic values and was used to calculate an autocorrelation-adjusted standard error. A Student's t-factor was then applied to obtain a 95% uncertainty estimate. The resulting relative wind-speed uncertainty was converted to an absolute flux uncertainty by multiplying it by the absolute value of the final CH_4 flux:

$$U_{\text{wind speed}} = |F_{\text{CH}_4}| \cdot u_{\text{wind speed}} \tag{9}$$

4.4.1.3: Wind direction uncertainty

Because the CH_4 flux estimate depends on the projected wind component, uncertainty in wind direction directly affects the flux. The wind direction was therefore changed in both directions using the variability in wind direction. The change in the wind component was used to calculate a relative wind direction uncertainty, which was converted to an absolute uncertainty by multiplying it by the final CH_4 flux estimate.

4.4.1.4: Kriging uncertainty

Kriging uncertainty was included as an absolute uncertainty term derived from the interpolated flux surface. In the processing workflow, the kriging uncertainty term represents the uncertainty associated with the spatial interpolation of the CH_4 enhancement across the flux plane. This term was therefore treated directly as an absolute uncertainty in kg CH_4 h^{-1} and included in the RSS calculation without conversion.

4.4.1.5: Measurement uncertainty

Measurement uncertainty represents the uncertainty caused by the precision of the sensor. The sensor precision is given as a CH_4 concentration uncertainty in ppm, but the final flux is reported in kg CH_4 h^{-1}. Therefore, the concentration uncertainty first had to be converted.

The ppm uncertainty was converted into a CH_4 density uncertainty using the local molar volume and the molar mass of CH_4. The density uncertainty was then multiplied by the representative projected wind speed, which describes the wind component crossing the flight plane. Finally, this was multiplied by the active kriged area, defined as the part of the

interpolation grid where valid flux values were present. This produced an absolute measurement uncertainty in kg CH_4 h^{-1}.

4.4.1.6: Baseline uncertainty

Baseline uncertainty represents the uncertainty in the estimated background CH_4 concentration. Since CH_4 flux is calculated from the enhancement above background, uncertainty in the baseline directly affects the final flux estimate. The baseline uncertainty was based on the 95% confidence interval of the estimated background concentration. As with measurement uncertainty, this concentration uncertainty was first converted from ppm to a CH_4 density uncertainty. It was then converted into a flux-equivalent uncertainty by multiplying it by the representative projected wind speed and the active kriged area. The resulting value represents the absolute uncertainty.

4.4.1.7: Total uncertainty

Fig. 12 summarises the conversion of each uncertainty component to absolute uncertainty used for the RSS. The final output of the uncertainty routine was an upper and lower flux bound:

$$F_{\text{upper}} = F_{\text{CH}_4} + U_{\text{total}}$$
$$F_{\text{lower}} = F_{\text{CH}_4} - U_{\text{total}} \quad (10)$$

Additionally, the relative contribution of each uncertainty component was reported to identify the dominant sources of uncertainty for each flight.

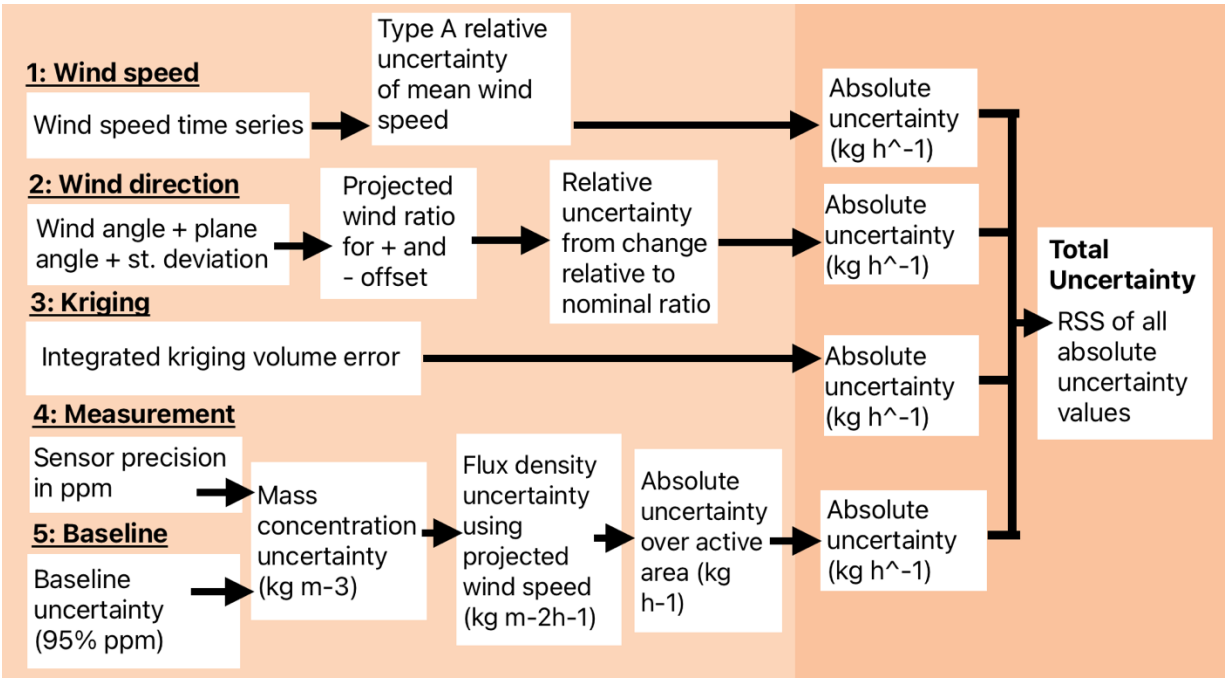

Fig. 12: Step-by-step calculation of absolute uncertainty for each component and propagation to total uncertainty.

4.4.2: Sensitivity testing

To assess the robustness of the emission estimates and identify key sources of methodological uncertainty, a targeted sensitivity analysis of selected processing parameters was conducted.

Sensitivity testing focuses on parameters that are both uncertain and expected to have a strong influence on the calculated CH_4 flux. Alternative processing configurations were implemented in Python to test sensitivity to:

i) Surface roughness (z_0),
ii) Change in methodology CH_4 baseline calculation

Surface roughness influences the representation of atmospheric turbulence and wind transport in the flux calculation, while baseline estimation directly affects the CH_4 concentration enhancement used to derive emissions. Both parameters therefore represent important methodological assumptions within the UAV-based emission estimation workflow. For each configuration: CH_4 flux was calculated, sensitivity relative to the baseline workflow was quantified and uncertainty with new parameters was estimated

4.4.2.2: Surface roughness (z_0)

In the original processing pipeline, Z_0 was estimated directly based on the mean wind speeds at the upper and lower mast heights. For the Z_0 sensitivity test, Z_0 was not recalculated from the anemometer data. Instead, a set of assumed aerodynamic roughness lengths was imposed, and the resulting changes in wind-speed scaling and CH_4 flux were evaluated. Z_0 ranges for landfills are normally between 0.3 m and 0.5 m (Brovkina et al., 2026; Dörenkämper et al., 2020). For the sensitivity testing, a wider range of values is tested (0.002 m – 0.8 m). Higher Z_0 values represent rougher surfaces and stronger near-surface drag, this changes the estimated wind speed at plume height and therefore changes the calculated CH_4 flux.

4.4.2.3: Baseline estimation

Two approaches were used to estimate background CH_4 concentrations: the original baseline method and an alternative time-varying baseline method. For each approach, CH_4 enhancement was calculated by subtracting the estimated background concentration from the observed CH_4 concentration.

The complete flux and uncertainty workflow was then repeated for both baseline approaches. The resulting emission estimates were compared to evaluate the sensitivity of the UAV-derived CH_4 fluxes to baseline estimation.

5 Results

5.1: Reproduction of the FOD model

The implemented IPCC Tier 2 FOD model reproduced national landfill CH_4 emissions reported in the NIR for the period 1952–2022 (Fig. 13). Modelled emissions increased steadily from the 1950s, reflecting rising waste deposition, and reached a maximum in the late 1980s. Peak modelled emissions occurred in 1989, with a value of 145.5 kt CH_4 yr^{-1}. Thereafter, emissions declined consistently, corresponding to reduced landfilling of DOC and increased CH_4 recovery. By 2022, emissions had decreased to 21.8 kt CH_4 yr^{-1}.

Comparison with officially reported inventory values for 1990–2022 shows agreement between the independently implemented model and the NIR estimates (Appendix Fig. A3). The mean absolute percentage difference over this period was 5.8%, with the largest deviation (21.32%) occurring in 2022. The root mean square error (RMSE) was 3.68kt CH_4 yr^{-1}, and the mean bias (model - official) was 3.52 kt CH_4 yr^{-1}.

The official inventory values consistently fall within the modelled 95% uncertainty envelope, indicating that the parameterisation and implementation of the FOD model are consistent with the national methodology.

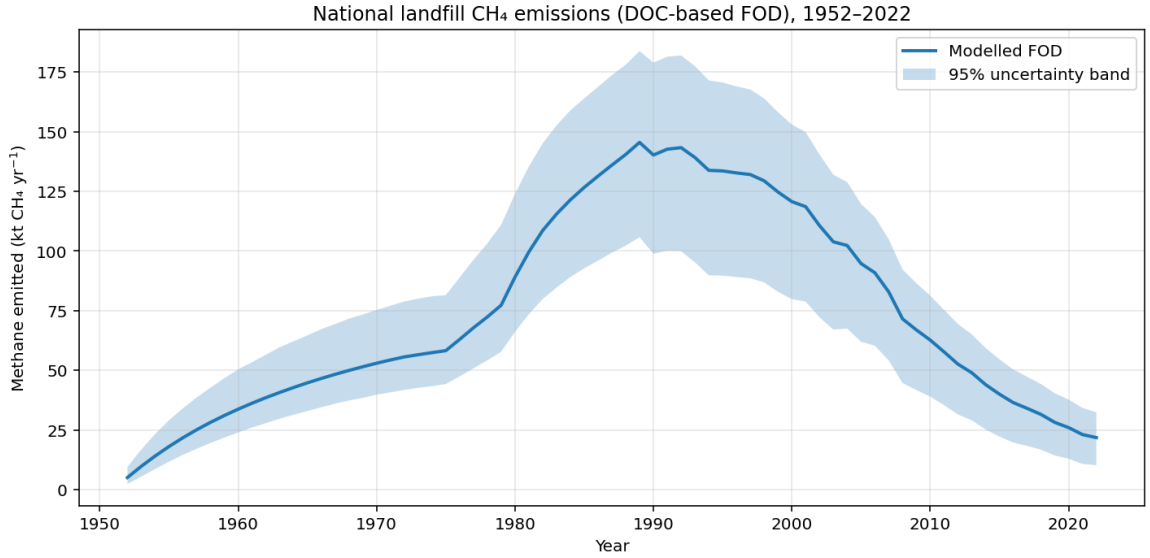

Fig. 13: National landfill CH_4 emissions (1951–2022) calculated using the IPCC Tier 2 FOD model and parameters from the Swedish National Inventory Report (NIR 2024). The blue line shows the modelled FOD and the light blue area represents propagated model uncertainty.

5.2: Site-specific FOD for Filborna

Fig. 14 shows the site-specific FOD model for Filborna, constructed using site-specific activity data and national model parameters. The model shows a similar temporal pattern to the national FOD model, with emissions increasing until a peak in the early 1990s, followed by a steady decline. According to the FOD model, emissions peaked in 1991 at 5805.5 t CH_4 yr^{-1}, equivalent to an annual-average emission rate of 662.7 kg CH_4 h^{-1}. By 2024, emissions had declined to 753.2 t CH_4 yr^{-1}, equivalent to an annual-average emission rate of 85.98 kg CH_4 h^{-1}. If the emissions were evenly distributed across the full 32 ha landfill area, the

corresponding whole-site average surface fluxes would be 2071 mg CH_4 m^{-2} h^{-1} in 1991 and 268.70 mg CH_4 m^{-2} h^{-1} in 2024.

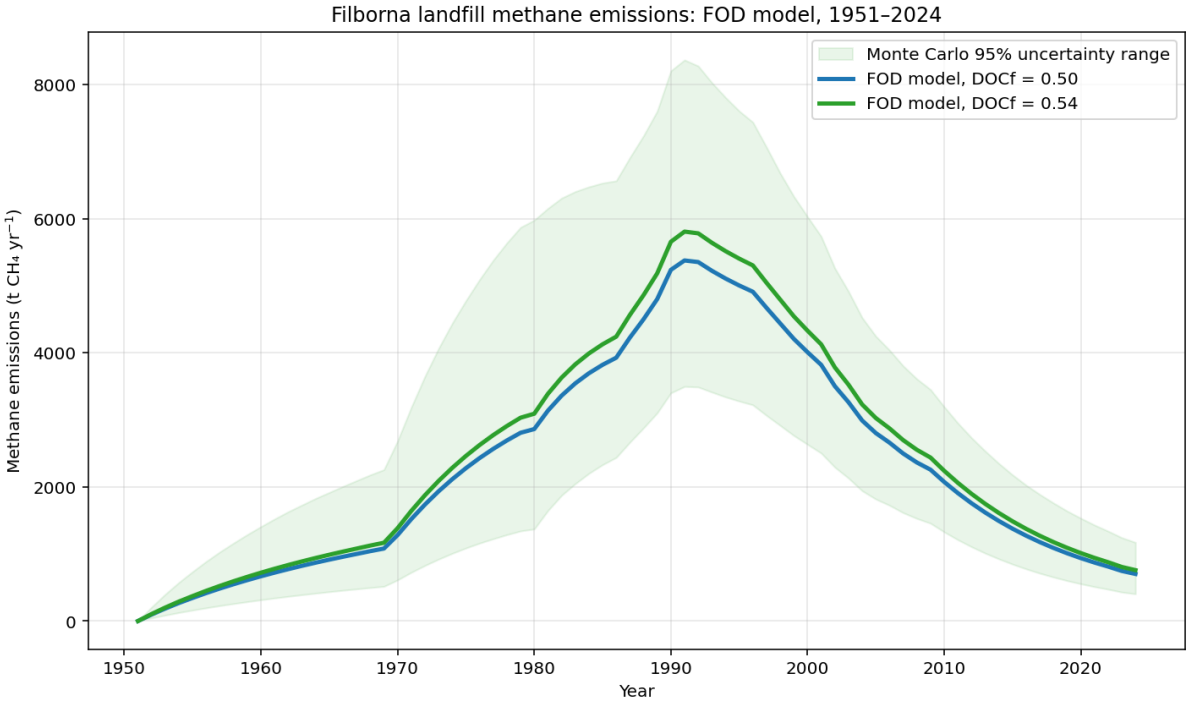

Fig. 14: FOD Model for Filborna Waste Facility 1951-2024 with the 95% uncertainty range (light green) around the FOD-model line with 0.54 DOCf (green), the blue line uses the national DOCf value 0.50 for comparison.

5.3: Comparison of methane estimation methods at Filborna

5.3.1: Site-reported annual emissions submitted to Naturvårdsverket.

Observed emissions (2001–2024) show lower values than the peak emissions predicted by the FOD model and generally decline from the early 2000s until approx. 2016, followed by moderate interannual variability and a slight increase in 2023–2024 (Fig. 16).

5.3.2: Satellite-derived CH_4 observations

Weekly GHGSat observations did not report quantifiable CH_4 emissions from the site during the study period.

5.3.3: UAV observations of fluxes

Fig. 15 shows the kriging estimates of the CH_4 flux planes for the first UAV flight in 2022 (A), 2023 (B), and 2024 (C). The plots provide a visual representation of the interpolated CH_4 flux distribution across the vertical measurement plane used in the mass balance calculation. For all three years, the flux is spatially heterogeneous and concentrated in localised plume structures rather than being evenly distributed across the full cross-section. In 2022, elevated fluxes are mainly located near the centre of the flux plane, with smaller plume features distributed across the transect. In 2023, the plume appears more spatially extensive, with several areas of enhanced flux across the middle and right-hand side of the plane. In 2025, the strongest enhancement is more localized, with a peak around the central part of the transect and

additional elevated areas toward the right side of the plane. The kriged flux planes are used as an intermediate step in the mass balance calculation, where the spatially resolved flux distribution is integrated to obtain a landfill-scale emission estimate for each flight.

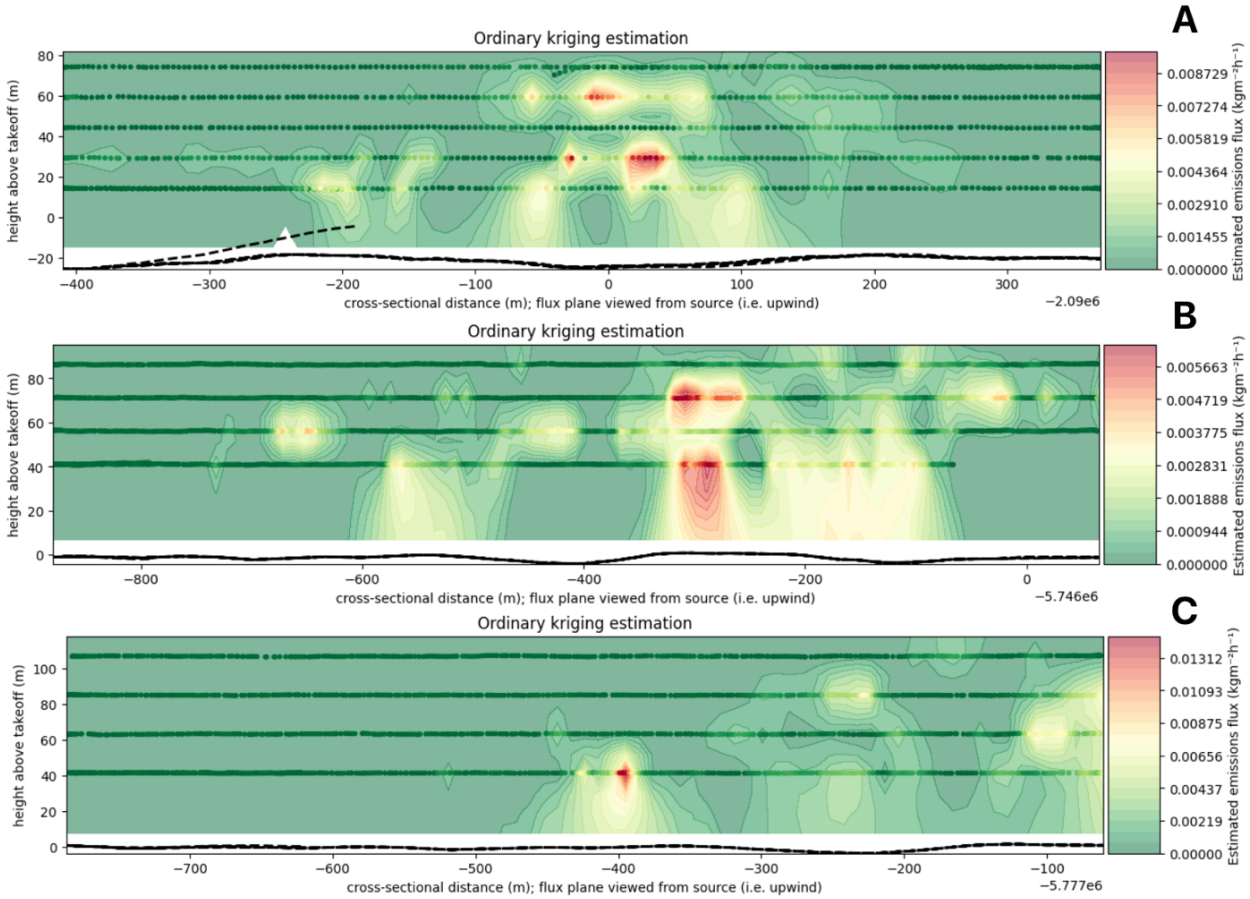

Fig. 15: Kriging estimates of the CH_4 flux plane for the first UAV flight in 2022, 2023, and 2024. Panels A B and C show the interpolated methane flux distribution across the vertical measurement plane for 2022, 2023, and 2024, respectively. Dark green points indicate the UAV measurement locations, while the colour scale represents the estimated CH_4 flux.

5.3.4: Comparing emissions

Modelled emissions generally exceed the interpolated, observed emissions across the entire measurement period (2001–2024) (Fig. 16). The largest discrepancies occur between 2008 and 2016, where observed emissions are lower than predicted by the FOD model. in recent years (2019–2024), modelled and observed emissions converge.

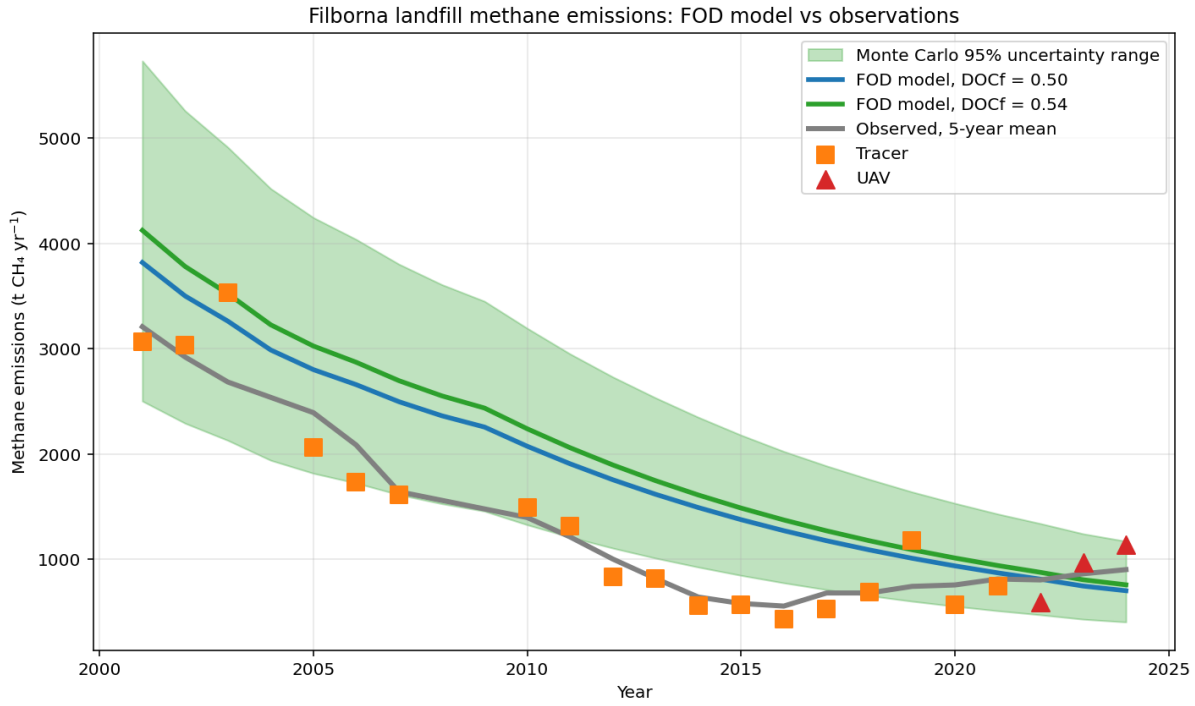

Fig. 16: Comparison observed CH_4 emissions and modelled CH_4 emissions for Filborna 2001 – 2024. The blue line represents the baseline FOD model estimate (DOCf 0.5) and the green line shows the FOD with DOCf 0.54. The shaded envelope is ±95% uncertainty around the green line. Observations are shown as individual measurements categorised by method (tracer: orange, and UAV: red), together with a 5-year moving mean for all (tracer and UAV) observations (grey line).

5.4: Evaluation and modification of UAV CH_4 flux processing workflows.

5.4.1: Uncertainty Propagation

The uncertainty values reported represent the propagated uncertainty of the UAV flux estimate based on the uncertainty sources explicitly included in the calculation. They describe how sensitive the calculated flux is to uncertainty in wind speed, wind direction, background concentration, sensor precision, and kriging interpolation.

5.4.1.1: 2022 uncertainty

Table 5 shows the results of the analysis of Flight 1 from 2022, 2023 and 2024 for comparison between the years. For all other flights, see Appendix Table A4 (2024), A5 (2023) and A6 (2022).

Flights 1-5 from 2022 had a relative uncertainty ranging between 23.9% and 29.8%. Most uncertainty came from the wind direction (22.9% - 26.9%). Following wind direction, uncertainty was due to wind speed (4.9% - 11.6%) and background (4.7% - 12.4%). Measurement and kriging remained low for all 2022 flights as well, with ranges between 1.3% - 2.6% and 0.01% - <0.01% respectively.

Table 5: Propagated uncertainty budget for Flight 1 for 2022, 2023 and 2024, showing the absolute uncertainty contribution of each source (kg h^{-1}) and its relative uncertainty contribution (%) to the estimated flux total. For all flights see Appendix Table A4, A5, A6. The percentages in brackets represent each uncertainty component expressed relative to the estimated flight emission, these percentages do not sum to the total relative uncertainty. Absolute values rounded to 2 decimals; percentages rounded to 1 decimal except for kriging (2 decimals) due to its small uncertainty values.

Absolute and Relative uncertainty for each source						
Flight	**Wind Speed**	**Wind direction**	**Kriging**	**Measurement**	**Background**	**Uncertainty total**
Flight 1 -2022	6.55 kg h^{-1} (11.6%)	13.73 kg h^{-1} (24.2%)	0.01 kg h^{-1} (0.01%)	0.73 kg h^{-1} (1.3%)	3.87 kg h^{-1} (6.8%)	15.71 kg h^{-1} (27.7%)
Flight 1 - 2023	5.71kg h^{-1} (6.8%)	26.81 kg h^{-1} (32.0%)	0.01 kg h^{-1} (0.01%)	1.22 kg h^{-1} (1.5%)	6.55 kg h^{-1} (7.8%)	28.21 kg h^{-1} (33.6%)
Flight 1 - 2024	8.17 kg h^{-1} (9.2%)	57.79 kg h^{-1} (65.2%)	0.00 kg h^{-11} (0.01%)	2.03 kg h^{-1} (2.3%)	11.64 kg h^{-1} (13.1%)	59.54 kg h^{-1} (67.1%)

5.4.1.2: 2023 uncertainty

For all flights from 2023, relative uncertainty ranged between 17.7% and 33.6%. Similarly to the 2022 uncertainty, most uncertainty is due to the wind direction, ranging between 11.8% and 32%. Following wind direction, background uncertainty ranged between 7.2% and 16.1% and wind speed uncertainty between 4.1% and 18.5%. Measurement uncertainty ranged between 1.1% and 2.4% for all flights an uncertainty for kriging was near-zero for all flights.

5.4.1.3: 2024 uncertainty analysis

The 2024 analysis shows that total uncertainty in the CH_4 flux estimates was dominated by wind direction across all analysed flights, with relative contributions ranging from 44.2% to 73.7%. Wind speed and background contributed similarly, between 3.1% and 9.2% for wind speed and 5% - 13.1% for background uncertainty. Sensor precision and kriging interpolation contributed marginally to the uncertainty budget.

5.4.2: Surface roughness

A sensitivity analysis was performed to evaluate how the assumed surface roughness length (z_0) influences wind scaling and the resulting CH_4 flux estimates. The projected wind speed used in the flux calculation increases with increasing roughness length due to the logarithmic wind profile applied to extrapolate wind measurements between mast heights and flight altitude (Fig. 17, left). Consequently, the estimated CH_4 flux also increases with increasing z_0 (Fig. 17, right).

For the sensitivity analysis, z_0 values between 0.02 and 0.8 m were tested, representing surfaces from short vegetation to forested terrain. For Flight 1 from 2024 shown in Figure 16, the estimated flux increased by approx. 31% from z_0 0.02 m to z_0 0.8 m. This demonstrates that the emission estimate is sensitive to assumptions about surface roughness. Other 2024 flights show a similar sensitivity to surface roughness, with an overall average flux variation of 28 kg CH_4 h^{-1} between z_0 0.02 m and z_0 0.8 m. Flights with higher fluxes show greater sensitivity to surface roughness assumptions than flights with lower fluxes. Appendix Table A7 shows the full sensitivity analysis output for all flights in 2024.

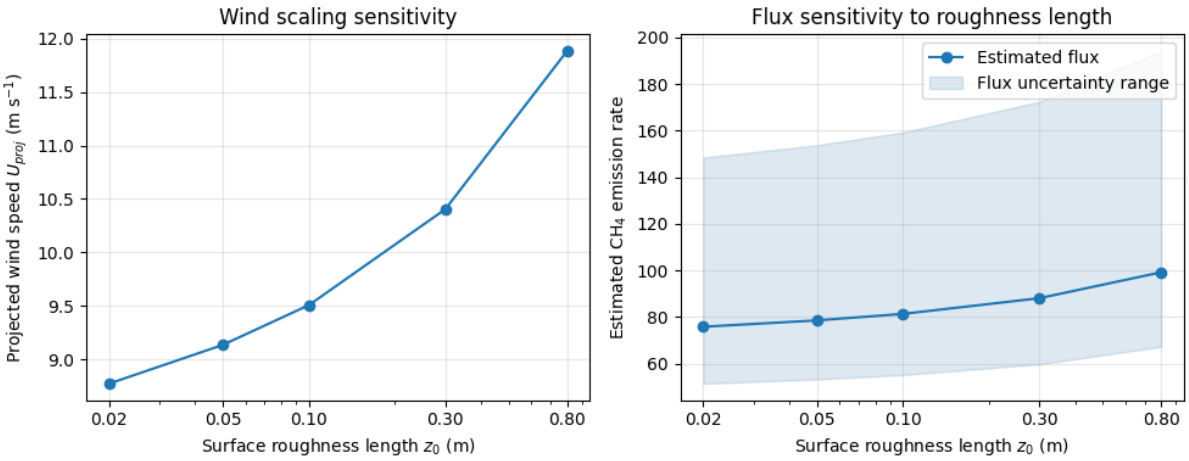

Fig. 17: Sensitivity of projected wind speed and CH₄ flux estimate to surface roughness length (z_0) for data from Filborna Flight 1 from 2024.
Left: Projected wind speed (U_{proj}) used in the flux calculation as a function of assumed aerodynamic surface roughness length. The projected wind speed (blue line) increases with increasing roughness due to the logarithmic wind profile used to scale wind measurements between the two mast heights and the flight altitude.
Right: The shaded region indicates the propagated flux uncertainty. Increasing z_0 leads to higher estimated fluxes (blue line) because the emission estimate scales approx. linearly with the projected wind speed.

5.4.3: Baseline estimation change

The static estimated background CH₄ concentration for Flight 3 from 2024 was approx. 2.002 ppm (Fig. 18).

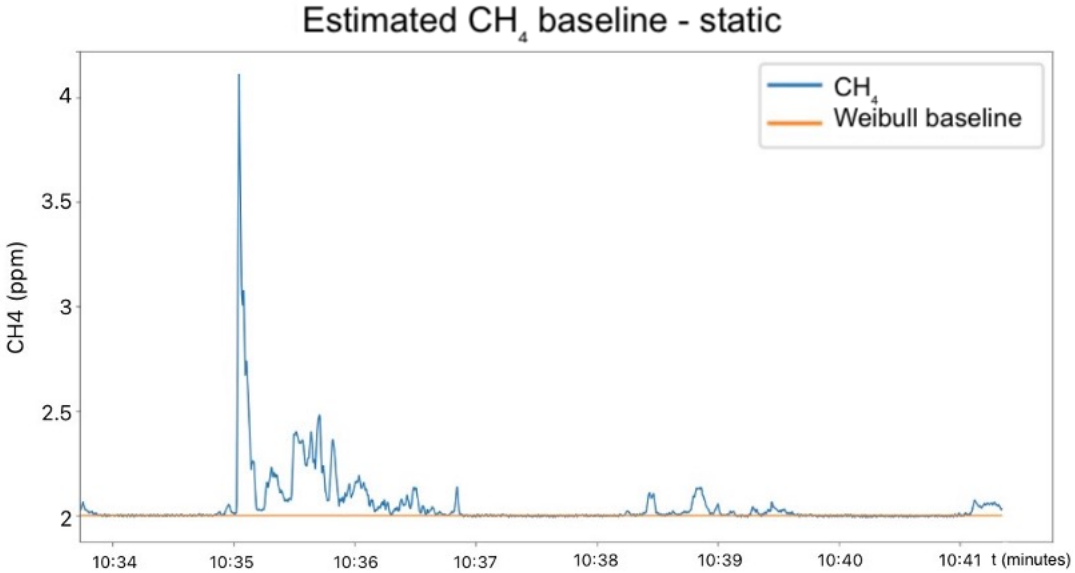

Fig. 18: Estimated CH₄ baseline using a static approach for Flight 3, 2024. The blue line shows the CH₄ plume and the orange line shows the estimated background concentration (baseline).

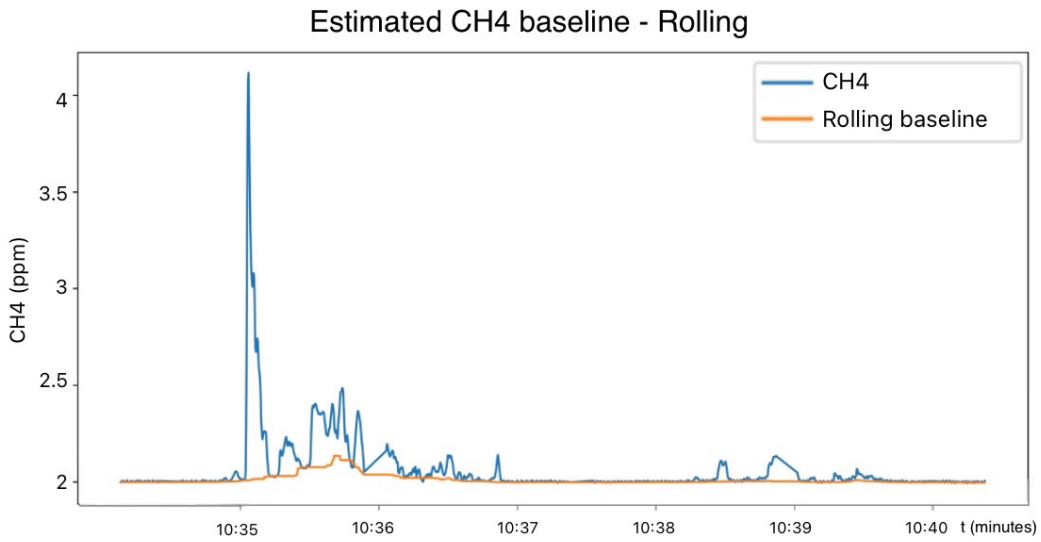

Fig. 19: Estimated CH_4 baseline using the Rolling approach for Flight 3, 2024. The blue line shows the CH_4 plume and the orange line shows the estimated background concentration (Rolling baseline).

Replacing the static baseline with a rolling baseline reduced the estimated emission volume from 172.6 kg h^{-1} to 143.3 kg h^{-1}. Fig. 19 shows that the CH_4 background signal sits near ~2.0 ppm for the duration of the flight, followed by a strong plume episode lasting roughly between 10:35 – 10:37, with one sharp peak above 4 ppm and a broader elevated period around 2.1–2.4 ppm. As seen in Fig. 19, the rolling baseline remains relatively stable, like the static baseline in Fig. 18. However, the rolling baseline shows a slight increase along the CH_4 plume around 10:35 – 10:36. The rolling method amounted to a slightly higher average background concentration of CH_4 (~2.1 ppm), resulting in a lower CH_4 enhancement and a lower estimated emission volume.

The uncertainty for background CH_4 estimation went down from 6.0% to 2.3% when using the rolling baseline instead of the static baseline (Fig. 20). The CH_4 plume's total relative uncertainty, however, remained nearly unchanged at 54.6% and 54.4% for the static and rolling baseline approach respectively. Baseline methodology had a substantial effect on the derived flux estimate, but only a limited effect on the overall propagated uncertainty,
which in both cases remained dominated by wind direction uncertainty.

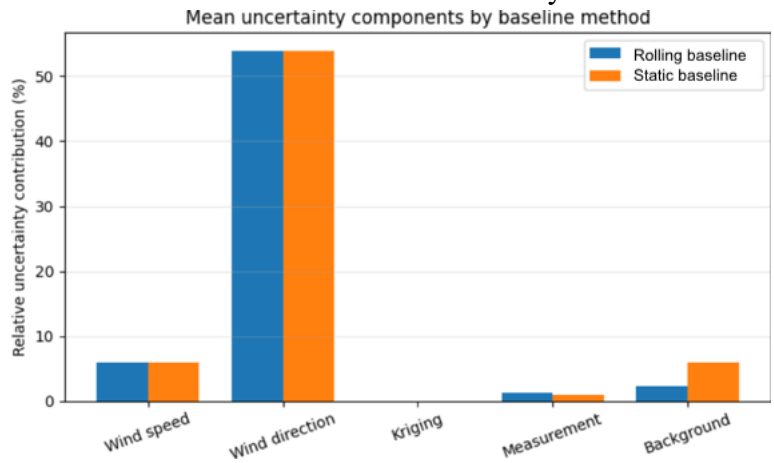

Fig. 20: Relative contribution of each uncertainty component to the total uncertainty for rolling and static baseline estimation approaches for Flight 3 from 2024. The orange columns show the static baseline uncertainty per component; the blue columns show the rolling baseline uncertainty per component.

Flight 3 from 2022 and Flight 1 from 2023 share similar patterns to Flight 3 from 2024 when changing the baseline methodology (Fig. 22), with a rolling baseline following strong plume signals. For Flight 1 in 2023, the CH_4 background concentration was estimated to be 2.0203 ppm, with a total emission flux of 83.9 kg CH_4 h^{-1}. Using the rolling background method shows a lower emission rate, with a total flux of 65.5 kg CH_4 h^{-1}. For Flight 3 in 2022, the static background method estimated an implied CH_4 background concentration of 2.0087 ppm and a total emission rate of 71.4 kg CH_4 h^{-1}. As observed for the 2024 and 2023 flights, the rolling background method produced a slightly lower CH_4 flux estimate, decreasing the emission rate to 69.7 kg CH_4 h^{-1}.

Similarly to 2024, 2022 and 2023 show that the relative uncertainty of background CH_4 estimation decreases when the rolling baseline approach is used instead of the static baseline-derived estimation (Appendix Fig. A4, A5). For Flight 3 from 2022, the relative contribution of background uncertainty to total uncertainty decreased from 4.7% to 1.3%. For Flight 1 2023, the relative contribution decreased from 7.8% to 3.7%. Total estimated uncertainty changed minimally for both Flight 3 from 2022 and Flight 1 from 2023, with 23.9% to 23.5% for 2022 and 33.6 % to 32.9% for 2023. Wind direction remained the main contributor to uncertainty. Other flights for 2022, 2023 and 2024 yielded similar results and are available in Appendix Table A8.

5.4.4: Comparison changes in Z_0 and Baseline approach

Change in baseline estimation and z_0 values did not affect each other and CH_4 emissions rose with an increase of z_0 at the same rate for either baseline estimation approaches (Fig. 21). The highest estimated emission rate of CH_4 for Flight 1 from 2024 was 96.74 kg CH_4 h^{-1}, using the static baseline and the highest tested z_0 (0.8). The emission rate was 57.60 kg CH_4 h^{-1}, for the lowest tested z_0 (0.02) in combination with the rolling baseline.

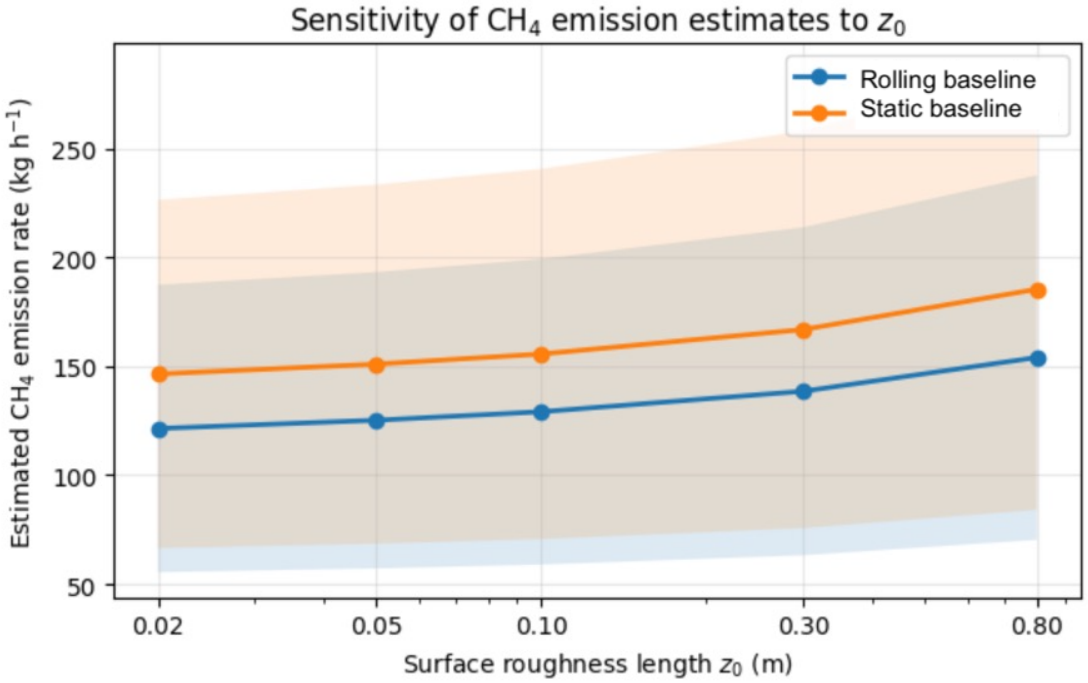

Fig. 21: CH_4 volume for all tested Z_0 and the 2 baseline approaches. Including the estimated uncertainty envelope for both static (orange) and rolling. (blue) baseline. Flight 1, transect C, 2024.

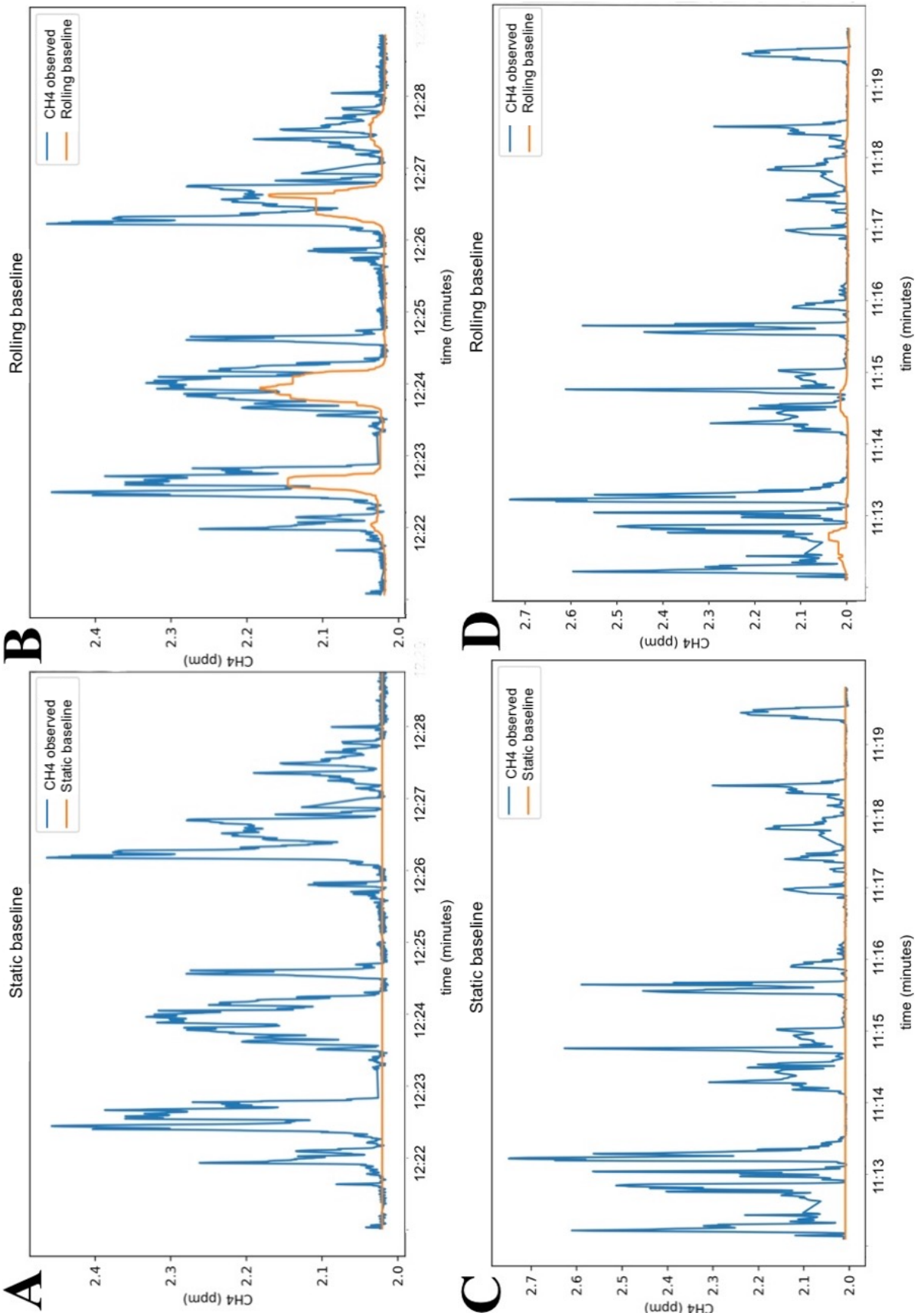

*Fig. 22: **A**: static baseline Flight 1, Transect C, 2023 **B**: rolling baseline Flight 1, Transect C, 2023 **C**: static baseline Flight 3, Transect W, 2022. **D**: rolling baseline Flight 3, Transect W, 2022. Orange lines indicate the estimated CH_4 baseline, while blue lines show the observed CH_4 concentration signal, including plume enhancements.*

6 Discussion

This study evaluated whether UAV-based CH_4 measurements can provide additional insight into landfill CH_4 emissions and their representation within Sweden's national GHG inventory. By reproducing the national FOD model, developing a site-specific model for the Filborna landfill, comparing these estimates with observational data from UAV and satellite measurements, and assessing uncertainties, the results provide insight into the strengths and limitations of current inventory approaches and emerging measurement technologies.

6.1 Reliability of the national landfill CH_4 inventory methodology

6.1.1: Comparison of the reproduced FOD Model with the NIR

The independently implemented IPCC Tier 2 FOD model reproduced national landfill CH_4 emissions reported in the NIR with high agreement. Modelled emissions closely followed the reported inventory time series for the period 1990–2022, with a mean absolute percentage difference of 5.8%. The difference between the reconstructed and official model is likely caused by the waste activity data used: the reconstructed model used rounded values from the NIR tables rather than the raw activity data used in the official inventory. The official inventory values consistently fell within the modelled 95% uncertainty interval. This indicates that the implemented model accurately represents the methodological framework used in the Swedish inventory and confirms that the implementation of the FOD model in this study are consistent with the national methodology.

6.1.2: Assessment of the Swedish Inventory Methodology

Although the reproduced model shows strong agreement with the national inventory, several limitations of the FOD approach must be considered when interpreting CH_4 emissions.

First, the FOD framework estimates CH_4 generation from decomposing waste rather than directly measured surface emissions. As a result, the model relies on assumptions regarding CH_4 oxidation in landfill covers, gas recovery efficiency, and the fraction of generated CH_4 that escapes to the atmosphere. The FOD model also uses nationally averaged parameters: these parameters are determined for national-scale inventory calculations, but they may not accurately represent individual landfill characteristics (Amini et al., 2013). Individual landfills can differ in waste composition and age, moisture and temperature and gas collection. Therefore, applying these parameters at a site-specific scale may result in biased emission estimates, particularly for landfills with atypical waste composition, cover systems, or gas management practices (Maliehe et al., 2026).

The model also relies on historical landfill activity data extending back to the 1950s. Over this period, definitions of municipal solid waste, household waste, and landfilling practices have evolved, potentially introducing inconsistencies in reported waste quantities. This limitation is supported by Maliehe et al. (2026), who note that possible misreporting in activity data is one

reason to be cautious when interpreting bottom-up CH_4 estimates. Furthermore, site-specific historical waste composition data are often incomplete or aggregated, which limits the accuracy of downscaled FOD estimates.

This is also a limitation in the case of Filborna. Although Filborna-specific activity data were used, most model parameters were based on national or default assumptions; only the waste composition and DOCf value were adjusted to better represent the site. As a result, the model may not fully capture Filborna-specific conditions. Mou et al. (2015) found that default IPCC parameter values overestimated CH_4 generation and emissions for four Danish landfills when compared with TDM measurements. However, they also showed that using site-specific parameters produced results that were more comparable to the measurements. For Filborna, the use of the site-specific adjusted DOCf value therefore likely improved the FOD model, but further site-specific information on gas recovery, oxidation, moisture conditions, cover type, and operational history would likely improve its accuracy further.

6.2 Comparison between modelled and observed emissions at Filborna

Differences between modelled and observed CH_4 emissions, both TDM measurements before 2022 and the UAV measurements for 2022, 2023, and 2024 at Filborna, partly reflect the different processes represented by the two approaches. The FOD model estimates annual CH_4 emissions from historical waste deposition and assumed decay dynamics, whereas in-situ measurements quantify atmospheric emissions during specific monitoring periods. These measurements therefore represent snapshots of emissions under particular meteorological and operational conditions, rather than annual averages.

This temporal mismatch is important because landfill CH_4 emissions can vary over short and seasonal timescales. Emissions may be influenced by temperature, soil moisture, atmospheric pressure, wind conditions, oxidation rates, cover conditions, and gas transport pathways. Studies of landfill CH_4 emissions have shown substantial temporal variability and sensitivity to meteorological conditions, including pressure changes and seasonal effects. For example, Kissas et al. (2022) found that temporal variability in CH_4 emissions from a Danish landfill was linked to changes in barometric pressure; an increase in atmospheric pressure leads to a decrease in CH_4 in a non-linear way, complicating the ability to estimate annual CH_4 emissions from landfill. Rees-White et al. (2019) found similar patterns, with higher CH_4 emissions under low-pressure. As a result, annualised observation-based estimates and FOD-based estimates are not directly equivalent. Observation-based values depend on when and under what conditions measurements were made, while the FOD model represents a smoothed annual estimate based on historical waste inputs. Differences between the two should be interpreted not as model error, but because of the difference of comparing a long-term bottom-up model with short-term top-down measurements.

The consistently higher emissions predicted by the FOD model compared with observed values can be explained by several site-specific processes that are not represented in the inventory

framework. The FOD model estimates CH_4 generation but does not represent spatial heterogeneity in landfill emissions, gas bypass pathways, or episodic release events driven by pressure changes. In addition, landfill closure activities, excavation, or reshaping of waste bodies may alter CH_4 generation and transport processes in ways not captured by the model (Mou et at., 2015 ; Amini et al.,2013).

For Filborna, modelled emissions generally exceed the interpolated observation-based emissions over most of the measurement period from 2001 to 2024. These findings are similar to Mou et al. (2015)'s, who found that IPCC parameter values overestimated CH_4 emissions for Danish landfills compared to observed, in-situ measurements. A reason for this overestimation is the low amount of organic waste in Danish landfills, since landfilling organic waste in Denmark has been banned since 1997. For Sweden, this ban has been active since 2005, meaning that Swedish landfills have similar low-organic waste landfills. The largest differences occur between approx. 2008 and 2016, when observed emissions decline more rapidly than predicted by the FOD model. This suggests that the modelled decay may not fully capture site-specific factors that reduced actual surface emissions during this period, such as changes in landfill management, or reduced emission pathways through the cover. However, as mentioned, the lower measured values could also be caused by the upscaled 'snapshot' measurements, which are not representative for annual emissions. In more recent years, from 2019 to 2024, the modelled and observed estimates converge, indicating closer agreement between the long-term FOD-based emission trajectory and measured site-scale emissions. Comparing the modelled and observed CH_4 emissions shows that the FOD model captures the broad decline in CH_4 generation over time but may be less able to represent shorter-term variability and operational controls affecting actual emissions.

Studies comparing top-down landfill CH_4 measurements with bottom-up inventory or FOD-based estimates generally suggest that atmospheric observations often yield higher emissions than reported inventory values, although site-level comparisons remain mixed and modelled emissions can also exceed measurements at individual landfills. Maliehe et al. (2026) state that studies may either overestimate or underestimate CH_4 emissions when using bottom-up approaches. Saunois et al. (2025) show bottom-up CH_4 estimations 30% larger than the estimated top-down estimations. The reason for these underestimations and overestimations is likely due to the limitations in bottom-up approaches, as discussed in 6.1 in combination with limitations from top-down approaches.

6.3 Satellite observations as an alternative monitoring strategy

Remote sensing technologies provide new opportunities to monitor CH_4 emissions from landfill sites. However, detection capabilities vary between measurement platforms. In this study, 12 observations were requested from GHGSat to assess the possibility of detecting CH_4 plumes over Filborna using satellites. Satellites are useful for detecting large CH_4 plumes over broad areas, but many Swedish landfill emissions may be too small, diffuse, or intermittent to be detected consistently, especially given cloud cover and satellite overpass limitations.

Gillespie et al. (2025) note that satellites can currently only detect CH_4 from a limited number of (high-emitting-) landfills, compared to in-situ measurements, which are able to quantify CH_4 for most accessible landfills.

6.3.1: Satellite measurements: no detected methane

No CH_4 was detected in any of the 12 GHGSat observations over Filborna. The modelled average emission rate for 2024, approx. 86 kg CH_4 h^{-1}, is below the lower bound of reported satellite detection thresholds under favourable atmospheric conditions, around 100 kg CH_4 h^{-1}. However, UAV-derived fluxes exceeding 100 kg CH_4 h^{-1} were measured during both the 2023 and 2024 campaigns, indicating that some emissions may have been within or close to the nominal detection range of 100 kg CH_4 h^{-1} (ESA, n.d.).

Detectability by satellite is strongly controlled by meteorological, atmospheric and surface conditions, including wind speed, cloud cover, background CH_4 variability, surface reflectance, and whether emissions occur as concentrated plumes or diffuse surface fluxes. McLinden et al. (2024) found that detection at approximately 100 kg CH_4 h^{-1} is possible only under ideal conditions, such as a flat, reflective surface and favourable atmospheric conditions. Under more typical conditions, they suggest that a detection limit of around 180 kg CH_4 h^{-1} is more representative.

The absence of GHGSat detections may therefore partly reflect that emissions at Filborna remained below, or only marginally above, the satellite detection threshold during the observation periods. This is especially likely when the more representative detection limit of approximately 180 kg CH_4 h^{-1} is considered, together with additional atmospheric and surface-related constraints. Wind conditions may also have contributed. Wind speeds in the study area ranged from 1.9 to 7.6 m s^{-1} (Appendix Table A9). Although some observation dates had wind speeds close to the optimal detection condition of approximately 3.0 m s^{-1}, these dates still did not produce significant CH_4 signals. This suggests that detectability is not controlled by wind speed alone, but by the combined influence of meteorological, atmospheric and surface conditions, as also shown by McLinden et al. (2024).

Another important factor is the likely diffuse character of landfill emissions. Daniels et al. (2023) noted that satellite detection thresholds may be too high for larger areas with spatially distributed diffuse emissions. GHGSat is primarily designed to detect CH_4 plumes that produce a clear concentration enhancement above background levels (McLinden et al., 2024). At landfills, however, the total flux may be distributed across multiple weak surface sources rather than emitted from a single compact point source. In such cases, CH_4 enhancements are diluted over a broader area and may remain below the satellite's column-detection threshold. This effect can be further strengthened by variable wind conditions, heterogeneous surface reflectance and unfavourable atmospheric conditions.

Therefore, the non-detection of CH_4 by GHGSat over Filborna does not necessarily imply negligible landfill emissions. Instead, it likely reflects a combination of relatively low emission

rates, diffuse and spatially heterogeneous surface emissions, and suboptimal atmospheric or surface conditions during the satellite observations.

6.3.2: Potential of UAV measurements to address satellite limitations

UAV-based CH_4 measurements offer several advantages compared with satellite observations for detecting emissions from moderate or spatially diffuse sources. Satellites provide valuable large-scale coverage and are particularly useful for identifying large CH_4 plumes, but their ability to detect smaller or short-lived emissions are limited (Yuvaraj et al., 2026). UAVs can measure CH_4 concentrations directly within or close to the plume, allowing smaller emission rates and diffuse surface emissions to be detected more effectively. This makes UAV measurements a useful method for medium-sized landfills such as Filborna, where emissions may fall near or below current satellite detection thresholds. UAV surveys can also be planned around favourable wind and weather conditions and can provide higher spatial detail than satellite observations, making them useful for identifying emission zones and supporting site-level mitigation.

However, UAV measurements also have limitations. They are more labour-intensive than satellite monitoring and require field access, suitable weather conditions, and repeated campaigns to capture temporal variability. UAV measurements are also limited in spatial coverage compared with satellites and usually represent short monitoring periods rather than continuous annual emissions. Overall, neither UAVs nor satellite observations are currently developed enough to replace inventory models on their own. For UAV-measurements, their main value lies in providing high-resolution, site-specific measurements whereas satellite monitoring could be used for large-scale coverage of sites with high emission rates well above the detection threshold.

6.4 Methodological uncertainties in UAV methane quantification

6.4.1: Uncertainty estimation

The uncertainty values reported in this study represent the propagated uncertainty of the UAV flux estimate based on the uncertainty sources included in the calculation: wind speed, wind direction, background concentration, sensor precision, and kriging interpolation.

Wind direction is the most dominant source of uncertainty for all flights in this study. This is because the flux calculation depends strongly on the wind component perpendicular to the flight plane. Even a small error can noticeably change the projected wind speed through the plume cross-section. Wind speed and background concentration also contributed to the total uncertainty, while CH_4 sensor precision and kriging uncertainty were comparatively small. However, these values represent only the uncertainty sources explicitly propagated in the flux calculation, and do not capture all possible sources of uncertainty, such as spatial mismatch between the anemometer and plume, turbulence, incomplete plume coverage, assumptions in the kriging, or the representativeness of individual flights for longer-term landfill emissions. The results should therefore be interpreted as a methodological uncertainty budget for the

UAV-derived flux estimates, rather than a complete uncertainty estimate for the true landfill emission rate.

Uncertainties in UAV-based CH_4 measurements remain difficult to quantify directly (van Ettinger et al., 2026). UAV-based CH_4 flux estimates rely on the assumption that plume morphology and source strength remain mostly constant over the duration of a flight (Yong et al., 2024). In addition, both emissions and the wind field are assumed to remain stable during an individual measurement period. These assumptions are necessary for the mass balance approach, but they also introduce uncertainty into the final CH_4 flux estimates.

Several studies have highlighted different dominant sources of uncertainty in UAV-based CH_4 measurements. Xu et al. (2025) reported that the largest source of uncertainty was the volumetric concentration of CH_4, which reflects both instrument measurement error and temporal variability in CH_4 concentrations. Yong et al. (2024) identified two main challenges affecting the accuracy of flux measurements: the accuracy of onboard wind measurements and the extent to which the plume is fully captured during sampling. They recommend wind speeds between 5 and 10 m s^{-1} for more reliable flux measurements. Spizzirri et al. (2026) likewise found that measurements collected with wind speeds above 2.3 m s^{-1} and wind direction variability below 33° were associated with lower uncertainties, although in their study uncertainty appeared to be driven primarily by atmospheric conditions and wind speed, while wind direction played a smaller role. In the uncertainty propagation for this study's 2024 transect, wind speed contributed a small share of the relative uncertainty contribution, ranging from 3.1% to 9.2% across flights, while wind direction was consistently the dominant component, contributing between 44.2% and 73.7%. Background uncertainty also played a notable role, ranging from 5% to 13.1% across flights. This differs from previous studies, in which uncertainty was more strongly associated with wind speed or broader atmospheric conditions. The relatively small contribution of wind-speed uncertainty in this study may be the result of the use of a Type A statistical uncertainty estimate, which may not fully capture within-flight variability or its practical influence on flux calculations.

Wind measurements remain one of the dominant drivers of uncertainty in mass balance flux calculations (Scheutz et al., 2025), while instrument error and temporal variability in CH_4 concentrations may also contribute substantially (Xu et al., 2025). For the transects used in this study, wind data were obtained from a nearby meteorological mast and extrapolated to the UAV flight altitude using a logarithmic wind profile. Any discrepancy between the measured wind field and the actual wind conditions within the CH_4 plume may therefore introduce additional uncertainty into the projected wind speed used in the flux calculation.

Table 6 shows how each flight (Flight 1 from 2022, 2023 and 2024) has a different relative uncertainty contribution. Notably, the uncertainty for 2024 is higher than in 2022 and 2023. This could be because the wind direction variability (58.54°) lies significantly above the maximum of 33° suggested by Spizzirri et al. (2026), leading to a higher uncertainty due to directionality. For 2022, wind speed uncertainty was higher (11.6%) compared to 2023 (6.8%) and 2024 (9.2%). A potential factor could be the lower wind speed observed for this year. As

mentioned, Yong et al. (2024) suggests wind speeds between 5 and 10 m s^{-1} for minimal wind speed uncertainties, a range that Flight 1 from 2022 does not reach. Additionally, wind speed variability for the 2022 flight is relatively higher to its wind speed (2.3 m/s to 3.3 m/s) than the wind variability to speed in 2023 (3.5 m/s to 7.6 m/s) and 2024 (3.14 m/s to 7.7 m/s). Lastly, background concentration was similar for 2022 (6.8%) and 2023 (7.8%) and higher for 2024 (13.1%). Van Ettinger et al. (2026) and Yong et al. (2024) note that relative background uncertainty increases under low-flux conditions, yet 2024 has the highest total flux of the three years. One possibility for the higher uncertainty could be a greater background variability or an unstable background estimate.

Table 6: Comparison of propagated uncertainty components for Flight 1 in 2022, 2023, and 2024. Values are shown as absolute uncertainty contributions in kg CH_4 h^{-1} and as relative uncertainty contributions expressed as a percentage of the estimated flux.

Flight	Direction U	Speed U	Background U	Wind speed	Wind speed V	Wind direction	Wind direction V	Total flux
2022	24%	12%	7%	3.3	2.3	207	40	57
2023	32%	7%	8%	7.6	3.5	294	20	66
2024	65%	9%	13%	7.7	3.14	279	59	89
U = Uncertainty. V = Variability. Wind speed given in m/s and wind direction in degrees. Total flux in kgh-1.								

6.4.2: Surface roughness length influences

The sensitivity analysis showed that the UAV-derived CH_4 flux estimates were affected by the assumed surface roughness length (z_0). In this study, z_0 was used in the logarithmic wind profile to scale measured wind speeds to the UAV flight altitude. Higher z_0 values produced higher scaled wind speeds at flight height, which in turn increased the calculated CH_4 flux. This is important because, in the mass-balance approach, the estimated flux is approx. proportional to the projected wind speed through the plume cross-section.

Across the tested z_0 range of 0.02–0.8 m over all 2024 flights, the average estimated CH_4 flux varied by approx. 28%, increasing from 100.3 to 128.6 kg CH_4 h^{-1}. This indicates that uncertainty in surface roughness can propagate into the final emission estimate through its effect on wind-speed scaling. However, the full tested range includes roughness lengths that may not all be equally representative of the Filborna landfill. Literature suggest that landfills or complex managed surfaces have z_0 values closer to intermediate roughness lengths between 0.3-0.5 m (Brovkina et al., 2026; Dörenkämper et al., 2020), although this depends on cover material, vegetation, buildings, waste morphology, and surrounding terrain.

As an example, Flight 1 from 2024 shows that the total flux ranged from approx. 74 to 97 kg CH_4 h^{-1} across the full tested z_0 range of 0.02–0.8 m. When considering the narrower range of 0.3–0.5 m, the flux range becomes smaller, approx. 86–91 kg CH_4 h^{-1}. Using the average of all 2024 flights, the estimated CH_4 flux increased by approximately 5% across the 0.3–0.5 m range, suggesting that careful selection of z_0 remains important, but that the sensitivity is considerably smaller when restricted to a more plausible roughness range.

Overall, the sensitivity analysis shows that z_0 can influence the final CH_4 flux estimate, but that the magnitude of this effect depends strongly on the roughness range considered. The full tested

range should therefore be interpreted as a broad assessment of model behaviour rather than as an equally likely range of true z_0 values. The original approach, in which roughness was estimated from height variability along the UAV transect, is likely more site-specific than applying generic land-cover values, because it reflects local terrain and surface variability encountered during the flight. However, this estimate should still be treated as approximate, since aerodynamic roughness is also affected by vegetation structure, obstacles, surface cover, waste morphology, and surrounding terrain. This highlights that z_0 should be selected or estimated carefully, but also that site-specific estimation may provide a more appropriate basis for UAV-based flux calculations than assuming a fixed literature value.

6.4.3: Baseline estimation stability

The baseline sensitivity analysis shows that the choice of background estimation method can have a clear effect on the calculated CH_4 flux, even when the overall propagated uncertainty remains almost unchanged. For the Flight 3 from 2024, replacing the static baseline with a rolling baseline reduced the estimated flux from 172.6 kg CH_4 h^{-1} to 143.3 kg CH_4 h^{-1}. This indicates that the rolling method produced a higher local background estimate during parts of the plume period, reducing the CH_4 enhancement above background.

For Flight 3 from 2024, both baseline methods estimated a relatively stable background close to 2.0 ppm. However, the rolling baseline increased slightly during the plume period, reaching approx. 2.1 ppm. This suggests that the rolling method may partially follow the plume signal when concentrations remain elevated for a period. As a result, part of the plume enhancement may be treated as background, which lowers the final flux estimate. Out of the 3 flights analysed in the results, this effect was strongest for Flight 1 from 2023, where the rolling baseline followed the CH_4 plume more closely than in 2022 and 2024. In Flight 1 from 2023, the static baseline method produced a flux of 83.9 kg CH_4 h^{-1}, while the rolling baseline reduced this to 65.5 kg CH_4 h^{-1}. In Flight 3 from 2022, the effect was smaller, with the flux decreasing from 71.4 to 69.7 kg CH_4 h^{-1}. This indicates that baseline sensitivity depends on the structure of the plume and the stability of the background signal. The rolling baseline produced lower flux estimates, but this likely reflects a methodological limitation rather than a true change in background CH_4. During plume periods, the rolling baseline partly followed the plume signal, causing some of the enhancement to be removed as background. Since true background CH_4 is not expected to vary strongly over a short flight, the static baseline was considered more appropriate for the flux calculation.

Even though the original static baseline methodology is likely more appropriate for this pipeline, the results show that baseline estimation is important for the CH_4 flux calculation. This highlights the need to select the baseline method carefully, particularly for flights where the plume is broad, persistent, or not clearly separated from the background signal.

6.5 Implications for methane monitoring and inventory improvement

The results of this study highlight the complementary roles of inventory modelling and direct measurement approaches for landfill CH_4 monitoring. The comparison between the FOD model

and site-level observations at Filborna shows that inventory-based estimates may not fully capture the variability of emissions at individual landfill sites.

Direct measurements, including UAV-based measurements, could help improve inventory methods by providing observational constraints on model assumptions. However, field flux measurements alone do not directly determine FOD parameters such as DOC, DOCf, k, or oxidation. The IPCC 2006 Guidelines state that direct measurements can be used to validate FOD model predictions and to support the selection of country-specific parameters, including the decay rate constant and CH_4 generation potential. In principle, repeated UAV or other plume-based measurements could therefore be used to evaluate current assumptions about CH_4 generation, oxidation, recovery, and emission behaviour by comparing measured CH_4 values to modelled values. This could support movement toward a more site-specific IPCC Tier 3 approach, which means that national estimates are based on measurement-derived or nationally developed parameters rather than default values alone.

Direct surface-emission measurements cannot simply be inserted into the national inventory without additional upscaling and representativeness assessment. UAV measurements capture actual emissions after gas recovery and oxidation, whereas the FOD model estimates CH_4 generation/emissions from waste degradation and assumed correction factors. To use UAV measurements in inventory development, repeated measurements would be needed across different seasons, meteorological conditions, landfill types, waste ages, sizes, cover systems, and recovery conditions. The IPCC guidance notes that surface emissions are spatially and temporally variable and that site-specific measurements should only be used for inventory estimation when their representativeness can be justified. UAV measurements are useful as part of a broader measurement database that can be used to validate the FOD model, calibrate parameters, or classify Swedish landfills into groups, but repeated measurement campaigns of landfills in Sweden under different seasons' meteorological conditions would be necessary.

A possible pathway would be to develop a Swedish landfill measurement programme where landfills are repeatedly measured. These measurements could then be compared with FOD estimates to identify systematic biases and refine country-specific parameters for different landfill classes. In this way, UAV measurements would not replace the FOD model directly but could provide evidence for improving the parameters and uncertainty ranges used in the national inventory.

6.6: Limitations methodology and data

Several limitations should be considered when interpreting the results of this study. First, the analysis is based on a limited number of UAV measurement campaigns. Landfill CH_4 emissions can vary with wind conditions, atmospheric pressure, meteorological conditions, cover moisture, and operational activities. Therefore, the UAV-derived fluxes represent short-term snapshots of emissions rather than continuous annual averages. Repeated measurements across different seasons and meteorological conditions would be needed to better assess temporal variability and improve comparison with annual FOD estimates.

Second, this study focuses on a single landfill site. Filborna provides a useful case study because of the availability of site-specific activity data and multiple years of observational measurements. However, Swedish landfills differ in waste composition, age, cover type, gas collection infrastructure, management history, and terrain. As a result, the findings cannot be assumed to be directly representative of all Swedish landfills. A larger dataset including several landfills with different characteristics would be needed to assess whether the patterns observed at Filborna are more generally applicable.

Third, the modelling component was limited to an IPCC-style FOD approach. Although this was appropriate for comparison with the NIR methodology, other landfill gas models, such as Afvalzorg or LandGEM-type models, were not tested. The Afvalzorg model, in particular, could have provided useful insight because it is commonly applied as a multiphase, site-specific landfill gas model (Vu et al., 2017). Comparing multiple model structures could help determine whether differences between modelled and observed emissions are mainly caused by parameter choices, site-specific input data, or the structure of the FOD model itself.

Finally, some site-specific parameters were not available in sufficient detail. Information on gas recovery efficiency, cover oxidation, moisture conditions, and operational changes was limited. These factors can influence the relationship between CH_4 generation and actual surface emissions. Consequently, the model should be interpreted as an approximate site-level application of the FOD framework rather than a fully calibrated landfill-specific emission model.

7 Summary and conclusions

This study evaluated UAV-based CH_4 measurements for the Filborna landfill and compared them with emissions estimates produced using an IPCC Tier 2 FOD model. The results show that the different approaches provide complementary, but not directly equivalent, information on CH_4 emissions. The FOD model describes long-term CH_4 generation and emissions based on historical waste deposition and assumed decay dynamics, while UAV measurements provide direct observations of atmospheric CH_4 emissions during specific measurement periods.

The comparison between modelled and observed emissions showed that the downscaled FOD model generally produced higher CH_4 emission estimates than the observation-based values for most of the 2001–2024 period. This indicates that the FOD model may not fully account for site-specific processes that affect surface emissions, such as gas recovery, oxidation in landfill cover material, operational changes, and spatially variable emission pathways. In recent years, the modelled and observed estimates converged more closely, suggesting that the FOD model captures the broad long-term decline in CH_4 generation. Nevertheless, the comparison should be interpreted carefully, as the observed emissions were scaled up to annual values. UAV measurements represent snapshots of conditions during individual flights and along specific transects, rather than continuous observations of the entire landfill. As a result, the upscaled observation-based estimates may not fully capture the temporal and spatial variability of landfill CH_4 emissions over a full year.

The uncertainty analysis showed that UAV-derived flux estimates were mainly sensitive to wind-related uncertainty. Across the analysed flights, wind direction was the dominant uncertainty component, while wind speed and background CH_4 concentration also contributed to the propagated uncertainty. This means that improving wind characterisation, especially wind direction at the plume location, would likely be one of the most effective ways to reduce uncertainty in future UAV-based landfill CH_4 estimates.

The sensitivity tests further demonstrated that processing choices can influence UAV-derived CH_4 flux estimates. The assumed surface roughness length affected the scaled wind speed, which influenced CH_4 fluxes. Baseline estimation also affected the magnitude of the flux estimate: using a rolling baseline generally reduced the estimated flux compared with the static baseline, but the rolling method followed the plume signal and may therefore have removed part of the true CH_4 enhancement. These results show that UAV-based flux estimates are not only dependent on measured CH_4 concentrations, but also on methodological choices in wind scaling and baseline estimation.

Overall, the FOD model provides a useful framework for estimating long-term landfill CH_4 emissions, but its application to a single heterogeneous and actively managed landfill is not without its limits. At Filborna, the model captured the general magnitude and expected long-term decline in emissions but could not fully explain the differences between modelled and

measured fluxes. This highlights the importance of combining bottom-up inventory models with direct measurements. Continuous satellite observations would be ideal, but because landfill emissions are diffuse, sensor performance is sensitive to atmospheric conditions, and CH_4 emission rates are relatively low, this is not currently feasible with existing satellite technology. UAV measurements are therefore particularly valuable, as they can capture spatial emission patterns and help evaluate whether inventory assumptions are reasonable for individual landfills.

These findings partly support the hypothesis that UAV-based measurements can capture site-specific spatial and operational variability that is not fully represented by inventory-based FOD modelling. However, the hypothesis can only be partly supported rather than fully verified, because the UAV campaigns were limited in temporal coverage and therefore cannot by themselves represent annual emissions. Instead, the results indicate that UAV-based methods are most valuable as a complementary approach to FOD modelling, especially for evaluating site-specific assumptions and identifying sources of uncertainty.

Future research should expand the temporal and spatial scope of landfill CH_4 measurements. More frequent UAV campaigns across different seasons, wind conditions, and operational states would improve understanding of temporal variability and make comparisons with annual FOD estimates more robust. Including additional Swedish landfills would also help determine whether the patterns observed at Filborna are representative of broader national landfill CH_4 emissions.

In summary, repeated UAV measurements, possibly combined with other direct measurement methods, could support the development of more representative FOD parameterisations for Sweden. Repeated site-specific observations could be used to constrain key FOD parameters, refine parameter values, and assess potential model biases. This could help reduce uncertainty in CH_4 emissions from the waste sector and improve the accuracy of the NIR.

8 References

Amini, H. R., Reinhart, D. R., & Niskanen, A. (2013). Comparison of first-order-decay modeled and actual field measured municipal solid waste landfill methane data. *Waste Management, 33*(12), 2720. https://doi.org/10.1016/j.wasman.2013.07.025

Avfall Sverige. (2025). *Svensk avfallshantering 2024.* Avfall Sverige. https://www.avfallsverige.se/media/xtbi3gst/svensk-avfallshantering-2024.pdf

Avfall Sverige. (2024). *Swedish Waste Management 2023.* https://www.avfallsverige.se/media/cwibhsx2/svensk_avfallshantering_2023_en.pdf

Avfall Sverige. (2024). *Methane Strategy of Avfall Sverige A strategy to minimise and systematically monitor methane emissions from municipal waste management.* https://www.avfallsverige.se/media/5bdpv2xf/CH4-strategy-of-avfall-sverige.pdf

Bergström S. and Fråne, A. (2011). *Uppskattning av framtida gaspotential i två skånska deponier- fallstudier av Filborna, Helsingborg och Albäck, Trelleborg*. [Master's thesis, Lund University]. Lund University Publications. https://lup.lub.lu.se/student-papers/search/publication/4468094

Björklund, A. E., & Finnveden, G. (2007). Life cycle assessment of a national policy proposal – The case of a Swedish waste incineration tax. *Waste Management, 27*(8), 1046-1058. https://doi.org/10.1016/j.wasman.2007.02.027

Brovkina, O., Pikl, M., Zemek, F., & Michálek, J. (2026). Detecting volume changes in municipal solid waste landfill using airborne laser scanning. *Waste Management Bulletin, 4*(1), https://doi.org/10.1016/j.wmb.2025.100272

Börjesson, G., Samuelsson, J. & Chanton, J. (2007). Methane Oxidation in Swedish Landfills Quantified with the Stable Carbon Isotope Technique in Combination with an Optical Method for Emitted Methane. *Environmental science & technology, 41*(19), 6684-6690. https://doi.org/10.1021/es062735v

Börjesson, G., Samuelsson, J., Chanton, J., Adolfsson, R., Galle, B., & Svensson, B. (2009). A national landfill methane budget for sweden based on field measurements, and an evaluation of ipcc models. *Tellus Series B-Chemical and Physical Meteorology, 61*(2), 424–435. https://doi.org/10.1111/j.1600-0889.2008.00409.x

Citrasari, N., Gautama, N. A. M., Larasati, D. A., Istiqomah, K., Isnadina, D. R. M., Hariyanto, S.,& Matsumoto, T. (2025). Comparative study of methane emission quantification in Indonesian landfills. *Official Journal of the Japan Society of Material Cycles and Waste Management (JSMCWM) and the Korea Society of Waste Management*. https://doi.org/10.1007/s10163-025-02390-6

Climate and Clean Air Coalition. (2021, November 2). *Global methane pledge.* https://www.ccacoalition.org/content/global-methane-pledge

Corvellec, H., & Hultman, J. (2012). From "less landfilling" to "wasting less": Societal narratives, socio-materiality, and organizations. *Journal of Organizational Change Management, 25*(2), 297-314. https://doi.org/10.1108/09534811211213964

Daniels, W. S., Wang, J. L., Ravikumar, A. P., Harrison, M., Roman-White, S. A., George, F. C., & Hammerling, D. M. (2023). Toward Multiscale Measurement-Informed Methane Inventories: Reconciling Bottom-Up Site-Level Inventories with Top-Down Measurements Using Continuous Monitoring Systems. *Environmental Science & Technology, 57*(32), 11823-11833. https://doi.org/10.1021/acs.est.3c01121

Dogniaux, M., Maasakkers, J. D., Girard, M., Jervis, D., McKeever, J., Schuit, B. J., Sharma, Lopez-Noreña, A., Varon, D. J., & Aben, I. (2025). Global satellite survey reveals uncertainty in landfill methane emissions. *Nature, 647*(8089), 397-402. https://doi.org/10.1038/s41586-025-09683-8

Dörenkämper, M., Olsen, B. T., Witha, B., Hahmann, A. N., Davis, N. N., Barcons, J., Ezber, Y., García-Bustamante, E., González-Rouco, J. F., Navarro, J., Sastre-Marugán, M., Sīle, T., Trei, W., Žagar, M., Badger, J., Gottschall, J., Sanz Rodrigo, J., & Mann, J. (2020). The making of the New European Wind Atlas – Part 2: Production and evaluation. *Geoscientific Model Development, 13*(10), 5079–5102. https://doi.org/10.5194/gmd-13-5079-2020

European Space Agency. (n.d.). *About GHGSat.* ESA Earth Online. Retrieved January 18, 2026, from https://earth.esa.int/eogateway/missions/ghgsat

Ferrari, A., Laneve, G., Tellez, R. A. C., Pampanoni, V., Saquella, S., & Guarini, R. (2025) Analysis of local methane emissions using near-simultaneous multi-satellite observations: Insights from landfills and oil-gas facilities. *In IGARSS 2025 – 2025 IEEE International Geoscience and Remote Sensing Symposium* (pp. 7570–7574). https://doi.org/10.1109/IGARSS55030.2025.11243473

Fosco, D., Molfetta, M., Renzulli, P., Notarnicola, B., Carella, C., & Fedele, G. (2025). Innovative drone-based methodology for quantifying methane emissions from landfills. *Waste Management, 195*, 79. https://doi.org/10.1016/j.wasman.2025.01.033

Fredenslund, A.M., Rees-White, T. C., Beaven, R. P., Delre, A., Finlayson, A., Helmore, J., Allenm G., & Scheutz, C. (2019). Validation and error assessment of the mobile tracer gas dispersion method for measurement of fugitive emissions from area sources. *Waste Management, 83*, 68-78. https://doi.org/10.1016/j.wasman.2018.10.036

GHG Protocol. (2024, August 7). *IPCC Global warming potential values: Version 2.0.* https://ghgprotocol.org/sites/default/files/2024-08/Global-Warming-Potential-Values%20%28August%202024%29.pdf

Gillespie, L. D., Ars, S., Worthy, C., Brantley, H., Green, R., Scarpelli, T. R.,Wunch, D. (2025). Comparison of Landfill CH_4 Emission Quantification Using Multiple Observation Methods. *ACS ES&T Air, 2*(12), 2786-2798. https://doi.org/10.1021/acsestair.5c00127

Government Offices of Sweden, Ministry of Climate and Enterprise. (2022, November 11). *Sweden's methane action plan: Mapping of Sweden's CH_4 emissions, projections, policies and measures*. https://www.government.se/reports/2022/11/swedens-CH4-action-plan

Gålfalk, M., Nilsson Påledal, S., & Bastviken, D. (2021). Sensitive drone mapping of methane emissions without the need for supplementary ground-based measurements. *ACS Earth and Space Chemistry, 5*(11), 2668–2676. https://doi.org/10.1021/acsearthspacechem.1c00106

IPCC (Intergovernmental Panel on Climate Change). (2000). *Good practice guidance and uncertainty management in national greenhouse gas inventories: Chapter 5: Waste. Institute for Global Environmental Strategies.* https://www.ipcc.ch/publication/good-practice-guidance-and-uncertainty-management-in-national-greenhouse-gas-inventories

IPCC (Intergovernmental Panel on Climate Change). (2021). *Climate change 2021: The physical science basis. Contribution of Working Group I to the Sixth Assessment Report of the Intergovernmental Panel on Climate Change* (V. Masson-Delmotte et al., Eds.). Cambridge University Press. https://doi.org/10.1017/9781009157896

IOGP, Ipieca, OGCI & Energy Institute. (2025). *Recommended practices for methane emissions detection and quantification technologies – upstream (*Report 661). International Association of Oil & Gas Producers. https://www.iogp.org/bookstore/product/recommended-practices-for-methane-emissions-detection-and-quantification-technologies-upstream

Jackson, R. B., Saunois, M., Martinez, A., Canadell, J. G., Yu, X., Li, M., Poulter, B., Raymond, P. A., Regnier; P., Ciais, P., Davis, S. J., & Patra, P.K. (2024). Human activities now fuel two-thirds of global methane emissions. *Environmental Research Letters, 19*(10), https://doi.org/10.1088/1748- 9326/ad6463

Jervis D., Girard M., MacLean J.W., Marshall D., McKeever J., Strupler M., Ramier A., Tarrant E., Young D., Maasakkers J.D,, Aben I., Scarpelli, T.R. (2025). Global energy sector methane emissions estimated by using facility-level satellite observations. *Science, 390*(6778), 1151-1157. https://doi.org/10.1126/science.adv3183

Kissas, K., Ibrom, A., Kjeldsen, P., & Scheutz, C. (2022). Methane emission dynamics from a Danish landfill. Waste Management, 138, 234. https://doi.org/10.1016/j.wasman.2021.11.043

Krause, M. J., Thoma, E. D., Bryant, A., Brantley, H., MacDonald, M., Green, R., & Thorneloe, S. (2025). A High-Resolution Satellite Survey of CH_4 Emissions from 60 North American Municipal Solid Waste Landfills. *Environmental Science & Technology, 59*(29), 15080-15091. https://doi.org/10.1021/acs.est.5c01409

Liu, S., Yang, X., & Zhou, X. (2021). Development of a low-cost UAV-based system for methane monitoring over oil fields. *Environmental technology, 42*(20), 3154-3163. https://doi.org/10.1080/09593330.2020.1724199

Maliehe, K. A., Goulding, J., Marsh, S., & Alam, M. S. (2026). A Bayesian inversion of TROPOMI methane observations over South Africa. *Science of the Total Environment, 1026.* https://doi.org/10.1016/j.scitotenv.2026.181650

Maurice, C., & Lagerkvist, A. (2003). LFG emission measurements in cold climatic conditions; seasonal variations and methane emissions mitigation. *Cold Regions Science and Technology, 36*(1-3), 37-46. https://doi.org/10.1016/S0165-232X(02)00094-0

McLinden, C. A., Griffin, D., Davis, Z., Hempel, C., Smith, J., Sioris, C., D, Dammers, E., Baray, S., Adams, C., Friesen, R., Stockdale, C., Bell, A., Conway, S., Makar, P. A., & Malo, A. (2024). An Independent Evaluation of GHGSat Methane Emissions. Journal of Geophysical Research. *Atmospheres, 129*(15), 1. https://doi.org/10.1029/2023JD039906

Ministry of the Environment. (2022, November 11*). Sweden's methane action plan: Mapping of Sweden's methane emissions, projections, policies and measures*. Government Offices of Sweden. https://www.government.se/reports/2022/11/swedens-methane-action-plan

Montoya, J. M., Olsson, A., Martensson, S., & Chilo, J. (2020). *Drone Gas Concentration Measurement System for Landfills*. 2020 IEEE International Instrumentation and Measurement Technology Conference (I2MTC) (pp. 1-5). IEEE. https://doi.org/10.1109/I2MTC43012.2020.9129192

Morales, R., Ravelid, J., Vinkovic, K., Korbeń, P., Tuzson, B., Emmenegger, L., Chen, H., Schmidt, M., Humbel, S., & Brunner, D. (2022). Controlled-release experiment to investigate uncertainties in UAV-based emission quantification for methane point sources. *Atmospheric Measurement Techniques, 15*(7), 2177-2198. https://doi.org/10.5194/amt-15-2177-2022

Möller, L. (2022*). Mätmetoder för ytemissioner av deponigas: En fallstudie på Filbornadeponin i Helsingborg* [Master's thesis, Lund University]. Lund University Publications. https://lup.lub.lu.se/student-papers/search/publication/9086724

Mou, Z., Scheutz, C., & Kjeldsen, P. (2015). Evaluation and application of site-specific data to revise the first-order decay model for estimating landfill gas generation and emissions at Danish landfills. *Journal of the Air & Waste Management Association, 65*(6), 686. https://doi.org/10.1080/10962247.2015.1008653

Mønster, J., Kjeldsen, P., & Scheutz, C. (2019). Methodologies for measuring fugitive CH_4 emissions from landfills – A review. *Waste Management, 87,* 835-859. https://doi.org/10.1016/j.wasman.2018.12.048

Naturvårdsverket. (2025, December 18*). Waste incineration and landfilling in the EU Emissions Trading System: Advantages and disadvantages* (Case No. NV-01705-24). Swedish Environmental Protection Agency. https://www.naturvardsverket.se/48d7d6/contentassets/82ba32d8069a4e619c123f587c0aa197/waste-incineration-and-landfilling-in-eu-ets.pdf

Naturvårdsverket. (2016). *Naturvårdsverkets föreskrifter om miljörapport* (NFS 2016:8). https://www.naturvardsverket.se/4ac4aa/globalassets/nfs/2016/nfs-2016-8.pdf

Naturvårdsverket. (2024) *National Inventory Report Sweden 2024: Greenhouse gas emission inventories 1990–2022 submitted under the United Nations Framework Convention on Climate Change and the Paris Agreement.* https://unfccc.int/sites/default/files/resource/NIR%20SE%20submission%202024.pdf

Naturvårdsverket. (2023, September 21*). Minskade utsläpp av metan: Redovisning av regeringsuppdrag*.https://www.naturvardsverket.se/48dbba/contentassets/a6f415dca04b468099ecc62bbbe76db3/regeringsuppdrag-minskade-utslapp-av-metan.pdf .

Naturvårdsverket. (n.d.). *Utsläpp i siffror*. Retrieved January, 2026, from https://utslappisiffror.naturvardsverket.se/sv/Sok/

Petrovic, B., French, H. K., Hanssen, O. J., Mæhlum, T., & Schöpke, C. (2026). Management of closed landfills: A qualitative study evaluating real case studies from Norway. *Cleaner Waste Systems, 13*. https://doi.org/10.1016/j.clwas.2026.100489

Rees-White, T., Mønster, J., Beaven, R., & Scheutz, C. (2019). Measuring methane emissions from a UK landfill using the tracer dispersion method and the influence of operational and environmental factors. *Waste Management, 87*, 870. https://doi.org/10.1016/j.wasman.2018.03.023

Saunois, M., Martinez, A., Poulter, B., Zhang, Z., Raymond, P. A., Regnier, P., Canadell, J. G., Jackson, R. B., Patra, P. K., Bousquet, P., Ciais, P., Dlugokencky, E. J., Lan, X., Allen, G. H., Bastviken, D., Beerling, D. J., Belikov, D. A., Blake, D. R., Castaldi, S., Crippa, M., ... Zhuang, Q. (2025).

Global methane budget 2000–2020. *Earth System Science Data, 17*(5), 1873–1958. https://doi.org/10.5194/essd-17-1873-2025

Scarpelli, T. R., Cusworth, D. H., Duren, R. M., Kim, J., Heckler, J., Asner, G. P., Thoma, E., Krause, M. J., Heins, D., & Thorneloe, S. (2024). Investigating Major Sources of Methane Emissions at US Landfills. *Environmental Science & Technology, 58*(49), 21545-21556. https://doi-org.ludwig.lub.lu.se/10.1021/acs.est.4c07572

Scheutz, C., Kissas, K., Mønster, J., Kolmert Strickland, Å., Kivistö, J., Arvidsson, I., Björling, I., Łakomiec, P., McQuilkin, J., & Sarno, A. (2020). *Quantification of landfill CH_4 emissions – a method comparison study*. Technical University of Denmark, FORCE Technology, ReSource International, Lund University, Sweco Environment. https://h2020-memo2.eu/wp-content/uploads/sites/198/2020/06/Quantification-of-landfill-CH_4-emissions-–-a-method-comparison-study_Final-4_june.pdf

Scheutz, C., & Kjeldsen, P. (2019). Guidelines for landfill gas emission monitoring using the tracer gas dispersion method. *Waste Management, 85,* 351-360. https://doi.org/10.1016/j.wasman.2018.12.048

Scheutz, C., Knudsen, J.E., Vechi, N.T., & Knudsen, J. (2025). Validation and demonstration of a drone-based method for quantifying fugitive methane *emissions. Journal of Environmental Management, 373.* https://doi.org/10.1016/j.jenvman.2024.123467

Spizzirri, U. G., Notarnicola, B., Molfetta, M. D., Renzulli, P. A., Astuto, F., Lovarelli, D., Selvaggi, M., Strazzullo, G., & Fosco, D. (2026). Direct measurement of methane emissions in cattle breeds by using UAV monitoring systems to improve data quality in LCA. *The International Journal of Life Cycle Assessment, 31, 1-17*. https://doi.org/10.1007/s11367-026-02620-5

Swedish Environmental Protection Agency. (2026*). National inventory document Sweden 2026: Annexes. Greenhouse gas emission inventories 1990–2024 submitted under the United Nations Framework Convention on Climate Change and the Paris Agreeme*nt. https://unfccc.int/sites/default/files/resource/NID%20SE%20submission%202026%20Annex.pdf

Swedish Government, Ministry of Climate and Enterprise. (2022, November 11*). Sweden's methane Action Plan: Mapping of Sweden's methane emissions, projections, policies and measures (Report* M2022/02106). https://www.government.se/contentassets/303c37911a6c4a9a895c3b4049b8ee9b/swedens-CH_4-action-plan---mapping-of-swedens-CH_4-emissions-projections-policies-and-measures.pdf

United Nations Framework Convention on Climate Change (UNFCC). (2015, December 12*). Paris Agreement. United Nations*. https://unfccc.int/sites/default/files/english_paris_agreement.pdf

van Ettinger, N., van Heuven, S. M. A. C., & Chen, H. (2026). *Evaluating the performance of a UAV-based in situ methane sensor for quantifying point source emissions*. EGUsphere. https://doi.org/10.5194/egusphere-2025-6209

Vu, H. L., Wai Ng, K. T. & Richter, A. (2017). Optimization of first order decay gas generation model parameters for landfills located in cold semi-arid climates. *Waste Management, 69*, 315. https://doi.org/10.1016/j.wasman.2017.08.028

Xu, D., Wang, C., Gu, T., Long, Z., Luan, H., Tang, Z., Gong, J., & Liu, Y. (2025). An unmanned aerial vehicle (UAV)-based methane quantification method for oil and gas sites. *Drones, 9*(11), Article 785. https://doi.org/10.3390/drones9110785

Yong, H., Allen, G., Mcquilkin, J., Ricketts, H., & Shaw, J. T. (2024). Lessons learned from a UAV survey and methane emissions calculation at a UK landfill. *Waste Management, 180,* 47-54. https://doi.org/10.1016/j.wasman.2024.03.025

Yuvaraj, R., Lauvaux, T., Abdallah, C., Ciais, P., Bonne, J., Akani Guery, J., Joly, L., & others. (2026). High-resolution modeling of methane plumes: Validation and sensitivity experiments to explore emission quantification approaches. *Environmental Science & Technology, 60*(5), 4029-4041. https://doi.org/10.1021/acs.est.5c15941

Zhang, S., Huang, X., Lei, M., Zhou, Y., Fei, X., Zhan, L., & Zhang, Y. (2026). Integrating inventory models and satellite observations for site-level methane emission quantification from MSW landfills in China. *Journal of Environmental Management, 399,* Article 128672. https://doi.org/10.1016/j.jenvman.2026.128672

9 Appendices

Table A1: Top ten uncertainty sources to the Swedish GHG inventory in 2022 – excluding land use and land use change (Retrieved from The National Inventory Report, 2024, Naturvårdsverket)

IPCC Source Category	GHG	Year 2022 emissions or removals (kt CO_2-eq.)	Combined uncertainty (%)	Relative contribution to variance in year 2022 (%)
3 D a 1 Inorganic N fertilizers	N2O	769.78	80.2	18.63
3 D a 6 Cultivation of organic soils (i.e. histosols)	N2O	604.36	85.1	12.96
1 A 1 a Public Electricity and Heat Production:Other Fuels	CO2	3 101.18	15.7	11.54
3 A 1 Non-dairy cattle	CH4	1 619.62	25.5	8.34
3 D b 1 Atmospheric deposition	N2O	83.52	400.5	5.48
2 F 1 Refrigeration and air conditioning	HFCs	785.82	38.4	4.46
3 D a 4 Crop residues applied to soils	N2O	360.22	82.5	4.32
3 B Indirect N2O emissions	N2O	72.50	400.5	4.13
5 A 1 Managed waste disposal sites	CH4	509.09	55.9	3.96
3 A 1 Dairy cattle	CH4	1 240.85	20.6	3.20
Total				**77%**

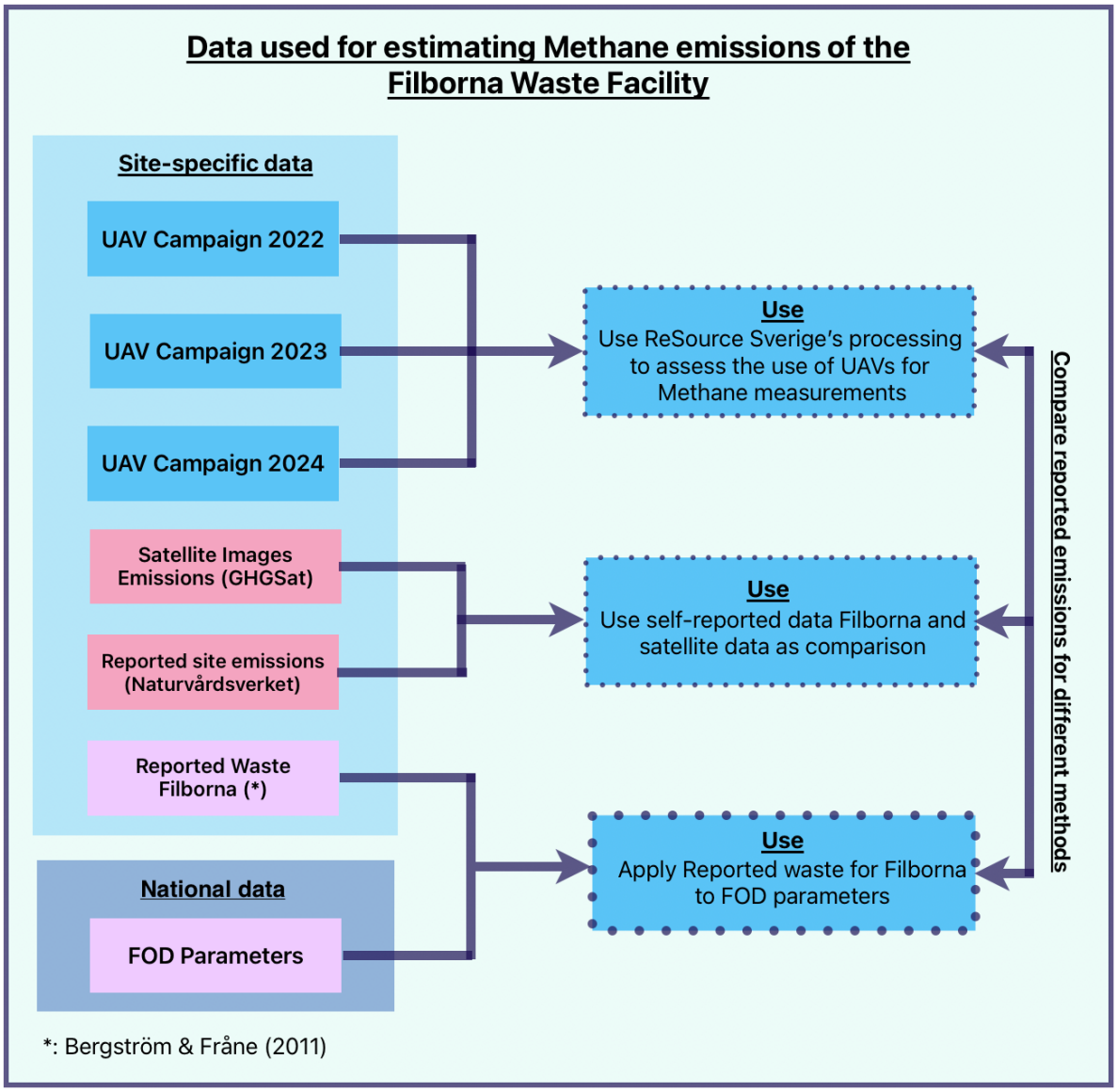

Fig. A1: Visual overview of the data sources and use of data for analysis.

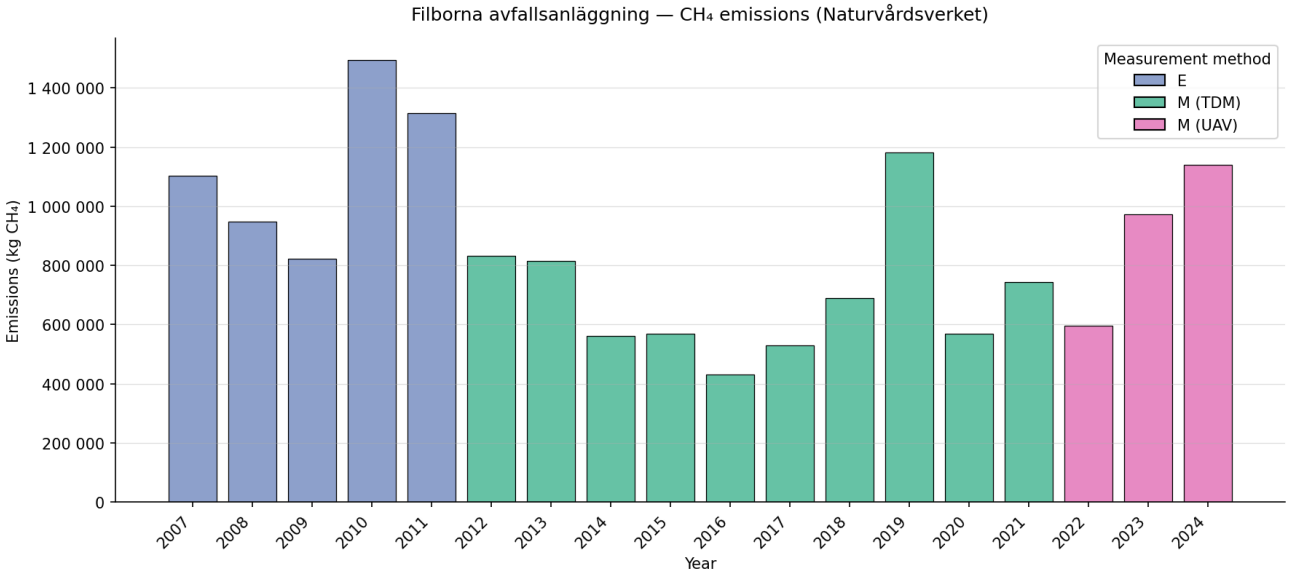

Fig. A2: Self-reported CH_4 Emissions Filborna landfill 2007-2024. Purple: estimated (E) emissions, green: TDM measured (M) emissions, pink: UAV measured (M) emissions. (data from Naturvårdsverket: Swedish Pollutant Release and Transfer Register)

Table A2: Parameter values and uncertainty range used for Monte Carlo-derived uncertainty in modelled Filborna CH_4 emissions. The default and uncertainty values are based on the Swedish NIR. The 95% range represents the 2.5th–97.5th percentile interval from repeated model simulation

Monte Carlo Uncertainty		
Parameter	Default Value	Uncertainty range
DOCf	0.5 (0.54 for Filborna (Börjesson et al. (2009)))	20%
F	0.5	5%
OX	0.1	0.05 - 0.15
Half life	7.5	20%
MCF	Before 1980: 0.6 After: 1	Before 1980: sampled between 0.30-0.96. After: 0.9 - 1
Activity data		30%

Table A3: Overview of model parameters, values and sources used for the IPCC FOD-model for Filborna landfill.

Model parameters, assumptions, and data sources
used for Filborna landfill methane emission modelling

Category	Parameter	Value / Assumption	Source
Observed data	CH_4 observations, 2007–2024	Annual site-scale CH_4 emission measurements	Naturvårdsverket
Observed data	CH_4 observations, 2001–2006	Surface flux study scaled to CH_4 yr^{-1}	Möller (2022)
FOD parameters	DOCf values	0.50 and 0.54; Monte Carlo uncertainty sampled around DOCf = 0.54	Börjesson et al. (2009); IPCC 2006
FOD parameters	F, CH_4 fraction in landfill gas	0.5	IPCC 2006; Sweden NIR 2024
FOD parameters	Oxidation factor, OX	0.1	Sweden NIR 2024; IPCC 2006
FOD parameters	Half-life, $t_{½}$	7.5 yr	IPCC 2006; Sweden NIR 2024
FOD parameters	Methane correction factor, MCF	0.6 before 1980 and 1.0 after 1980	IPCC 2006; Sweden NIR 2024
Activity data	Site-specific waste inputs	Annual deposited waste by category, 1951–2008	Bergström and Fråne (2011)
Activity data	DOC conversion	Category-specific DOC fractions applied to annual waste inputs	IPCC 2006 Guidelines
Activity data	Post-2008 DOC input	Representative DOC fraction derived from 2000-2008 site-specific waste composition	Avfall Sverige 2024
Uncertainty	Model uncertainty	Monte Carlo uncertainty propagation using sampled DOCf, F, $t_{½}$, MCF, OX, and activity-data uncertainty	IPCC 2006; Sweden NIR 2024

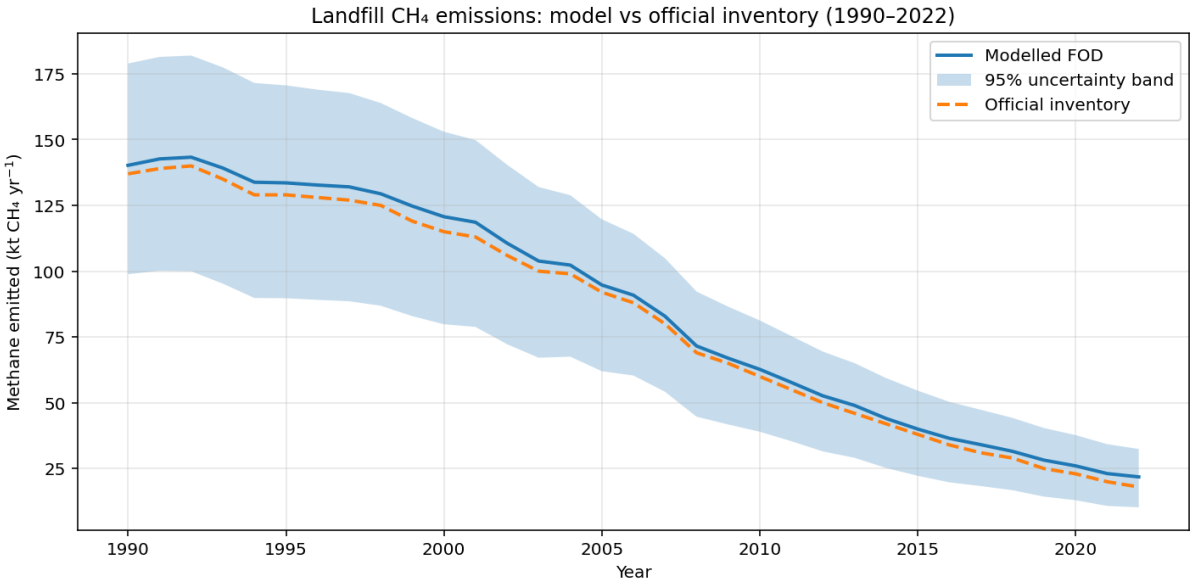

Fig. A3: Comparison between independently modelled landfill CH_4 emissions and officially reported UNFCCC inventory values for Sweden (1990–2022). The blue line shows the modelled CH_4 emissions for each year, with the light blue envelope indicating the 95% uncertainty band. The orange line shows the CH_4 emissions for each year as reported by the NIR in 2024.

Table A4: Propagated uncertainty for each component 2024 flight 1 – 9. showing the absolute uncertainty contribution of each source (kg h^{-1}) and its relative uncertainty contribution (%) to the estimated flux total. The percentages in brackets represent each uncertainty component expressed relative to the estimated flight emission, these percentages do not sum to the total relative uncertainty. Absolute values rounded to 2 decimals; percentages rounded to 1 decimal except for kriging due to its small uncertainty values.

Flight	Wind Speed	Wind direction	Kriging	Measurement	Background	Uncertainty total
Flight 1	8.17 kg h^{-1} (9.2%)	57.79 kg h^{-1} (65.2%)	0.00 kg h^{-1} (0.01%)	2.03 kg h^{-1} (2.3%)	11.64 kg h^{-1} (13.1%)	59.54 kg h^{-1} (67.1%)
Flight 2	4.56 kg h^{-1} (5%)	59.95 kg h^{-1} (65.2%)	0.01 kg h^{-1} (0.01%)	1.91 kg h^{-1} (2.1%)	11.48 kg h^{-1} (12.5%)	61.24kg h^{-1} (66.7%)
Flight 3	10.31 kg h^{-1} (6%)	93.11 kg h^{-1} (54.0%)	0.01kg h^{-1} (0.01%)	1.79 kg h^{-1} (1.0%)	10.39 kg h^{-1} (6.0%)	94.27 kg h^{-1} (54.6%)
Flight 4	4.57 kg h^{-1} (5.9%)	53.28 kg h^{-1} (68.9%)	0.00 kg h^{-1} (0.00%)	0.86 kg h^{-1} (1.1%)	3.86 kg h^{-1} (5%)	53.62 kg h^{-1} (69.4%)
Flight 5	8.32 kg h^{-1} (7.2%)	64.08 kg h^{-1} (55.8%)	0.01 kg h^{-1} (0.01%)	1.80 kg h^{-1} (1.6%)	8.41 kg h^{-1} (7.3%)	65.19 kg h^{-1} (56.8%)
Flight 6	4.49 kg h^{-1} (3.1%)	63.02 kg h^{-1} (44.2%)	0.01 kg h^{-1} (0.01%)	1.90 kg h^{-1} (1.3%)	10.46 kg h^{-1} (7.3%)	64.07 kg h^{-1} (44.9%)
Flight 7	6.84 kg h^{-1} (7.3%)	60.13 kg h^{-1} (64.1%)	0.01kg h^{-1} (0.01%)	2.00 kg h^{-1} (2.1%)	11.38 kg h^{-1} (12.1%)	61.61 kg h^{-1} (65.7%)
Flight 8	7.93 kg h^{-1} (5.5%)	84.62 kg h^{-1} (58.9%)	0.01kg h^{-1} (0.01%)	1.97 kg h^{-1} (1.4%)	11.06 kg h^{-1} (7.7%)	85.73 kg h^{-1} (59.6%)
Flight 9	8.74 kg h^{-1} (5.8%)	111.35 kg h^{-1} (73.7%)	0.02 kg h^{-1} (0.01%)	2.11 kg h^{-1} (1.4%)	10.74 kg h^{-1} (7.1%)	112.23 kg h^{-1} (74.3%)

Table A5: Propagated uncertainty for each component 2023 flight 1 – 8. showing the absolute uncertainty contribution of each source (kg h^{-1}) and its relative uncertainty contribution (%) to the estimated flux total. The percentages in brackets represent each uncertainty component expressed relative to the estimated flight emission, these percentages do not sum to the total relative uncertainty. Absolute values rounded to 2 decimals; percentages rounded to 1 decimal except for kriging due to its small uncertainty values.

Flight	Wind Speed	Wind direction	Kriging	Measure ment	Background	Uncertainty total
Flight 1	5.71kg h^{-1} (6.8%)	26.81 kg h^{-1} (32.0%)	0.01 kg h^{-1} (0.01%)	1.22 kg h^{-1} (1.5%)	6.55 kg h^{-1} (7.8%)	28.21 kg h^{-1} (33.6%)
Flight 2	6.78 kg h^{-1} (5.6%)	30.79 kg h^{-1} (25.4%)	0.01 kg h^{-1} (0.01%)	1.37 kg h^{-1} (1.1%)	8.78 kg h^{-1} (7.2%)	32.76 kg h^{-1} (27.0%)
Flight 3	6.17 kg h^{-1} (5.2%)	20.30 kg h^{-1} (17.2%)	0.01 kg h^{-1} (0.01%)	1.55 kg h^{-1} (1.3%)	10.41kg h^{-1} (8.8%)	23.7 kg h^{-1} (20.1%)
Flight 4	3.69 kg h^{-1} (18.5%)	2.36 kg h^{-1} (11.8%)	0.02 g h^{-1} (0.08%)	0.48kg h^{-1} (2.4%)	3.21 kg h^{-1} (16.1%)	5.45 kg h^{-1} (27.3%)
Flight 5	5.52 kg h^{-1} (4.3%)	20.47 kg h^{-1} (15.9%)	0.01 kg h^{-1} (0.01%)	1.45kg h^{-1} (1.1%)	8.12 kg h^{-1} (6.3%)	22.75kg h^{-1} (17.7%)
Flight 6	4.91kg h^{-1} (4.5%)	21.84 kg h^{-1} (20.2%)	0.01kg h^{-1} (0.00%)	1.55 kg h^{-1} (1.4%)	8.54 kg h^{-1} (7.9%)	24.01 kg h^{-1} (22.2%)
Flight 7	4.09 kg h^{-1} (4.1%)	18 kg h^{-1} (18.1%)	0.00 kg h^{-1} (0.00%)	1.5 kg h^{-1} (1.5%)	9.03 kg h^{-1} (9.1%)	20.6 kg h^{-1} (20.7%)
Flight 8	5.5 kg h^{-1} (6.8%)	15.6 kg h^{-1} (19.2%)	0.01 kg h^{-1} (0.01%)	1.08 kg h^{-1} (1.3%)	7.57 kg h^{-1} (9.3%)	18.19 kg h^{-1} (22.5%)

Table A6: Propagated uncertainty for each component 2022 flight 1 –5. showing the absolute uncertainty contribution of each source (kg h^{-1}) and its relative uncertainty contribution (%) to the estimated flux total. The percentages in brackets represent each uncertainty component expressed relative to the estimated flight emission, these percentages do not sum to the total relative uncertainty. Absolute values rounded to 2 decimals; percentages rounded to 1 decimal except for kriging due to its small uncertainty values.

Flight	Wind Speed	Wind direction	Kriging	Measurement	Background	Uncertainty total
Flight 1	6.55 kg h^{-1} (11.6%)	13.73 kg h^{-1} (24.2%)	0.01kg h^{-1} (0.01%)	0.73 kg h^{-1} (1.3%)	3.87 kg h^{-1} (6.8%)	15.71 kg h^{-1} (27.7%)
Flight 2	5.56 kg h^{-1} (11.4%)	13.08 kg h^{-1} (26.9%)	0.00 kg h^{-1} (0.01%)	0.67 kg h^{-1} (1.4%)	2.94 kg h^{-1} (6.0%)	14.53 kg h^{-1} (29.8%)
Flight 3	3.52 kg h^{-1} (4.9%)	16.35 kg h^{-1} (22.9%)	0.01kg h^{-1} (0.01%)	1.03 kg h^{-1} (1.4%)	3.36 kg h^{-1} (4.7%)	17.09 kg h^{-1} (23.9%)
Flight 4	4.77 kg h^{-1} (9.3%)	12.89 kg h^{-1} (25.1%)	0.00 kg h^{-1} (0.00%)	0.7 kg h^{-1} (1.4%)	4.40 kg h^{-1} (8.6%)	14.45 kg h^{-1} (28.1%)
Flight 5	4.15 kg h^{-1} (9.0%)	10.58 kg h^{-1} (23.0%)	0.00 kg h^{-1} (0.00%)	1.20 kg h^{-1} (2.6%)	5.72 kg h^{-1} (12.4%)	12.78 kg h^{-1} (27.8%)

*Table A7: Sensitivity Analysis Flights 2024 for change in surface roughness (z_0). *: CH_4 flux in kg h^- Surface Roughness Length values range between 0-1. Absolute values rounded to 2 decimals.*

F	Time of flight (local)	CH_4 * z_0 0.02 **	CH_4* z_0**0.05	CH_4* z_0**0.10	CH_4 flux* z_0**0.30	CH_4*z_0** 0.80	Difference z_0
1	2024-11-15 11:04:28 - 11:10:03	73.71	76.39	79.15	85.78	96.74	23.03
2	2024-11-15 11:21:30 - 11:27:11	75.86	78.58	81.38	88.11	99.22	23.36
3	2024-11-15 11:34:32 - 11:40:20	146.41	150.95	155.60	166.82	185.33	38.92
4	2024-11-15 11:47:12 - 11:50:41	70.15	72.47	74.84	80.56	90.00	19.84
5	2024-11-15 14:56:16 - 15:02:14	97.06	100.20	103.43	111.20	124.03	26.97
6	2024-11-15 15:10:55 - 15:16:52	121.17	125.03	128.98	138.52	154.24	33.07
7	2024-11-15 15:25:56 - 15:31:53	74.77	77.22	79.73	85.79	95.78	21.02
8	2024-11-15 15:38:59 - 15:45:12	120.57	124.38	128.30	137.73	153.29	32.72
9	2024-11-15 15:52:55 - 15:58:10	123.09	127.23	131.48	141.73	158.63	35.54
Average		**100.31**	**103.61**	**106.99**	**115.14**	**128.58**	**28.27**

2023

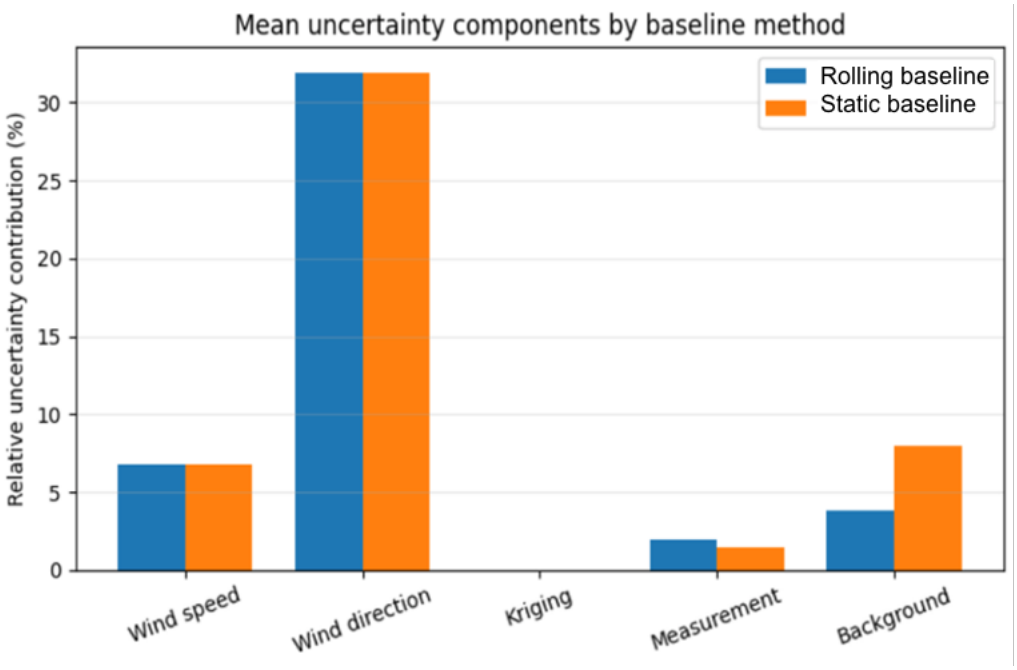

Fig. A4: Relative contribution of each uncertainty component to the total uncertainty for rolling (blue) and static (orange) baseline estimation approaches, Transect C, 2023.

2022

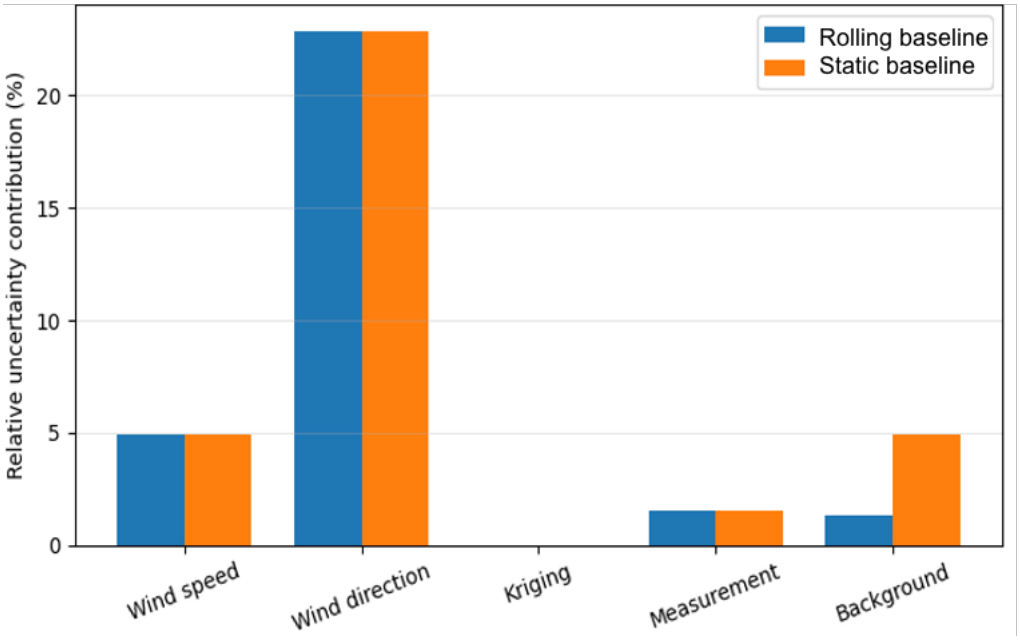

Fig. A5: Relative contribution of each uncertainty component to the total uncertainty for rolling (blue) and static (orange) baseline estimation approaches, Transect W, 2022.

Table A8: Output rolling / static baseline total uncertainty and uncertainty per component for all flights from 2022, 2023 and 2024. The column CH_4 kg h^- gives the total flux for the flight rounded to 2 decimals. Uncertainty CH_4 kg h^- gives the absolute uncertainty contribution in CH_4 kg h^- rounded to 2 decimals and relative uncertainty % is the relative uncertainty contribution expressed as a percentage of the estimated flux rounded to 2 decimals.

2022: Flight 1

Method	Component	CH_4 kgh	Uncertainty CH_4 kgh	Relative uncertainty %
static	wind speed	56.67	6.55	11.55
static	wind direction	56.67	13.73	24.23
static	kriging	56.67	0.01	0.01
static	measurement	56.67	0.73	1.28
static	background	56.67	3.87	6.83
static	total	56.67	15.71	27.73
static	total_uncertainty_high	56.67	72.38	127.73
static	total_uncertainty_low	56.67	40.96	72.27
rolling	wind speed	56.91	6.57	11.55
rolling	wind direction	56.91	13.79	24.23
rolling	kriging	56.91	0.01	0.01
rolling	measurement	56.91	0.73	1.28
rolling	background	56.91	1.16	2.03
rolling	total	56.91	15.34	26.95
rolling	total_uncertainty_high	56.91	72.25	126.95
rolling	total_uncertainty_low	56.91	41.57	73.05

2022: Flight 2

Method	Component	CH_4 kgh	Uncertainty CH_4 kgh	Relative uncertainty %
static	wind speed	48.68	5.56	11.43
static	wind direction	48.68	13.08	26.86
static	kriging	48.68	0.0	0.01
static	measurement	48.68	0.67	1.39
static	background	48.68	2.94	6.05
static	total	48.68	14.53	29.84
static	total_uncertainty_high	48.68	63.21	129.84
static	total_uncertainty_low	48.68	34.16	70.16
rolling	wind speed	44.77	5.12	11.43
rolling	wind direction	44.77	12.02	26.86
rolling	kriging	44.77	0.0	0.01
rolling	measurement	44.77	0.67	1.51
rolling	background	44.77	0.88	1.96
rolling	total	44.77	13.11	29.29
rolling	total_uncertainty_high	44.77	57.88	129.29
rolling	total_uncertainty_low	44.77	31.65	70.71

2022: Flight 3

Method	Component	CH_4 kgh	Uncertainty CH_4 kgh	Relative uncertainty %
static	wind speed	76.5	3.52	4.94
static	wind direction	71.41	16.35	22.89
static	kriging	71.41	0.01	0.01
static	measurement	71.41	1.03	1.44
static	background	71.41	3.36	4.7
static	total	71.41	17.09	23.93
static	total_uncertainty_high	71.41	88.5	123.93
static	total_uncertainty_low	71.41	54.33	76.07
rolling	wind speed	69.72	3.44	4.94
rolling	wind direction	69.72	15.96	22.89
rolling	kriging	69.72	0.01	0.01
rolling	measurement	69.72	1.03	1.47
rolling	background	69.72	0.87	1.25
rolling	total	69.72	16.38	23.5
rolling	total_uncertainty_high	69.72	86.1	123.5
rolling	total_uncertainty_low	69.72	53.34	76.5

2022: Flight 4

Method	Component	CH_4 kgh	Uncertainty CH_4 kgh	Relative uncertainty %
static	wind speed	51.44	4.77	9.28
static	wind direction	51.44	12.89	25.07

static	kriging	51.44	0.0	0.0
static	measurement	51.44	0.7	1.36
static	background	51.44	4.4	8.55
static	total	51.44	14.45	28.1
static	total_uncertainty_high	51.44	65.9	128.1
static	total_uncertainty_low	51.44	36.99	71.9
rolling	wind speed	45.83	4.25	9.28
rolling	wind direction	45.83	11.49	25.07
rolling	kriging	45.83	0.0	0.0
rolling	measurement	45.83	0.7	1.53
rolling	background	45.83	1.95	4.26
rolling	total	45.83	12.42	27.11
rolling	total_uncertainty_high	45.83	58.25	127.11
rolling	total_uncertainty_low	45.83	33.4	72.89

2022: Flight 5

Method	Component	CH_4 kgh	Uncertainty CH_4 kgh	Relative uncertainty %
static	wind speed	46.04	4.15	9.01
static	wind direction	46.04	10.58	22.98
static	kriging	46.04	0.0	0.0
static	measurement	46.04	1.2	2.61
static	background	46.04	5.72	12.42
static	total	46.04	12.78	27.75
static	total_uncertainty_high	46.04	58.82	127.75
static	total_uncertainty_low	46.04	33.26	72.25
rolling	wind speed	45.1	4.06	9.01
rolling	wind direction	45.1	10.36	22.98
rolling	kriging	45.1	0.0	0.0
rolling	measurement	45.1	1.2	2.67
rolling	background	45.1	1.59	3.52
rolling	total	45.1	11.31	25.08
rolling	total_uncertainty_high	45.1	56.41	125.08
rolling	total_uncertainty_low	45.1	33.79	74.92

2023: Flight 1

Method	Component	CH_4 kgh	Uncertainty CH_4 kgh	Relative uncertainty %
static	wind speed	83.9	5.71	6.81
static	wind direction	83.9	26.81	31.96
static	kriging	83.9	0.01	0.01
static	measurement	83.9	1.22	1.46
static	background	83.9	6.55	7.8
static	total	83.9	28.21	33.63
static	total_uncertainty_high	83.9	112.11	133.63
static	total_uncertainty_low	83.9	55.69	66.37
rolling	wind speed	65.53	4.46	6.81
rolling	wind direction	65.53	20.94	31.96
rolling	kriging	65.53	0.01	0.01
rolling	measurement	65.53	1.22	1.86
rolling	background	65.53	2.44	3.72
rolling	total	65.53	21.59	32.94
rolling	total_uncertainty_high	65.53	87.12	132.94
rolling	total_uncertainty_low	65.53	43.95	67.06

2023: Flight 2

Method	Component	CH_4 kgh	Uncertainty CH_4 kgh	Relative uncertainty %
static	wind speed	121.25	6.78	5.59
static	wind direction	121.25	30.79	25.4
static	kriging	121.25	0.01	0.01
static	measurement	121.25	1.37	1.13
static	background	121.25	8.78	7.24
static	total	121.25	32.76	27.02
static	total_uncertainty_high	121.25	154.01	127.02
static	total_uncertainty_low	121.25	88.49	72.98
rolling	wind speed	103.6	5.79	5.59
rolling	wind direction	103.6	26.31	25.4
rolling	kriging	103.6	0.01	0.01
rolling	measurement	103.6	1.37	1.32
rolling	background	103.6	2.77	2.67
rolling	total	103.6	27.12	26.17
rolling	total_uncertainty_high	103.6	130.71	126.17

rolling	total_uncertainty_low	103.6	76.48	73.83

2023: Flight 3

Method	Component	CH_4 kgh	Uncertainty CH_4 kgh	Relative uncertainty %
static	wind speed	118.05	6.17	5.23
static	wind direction	118.05	20.3	17.19
static	kriging	118.05	0.01	0.01
static	measurement	118.05	1.55	1.32
static	background	118.05	10.41	8.82
static	total	118.05	23.68	20.06
static	total_uncertainty_high	118.05	141.73	120.06
static	total_uncertainty_low	118.05	94.37	79.94
rolling	wind speed	89.52	4.68	5.23
rolling	wind direction	89.52	15.39	17.19
rolling	kriging	89.52	0.01	0.01
rolling	measurement	89.52	1.55	1.74
rolling	background	89.52	4.34	4.84
rolling	total	89.52	16.73	18.69
rolling	total_uncertainty_high	89.52	106.25	118.69
rolling	total_uncertainty_low	89.52	72.78	81.31

2023: Flight 4

Method	Component	CH_4 kgh	Uncertainty CH_4 kgh	Relative uncertainty %
static	wind speed	19.99	3.69	18.48
static	wind direction	19.99	2.36	11.82
static	kriging	19.99	0.02	0.08
static	measurement	19.99	0.48	2.42
static	background	19.99	3.21	16.05
static	total	19.99	5.45	27.29
static	total_uncertainty_high	19.99	25.44	127.29
static	total_uncertainty_low	19.99	14.53	72.71
rolling	wind speed	14.3	2.64	18.48
rolling	wind direction	14.3	1.69	11.82
rolling	kriging	14.3	0.01	0.09
rolling	measurement	14.3	0.48	3.38
rolling	background	14.3	1.92	13.46
rolling	total	14.3	3.71	25.96
rolling	total_uncertainty_high	14.3	18.02	125.96
rolling	total_uncertainty_low	14.3	10.59	74.04

2023: Flight 5

Method	Component	CH_4 kgh	Uncertainty CH_4 kgh	Relative uncertainty %
static	wind speed	128.46	5.52	4.3
static	wind direction	128.46	20.47	15.94
static	kriging	128.46	0.01	0.01
static	measurement	128.46	1.45	1.13
static	background	128.46	8.12	6.32
static	total	128.46	22.75	17.71
static	total_uncertainty_high	128.46	151.21	117.71
static	total_uncertainty_low	128.46	105.71	82.29
rolling	wind speed	89.13	3.83	4.3
rolling	wind direction	89.13	14.2	15.94
rolling	kriging	89.13	0.01	0.01
rolling	measurement	89.13	1.45	1.63
rolling	background	89.13	2.74	3.08
rolling	total	89.13	15.04	16.87
rolling	total_uncertainty_high	89.13	104.17	116.87
rolling	total_uncertainty_low	89.13	74.1	83.13

2023: Flight 6

Method	Component	CH_4 kgh	Uncertainty CH_4 kgh	Relative uncertainty %
static	wind speed	108.27	4.91	4.54
static	wind direction	108.27	21.84	20.18
static	kriging	108.27	0.01	0.0
static	measurement	108.27	1.55	1.44
static	background	108.27	8.54	7.89
static	total	108.27	24.01	22.18
static	total_uncertainty_high	108.27	132.28	122.18

static	total_uncertainty_low	108.27	84.25	77.82
rolling	wind speed	82.22	3.73	4.54
rolling	wind direction	82.22	16.59	20.18
rolling	kriging	82.22	0.0	0.0
rolling	measurement	82.22	1.55	1.89
rolling	background	82.22	2.75	3.35
rolling	total	82.22	17.29	21.03
rolling	total_uncertainty_high	82.22	99.52	121.03
rolling	total_uncertainty_low	82.22	64.93	78.97

2023: Flight 7

Method	Component	CH_4 kgh	Uncertainty CH_4 kgh	Relative uncertainty %
static	wind speed	99.65	4.09	4.1
static	wind direction	99.65	18.0	18.06
static	kriging	99.65	0.0	0.0
static	measurement	99.65	1.5	1.5
static	background	99.65	9.03	9.06
static	total	99.65	20.6	20.67
static	total_uncertainty_high	99.65	120.25	120.67
static	total_uncertainty_low	99.65	79.05	79.33
rolling	wind speed	73.76	3.03	4.1
rolling	wind direction	73.76	13.32	18.06
rolling	kriging	73.76	0.0	0.0
rolling	measurement	73.76	1.5	2.03
rolling	background	73.76	3.11	4.22
rolling	total	73.76	14.09	19.1
rolling	total_uncertainty_high	73.76	87.85	119.1
rolling	total_uncertainty_low	73.76	59.67	80.9

2023: Flight 8

Method	Component	CH_4 kgh	Uncertainty CH_4 kgh	Relative uncertainty %
static	wind speed	80.98	5.5	6.79
static	wind direction	80.98	15.57	19.23
static	kriging	80.98	0.01	0.01
static	measurement	80.98	1.08	1.34
static	background	80.98	7.57	9.34
static	total	80.98	18.19	22.47
static	total_uncertainty_high	80.98	99.18	122.47
static	total_uncertainty_low	80.98	62.79	77.53
rolling	wind speed	50.17	3.4	6.79
rolling	wind direction	50.17	9.64	19.23
rolling	kriging	50.17	0.01	0.01
rolling	measurement	50.17	1.08	2.16
rolling	background	50.17	3.04	6.06
rolling	total	50.17	10.73	21.38
rolling	total_uncertainty_high	50.17	60.89	121.38
rolling	total_uncertainty_low	50.17	39.44	78.62

2024: Flight 1

Method	Component	CH_4 kgh	Uncertainty CH_4 kgh	Relative uncertainty %
static	wind speed	88.68	8.17	9.21
static	wind direction	88.68	57.79	65.16
static	kriging	88.68	0.0	0.01
static	measurement	88.68	2.03	2.29
static	background	88.68	11.64	13.12
static	total	88.68	59.54	67.14
static	total_uncertainty_high	88.68	148.23	167.14
static	total_uncertainty_low	88.68	29.14	32.86
rolling	wind speed	69.61	6.41	9.21
rolling	wind direction	69.61	45.36	65.16
rolling	kriging	69.61	0.0	0.0
rolling	measurement	69.61	2.03	2.92
rolling	background	69.61	3.21	4.62
rolling	total	69.61	45.97	66.03
rolling	total_uncertainty_high	69.61	115.57	166.03
rolling	total_uncertainty_low	69.61	23.64	33.97

2024: Flight 2

Method	Component	CH_4 kgh	Uncertainty CH_4 kgh	Relative uncertainty %
static	wind speed	91.85	4.56	4.97
static	wind direction	91.85	59.95	65.27
static	kriging	91.85	0.01	0.01
static	measurement	91.85	1.91	2.08
static	background	91.85	11.48	12.5
static	total	91.85	61.24	66.67
static	total_uncertainty_high	91.85	153.08	166.67
static	total_uncertainty_low	91.85	30.61	33.33
rolling	wind speed	83.29	4.14	4.97
rolling	wind direction	83.29	54.36	65.27
rolling	kriging	83.29	0.0	0.01
rolling	measurement	83.29	1.91	2.29
rolling	background	83.29	3.03	3.63
rolling	total	83.29	54.64	65.6
rolling	total_uncertainty_high	83.29	137.92	165.6
rolling	total_uncertainty_low	83.29	28.65	34.4

2024: Flight 3

Method	Component	CH_4 kgh	Uncertainty CH_4 kgh	Relative uncertainty %
static	wind speed	172.56	10.32	5.98
static	wind direction	172.56	93.11	53.96
static	kriging	172.56	0.01	0.01
static	measurement	172.56	1.79	1.04
static	background	172.56	10.39	6.02
static	total	172.56	94.27	54.63
static	total_uncertainty_high	172.56	266.83	154.63
static	total_uncertainty_low	172.56	78.29	45.37
rolling	wind speed	143.3	8.57	5.98
rolling	wind direction	143.3	77.32	53.96
rolling	kriging	143.3	0.01	0.01
rolling	measurement	143.3	1.79	1.25
rolling	background	143.3	3.33	2.33
rolling	total	143.3	77.89	54.35
rolling	total_uncertainty_high	143.3	221.18	154.35
rolling	total_uncertainty_low	143.3	65.41	45.65

2024: Flight 4

Method	Component	CH_4 kgh	Uncertainty CH_4 kgh	Relative uncertainty %
static	wind speed	77.32	4.57	5.91
static	wind direction	77.32	53.28	68.9
static	kriging	77.32	0.0	0.0
static	measurement	77.32	0.86	1.11
static	background	77.32	3.86	4.99
static	total	77.32	53.62	69.35
static	total_uncertainty_high	77.32	130.94	169.35
static	total_uncertainty_low	77.32	23.7	30.65
rolling	wind speed	41.86	2.48	5.91
rolling	wind direction	41.86	28.84	68.9
rolling	kriging	41.86	0.0	0.0
rolling	measurement	41.86	0.86	2.04
rolling	background	41.86	1.36	3.25
rolling	total	41.86	29.0	69.26
rolling	total_uncertainty_high	41.86	70.86	169.26
rolling	total_uncertainty_low	41.86	12.87	30.74

2024: Flight 5

Method	Component	CH_4 kgh	Uncertainty CH_4 kgh	Relative uncertainty %
static	wind speed	114.83	8.32	7.24
static	wind direction	114.83	64.08	55.81
static	kriging	114.83	0.01	0.01
static	measurement	114.83	1.8	1.57
static	background	114.83	8.41	7.33
static	total	114.83	65.19	56.77
static	total_uncertainty_high	114.83	180.02	156.77
static	total_uncertainty_low	114.83	49.63	43.23
rolling	wind speed	85.36	6.18	7.24
rolling	wind direction	85.36	47.64	55.81
rolling	kriging	85.36	0.0	0.01
rolling	measurement	85.36	1.8	2.11

rolling	background	85.36	3.2	3.75
rolling	total	85.36	48.18	56.44
rolling	total_uncertainty_high	85.36	133.53	156.44
rolling	total_uncertainty_low	85.36	37.18	43.56

2024: Flight 6

Method	Component	CH_4 kgh	Uncertainty CH_4 kgh	Relative uncertainty %
static	wind speed	142.68	4.49	3.14
static	wind direction	142.68	63.02	44.17
static	kriging	142.68	0.01	0.01
static	measurement	142.68	1.9	1.33
static	background	142.68	10.46	7.33
static	total	142.68	64.07	44.9
static	total_uncertainty_high	142.68	206.75	144.9
static	total_uncertainty_low	142.68	78.62	55.1
rolling	wind speed	118.69	3.73	3.14
rolling	wind direction	118.69	52.42	44.17
rolling	kriging	118.69	0.01	0.01
rolling	measurement	118.69	1.9	1.6
rolling	background	118.69	2.82	2.38
rolling	total	118.69	52.66	44.37
rolling	total_uncertainty_high	118.69	171.35	144.37
rolling	total_uncertainty_low	118.69	66.02	55.63

2024: Flight 7

Method	Component	CH_4 kgh	Uncertainty CH_4 kgh	Relative uncertainty %
static	wind speed	93.77	6.84	7.3
static	wind direction	93.77	60.13	64.12
static	kriging	93.77	0.01	0.01
static	measurement	93.77	2.0	2.14
static	background	93.77	11.38	12.13
static	total	93.77	61.61	65.7
static	total_uncertainty_high	93.77	155.39	165.7
static	total_uncertainty_low	93.77	32.16	34.3
rolling	wind speed	77.85	5.68	7.3
rolling	wind direction	77.85	49.92	64.12
rolling	kriging	77.85	0.0	0.01
rolling	measurement	77.85	2.0	2.57
rolling	background	77.85	2.92	3.75
rolling	total	77.85	50.36	64.7
rolling	total_uncertainty_high	77.85	128.21	164.7
rolling	total_uncertainty_low	77.85	27.48	35.3

2024: Flight 8

Method	Component	CH_4 kgh	Uncertainty CH_4 kgh	Relative uncertainty %
static	wind speed	143.78	7.93	5.52
static	wind direction	143.78	84.62	58.85
static	kriging	143.78	0.01	0.01
static	measurement	143.78	1.97	1.37
static	background	143.78	11.06	7.69
static	total	143.78	85.73	59.62
static	total_uncertainty_high	143.78	229.51	159.62
static	total_uncertainty_low	143.78	58.05	40.38
rolling	wind speed	127.18	7.02	5.52
rolling	wind direction	127.18	74.85	58.85
rolling	kriging	127.18	0.01	0.01
rolling	measurement	127.18	1.97	1.55
rolling	background	127.18	3.49	2.75
rolling	total	127.18	75.28	59.19
rolling	total_uncertainty_high	127.18	202.46	159.19
rolling	total_uncertainty_low	127.18	51.9	40.81

2024: Flight 9

Method	Component	CH_4 kgh	Uncertainty CH_4 kgh	Relative uncertainty %
static	wind speed	151.04	8.74	5.79
static	wind direction	151.04	111.35	73.72
static	kriging	151.04	0.02	0.01
static	measurement	151.04	2.11	1.4
static	background	151.04	10.74	7.11

static	total	151.04	112.23	74.31
static	total_uncertainty_high	151.04	263.27	174.31
static	total_uncertainty_low	151.04	38.81	25.69
rolling	wind speed	118.92	6.88	5.79
rolling	wind direction	118.92	87.67	73.72
rolling	kriging	118.92	0.01	0.01
rolling	measurement	118.92	2.11	1.77
rolling	background	118.92	3.15	2.65
rolling	total	118.92	88.02	74.02
rolling	total_uncertainty_high	118.92	206.94	174.02
rolling	total_uncertainty_low	118.92	30.89	25.98

Table A9: 10 m Wind speed (U10) from SMHI (station 62040, Helsingborg A) matched to GHGSat overpass times.

scene_id	Overpass time (UTC)	SMHI time used (UTC)	Wind speed U10 (m/s)
Ii98UjV	2024-01-01 12:06:32	2024-02-01 12:00:00	7.6
Ejd-zjV	2024-05-07 11:09:16	2024-05-07 11:00:00	2.3
Mo48zjV	2025-02-14 12:41:41	2025-02-14 13:00:00	2.9
Ita9zjV	2026-02-03 12:10:51	2026-02-03 12:00:00	6.8
ltlB3mi	2026-02-14 12:09:35	2026-02-14 12:00:00	2.9
CtqAUjV	2026-02-19 13:45:40	2026-02-19 14:00:00	1.9
Cu3EYmi	2026-03-04 14:34:14	2026-03-04 15:00:00	2.9
Hu54UjV	2026-03-06 11:01:49	2026-03-06 11:00:00	3.7
hu94Ymi	2026-03-10 11:18:04	2026-03-10 11:00:00	2.7
Wui83mi	2026-04-16 09:43:16	2026-04-16 10:00:00	1.4
KupDYmi	2026-04-23 15:15:10	2026-04-23 15:00:00	6.1
Our-Ymi	2026-04-27 09:36:17	2026-04-27 10:00:00	2.1
Gv1CYmi	2026-05-05 14:56:03	2026-05-05 15:00:00	3.6

References (Appendices)

Naturvårdsverket. (n.d.). *Utsläpp i siffror.* Retrieved January, 2026, from https://utslappisiffror.naturvardsverket.se/sv/Sok/

Naturvårdsverket. (2024) *National Inventory Report Sweden 2024*: *Greenhouse gas emission inventories 1990–2022 submitted under the United Nations Framework Convention on Climate Change and the Paris Agreement*.
https://unfccc.int/sites/default/files/resource/NIR%20SE%20submission%202024.pdf

Swedish Meteorological and Hydrological Institute (SMHI). (n.d.). *Meteorological observations: Wind speed and wind direction*. SMHI Open Data. Retrieved April, 2026, from https://opendata.smhi.se/metobs/introduction